

Cohesive Crack Growth in Macro-Synthetic Fiber Reinforced Concrete

K Chiranjeevi Reddy
CE13M1001

A Dissertation Submitted to
Indian Institute of Technology Hyderabad
In Partial Fulfilment of the Requirements for
The Degree of Master of Technology



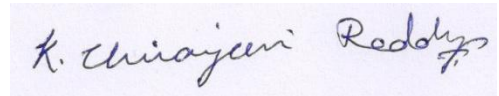
भारतीय प्रौद्योगिकी संस्थान हैदराबाद
Indian Institute of Technology Hyderabad

Department of Civil Engineering
Indian Institute of Technology, Hyderabad

July, 2015

Declaration

I declare that this written submission represents my ideas in my own words, and where others' ideas or words have been included, I have adequately cited and referenced the original sources. I also declare that I have adhered to all principles of academic honesty and integrity and have not misrepresented or fabricated or falsified any idea/data/fact/source in my submission. I understand that any violation of the above will be a cause for disciplinary action by the Institute and can also evoke penal action from the sources that have thus not been properly cited, or from whom proper permission has not been taken when needed.

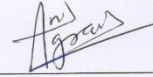
A handwritten signature in blue ink on a light purple background. The signature reads "K. Chiranjeevi Reddy" with a stylized flourish at the end.

K. Chiranjeevi Reddy

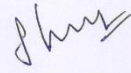
CE13M1001

Approval Sheet

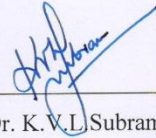
This thesis entitled "*Cohesive Crack Growth in Macro-synthetic Fiber Reinforced Concrete*" by K.Chiranjeevi Reddy is approved for the degree of Master of Technology from IIT Hyderabad.



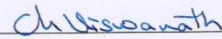
Dr. Anil Agarwal
Examiner



Dr. S.Suriya Prakash
Examiner



Dr. K.V.L. Subramaniam
Adviser



Dr. Viswanath Chinthapenta
Chairman

Acknowledgements

I would like to convey my gratitude to my advisor, Dr. K.V.L.Subramaniam for his guidance throughout this project. His suggestions during the three stages of my research, i.e. experimental, analytical and numerical work, have contributed to my knowledge and have vastly improved the quality of this thesis. I would also like to thank Dr. S.Suriya Prakash for his feedback on my experiments.

I extend my special gratitude to my fellow student, G. Sahith Reddy, for his guidance and help in conducting experiments. Thanks are also due to G.V.P. Bhagath Singh for his valuable support in the laboratory.

Finally, my friends, Kondapalli Sravani, Jaya Prakash Vemuri, B. Durga Prasad and Surepally Naresh provided me good company during this period. I will always cherish the time spent with them.

Dedicated to

My Parents

Nomenclature

P_1	First peak load
P_u	Peak load in load deflection response
δ_u	Deflection corresponding to P_u
P_{crit}	Load corresponding to immediate lowest point after peak load
δ_u	Deflection corresponding to P_{crit}
δ_p	Net deflection at peak
δ_1	first-peak loads
F_p	Peak Strength
f_1	First-Peak Strength
P_D^{600}	Residual load at net deflection of L/600
f_D^{600}	Residual Strength at net deflection of L/600
P_D^{150}	Residual load at net deflection of L/150
f_D^{150}	Residual Strength at net deflection of L/150
T_D^{150}	Area under the load vs. net deflection curve 0 to L/150
$R_{T,D}^{150}$	Equivalent flexural strength
T_{JSCE}	Toughness
F_{JSCE}	Toughness factor
CMOD	Crack mouth opening displacement
LOP	Limit of proportionality
F_L	load corresponding to LOP
$f_{ct,Lf}$	Strength corresponding to LOP
F_i	load corresponding to with CMOD = CMOD _j or $\delta = \delta_i$ (I = 1,2,3,4)
$f_{R,j}$	Residual flexural Tensile Strength corresponding with CMOD = CMOD _j where (i= 1.5, 2.5, 3.5, 4.5)
CTOD	Crack Tip opening displacement
P_{If}	First crack load
f_{If}	first crack strength
SNFRC	Synthetic Nylon Fiber Reinforced Concrete.
SPFRC	Synthetic Polypropylene Fiber Reinforced Concrete.

Table of Contents

Declaration	ii
Approval sheet.....	iii
Acknowledgements	iv
Dedicated to.....	v
List of figures	ix
List of Tables.....	xi
Chapter 1	1
Introduction.....	1
1.1 Introduction	1
1.2 Objectives.....	2
1.3 Organization of thesis.....	3
Chapter 2	4
Review of Standard Test methods and Literature	4
2.1 Introduction	4
2.1.1 Steel Fibers	6
2.1.2 Polypropylene Fibers	7
2.1.3 Macro-synthetic Polypropylene fiber	8
2.2 Cohesive behaviour	12
2.3 Standard Test Methods.....	17
2.3.1 ASTM 1609 test procedure.....	17
2.3.2 ASTM 1018 test procedure.....	19
2.3.3 JSCE SF24.....	20
2.3.5 UNI 11039-2 Test Procedure.....	22
2.3.6 EN 14651 Test Procedure.....	24
Chapter 3	26
Materials and Methods.....	26
3.1 Introduction	26
3.1.1 Cement.....	26
3.1.2 Fly Ash	26
3.1.3 Aggregates	26
3.1.4 Synthetic Fibers	26
3.1.5 Admixture.....	27

3.2 Experimental program and Mix Proportions.....	27
3.2.1 Casting and Curing of Specimens	28
3.3 Test Methods	28
3.3.1 Slump.....	28
3.3.2 Compression Strength Testing.....	29
3.3.3 Four-point-bending test	29
3.3.4 Three-point-bending test (For notch beam).....	30
Chapter 4.....	31
Experimental Results	31
4.1 Introduction	31
4.2 Compressive strength	31
4.3 Flexural Testing as per ASTM C1609 (Unnotched Beams)	34
4.4 Flexure Testing on Notched Specimens (EN 14651).....	39
4.5 Analysis of Data	42
4.6 Summary of Findings	45
Chapter 5.....	46
Digital Image Correlation Results	46
5.1 Introduction	46
5.2 Background	46
5.3 Results	47
5.4 Analysis of Results.....	56
5.5 Summary and Findings	57
Chapter 6.....	58
Analytical Model	58
6.1 Introduction	58
6.2 Load deflection curve from moment curvature analysis	60
6.3 Proposed Analytical Formulation for multi-linear softening	63
6.4 Inverse analysis	68
Chapter 7.....	73
Summary of findings and Future Works.....	73
References	74

List of figures

Fig 2.1 1: The composite stress-strain curves for fiber-reinforced brittle matrix	5
Fig 2.1 2: Strain hardening response of polypropylene fiber composites.....	6
Fig 2.1 3: Effect of steel fiber shape on the load response in flexure.....	7
Fig 2.1.4 Various types of synthetic fibers tested in the present study.....	9
Fig 2.1.5 Comparison of absorbed energies from pullout tests for various fiber types.....	9
Fig 2.1.6 Pullout/ fiber strength with indentation pressure.....	9
Fig 2.1.7 Load–deflection curves for Hooked end steel fibers and Synthetic fibers.	10
Fig 2.1.8 Equivalent Flexural Strength Ratio of steel and Synthetic fiber	11
Fig 2.1 9 Load CMOD response of synthetic fiber with varying volume fraction.....	12
Fig 2.2.1 A crack in plain concrete and the essential features: zone with fiber bridging, the process zone and aggregate interlock together with the FCM.	13
Fig 2.2.2 A crack in FRC and the essential features: zone with fibre bridging, the process zone and aggregate interlock together with the FCM.	13
Fig 2.2.3 Stress Crack opening Relationships	14
Fig 2.2.4 Bi-linear stress crack opening relationship	14
Fig 2.2.5 Typical stress-crack opening relationships	15
Fig 2.2.6 Stress Crack opening Relationships for Steel FRC	16
Fig 2.3.1 Diagrammatic View of a Suitable Apparatus for Flexure Test of Concrete by Third-Point Loading Method	18
Fig 2.3.2 Example of Parameter Calculations	18
Fig 2.3.3 Important Characteristics of the Load-Deflection Curve	19
Fig 2.3.4 Definition of Toughness Indices for Elastic-Plastic Material Behaviour.....	20
Fig 2.3.5 Definitions of JSCE Toughness and Toughness Factor	21
Fig 2.3.6 Schematic diagram of the UNI 11309 four-point bending test setup.....	22
Fig 2.3.7(a) Basic concrete load-CTOD, (b) Load–CTOD	23
Fig 2.3.8 Typical arrangement of measuring CMOD	24
Fig 2.3.9 Load-CMOD and F_j ($j=1.5, 2.5, 3.5, 4.5$).....	25
Fig 3.1.1 FibreTuff™ Monofilament structural polypropylene fiber	27
Fig 4.1 Compressive Stress vs Strain of Cylinders.....	33
Fig 4.2 Failure in fiber reinforced concrete specimens; (a) cylinder; (b) cube.....	33
Fig 4.3 Load deflection response control specimen.....	34
Fig 4.4 Load deflection response from flexure test for 4 kg/m^3	34
Fig 4.5 Load deflection response from flexure test for 6 kg/m^3	35
Fig 4. 6 Load deflection response from flexure test for 8 kg/m^3	35
Fig 4.7 Load deflection response of SPFRC at 28 days	36
Fig 4.8 Load deflection response of SNFRC at 28 days.....	36
Fig 4.9. Idealized load response for beams tested in flexure	37

Fig 4.10 Load CMOD response of control at 28 days	39
Fig 4.11 Load CMOD response of 4 kg/m ³ at 28 days (a) SPFRC and (b) SNFRC	39
Fig 4.12 Load CMOD response of 6 kg/m ³ at 28 days (a) SPFRC and (b) SNFRC	40
Fig 4.13 Load CMOD response of 8 kg/m ³ at 28 days (a) SPFRC and (b) SNFRC	40
Fig 4.14 Load CMOD response SPFRC at 28 days	41
Fig 4.15 Load CMOD response SNFRC at 28 days	41
Fig 4.16 Residual Strength at L/600 as per ASTM C 1609	43
Fig 4.17 Residual Strength at L/150 as per ASTM C 1609	43
Fig 4.18 Equivalent Flexural strength Ratio as per ASTM C 1609	43
Fig 4.19 Toughness factor as per JSCE 1609	44
Fig 4.20 Residual Flexural Strength of SPFRC as per EN14651	44
Fig 4.21 Residual Flexural Strength of SNFRC as per EN14651	45

Fig 5. 1: (a) Load-CMOD of plot of SPFRC specimen with 6kg/m ³ fibers. The CTOD measured during the test is also shown in the Figure; (b) ϵ_{xx} at 10.5 kN (pre-peak); (c) ϵ_{xx} at 12.1 kN (prepeak); (d) ϵ_{xx} at 12.7 (postpeak); (e) ϵ_{xx} at 11.4 kN (postpeak); (f) ϵ_{xx} at 10.1 kN (postpeak); and (g) ϵ_{xx} at 7 kN (postpeak)	48
Fig 5.2 Horizontal strips for strain computations	49
Fig 5.3: (a) Typical load response of control; (b) displacement profile at line 1; (c) strain profile at line 1 at distinct load points	50
Fig 5.4: (a) Typical load response of 4 kg/m ³ Polyprpylene fibers; (b) displacement profile at line 1; (c) strain profile at line 1 at distinct load points	50
Fig 5.5: (a) Typical load response of 6 kg/m ³ Polypropylene fibers (b) displacement profile at line 1; (c) strain profile at line 1 at distinct load points	51
Fig 5.6: (a) Typical load response of 8 kg/m ³ Polypropylene fibers (b) displacement profile at line 1; (c) strain profile at line 1 at distinct load points	51
Fig 5.7: (a) Typical load response of 4 kg/m ³ Nylon (b) displacement profile at line 1; (c) strain profile at line 1 at distinct load points	52
Fig 5.8: (a) Typical load response of 6 kg/m ³ PP; (b) displacement profile at line 1; (c) strain profile at line 1 at distinct load points	52
Fig 5.9: (a) Typical load response of 8 kg/m ³ Nylon (b) displacement profile at line 1; (c) strain profile at line 1 at distinct load points	53
Fig 5.10 Variation of Strain value (ϵ_{xx}) on lines along the depth of section at distinct loads for control Specimen	54
Fig 5.11 Variation of Strain value (ϵ_{xx}) on lines along the depth of section at distinct loads for polypropylene with 6 kg/m ³ volume	55
Fig 5.12 Crack Depth vs CTOD of typical SPFRC beams and control	56

Fig 6.1 Geometry, Loading, and Deformation of Cracked Incremental	59
Fig 6.2 Definition of Parameters of Bilinear Stress-Crack opening relationship	59
Fig 6.3 Distinct Phases of Stress Distribution during propagation of the crack in the section	60
Fig 6.4 Model representation of simply supported beam after cracking	60
Fig 6.5 Load deflection curves by using bilinear stress crack opening relationship	62

Fig 6.6 Experimental Load deflection curves	63
Fig 6.7 Definition of Parameters of Multi linear Stress-Crack relationship	64
Fig 6.8 General Stress distribution for multi linear case	64
Fig 6.9 Comparison of Moment Rotation relationship for Oleson formulae and current formulae	66
Fig 6.10 Load deflection curves by using tetra linear stress crack opening relationship	68
Fig 6.11. Stress Crack opening relationship of SPFRC beams.....	70
Fig 6.12 Stress Crack opening relationship of SNFRC beams	70
Fig 6.13 Experimental and matched theoretical curves of SNFRC 6 kg/m ³ beams.	71
Fig 6.14 Crack depth vs Crack width for mean Crack opening parameters of SPFRC	72
Fig 6.15 Crack depth vs Crack width for mean Crack opening parameters of SNFRC	72

List of Tables

Table 2.1: Typical Properties of Fibers.....	4
Table 2.2: Properties of various types of polypropylene fiber.....	8
Table 3.1 Summary of weight proportion of the various mixes	28
Table 4.1 28- Day Compressive strength results	32
Table 4.2 90-day compressive strength results	32
Table 4.3 Key Parameters in the flexural load response of SPFRC	37
Table 4.4 Key Parameters in the flexural load response of SNFRC.....	37
Table 4.5 Key Parameters in the flexural load response of SPFRC from notched beams.....	42
Table 4.6 Key Parameters in the flexural load response of SNFRC from notched beams	42
Table 5.1 Locations of lines.....	49
Table 6.1 Mean (Std dev) Values Of crack opening parameters of SPFRC Beam	70
Table 6.2 Mean (Std dev) Values Of crack opening parameters of SPFRC Beam	71

Chapter 1

Introduction

1.1 Introduction

Fibers act like discrete reinforcement, which provide tensile stress transfer across a crack. Fibers bridging a crack increase the load carrying capacity of the material even after the formation of a crack. A concrete beam containing fibres suffers damage by gradual development of single or multiple cracks with increasing deflection, but retains some degree of structural integrity and post-crack resistance even under considerable deflection. A similar beam without fibres fails suddenly at a small deflection by separation into two pieces. The addition of the fibres to concrete therefore enhances the toughness of concrete. The ability of fibre-reinforced concrete composites to absorb energy has long been recognised as one of the most important benefits of the incorporation of fibres in plain concrete. The toughening effect is the result of crack closing stresses provided by the fibers results from several types of fiber/matrix interactions, leading to energy absorption in the fiber-bridging zone of a fiber-reinforced concrete (FRC). These processes include fiber bridging, fiber debonding, fiber pullout (sliding) and fiber rupture as a crack propagates across a fiber through the matrix [1].

There are many kinds of fibers, both metallic and polymeric, which have been used in concrete to improve specific engineering properties of the material. Steel fibers are used in a wide range of structural applications, in general, when the control of concrete cracking is important such as industrial pavements [2, 3] precast structural elements [4] and tunnel linings [5]. Steel fibers have high elastic modulus and stiffness and produce improvements in compressive strength and toughness of concrete [6]. Improvements in flexural strength of the material are also obtained by the use of steel fibers in concrete. Increase in flexural strength is achieved with increasing fiber aspect ratio (length to diameter ratio) and fiber volume fraction; significant improvements are obtained at high volume fractions [7]. In general, addition of steel fibers influences the compressive strain at ultimate load and ductility in flexure more significantly than the improvements in strength [8]. Steel fibers, however, increase structure weight of concrete and exhibit balling effect during mixing, which lowers the workability of the mix. In addition, steel fibers easily basset and rust, and it also has the problem of conductive electric and magnetic fields.

Synthetic fibres are less stiff than steel fibres and are most typically used in industrial pavements to reduce the cracking induced by shrinkage. Synthetic fibres are mainly effective in reducing crack formation, particularly at an early stage of the cast and in severe weather conditions (e.g. in dry climatic zones), when hygrometric shrinkage brings along some weak tensile stress which is yet too high for the fresh mixture to withstand. Synthetic fibers made using nylon Polypropylene and acrylic are available commercially. Polypropylene fibers are available in two different forms; Monofilaments and Fibrillated. Monofilament fibers are single strand of fibers having uniform cross-sectional. Fibrillated fibers are manufactured in the form of films or tapes that are slit in such a way that they have net like physical structure.

Polypropylene fibers have good ductility, fineness, and dispersion so they can restrain the plastic cracks [9].

Improvements are being made to optimize synthetic fibers to suit structural applications. Recently, macro-synthetic fibres have been produced with the aim of substituting steel fibres in structural applications. There has been a growing interest on synthetic fibres, owing to some substantial advantages over metallic ones, such as strong chemical stability in alkaline and generally aggressive environments, exemption from oxidation, lightness and, in turn, convenient stocking and handling, a-toxicity and electromagnetic transparency. This latter aspect is relevant, for instance, when either dealing with special equipment (ranging from mobile phones to CT diagnostics) or in industrial buildings wherein, say, automated toll collection booths employing electromagnetic vehicle detectors are planned. The availability of a structural synthetic fibre, capable of contributing to the load carrying capacity of an element while increasing its toughness and durability at a reasonable cost, is an important asset for an improved building technology. The knowledge of the fracture properties of concrete reinforced with these fibres is still limited.

In this thesis the influence of two commercially available macro-synthetic fibers on the toughness and ductility of concrete is investigated. Structural polypropylene and Nylon fibers with embossed surface patterns to optimize strength and pullout response from concrete matrix are used in this study. Crack propagation in concrete reinforced with discrete macro-synthetic fibers in flexure is studied using a full-field optical technique known as digital image correlation. An interpretation of the observed tension response of fiber reinforced concrete is attempted in terms of crack propagation and toughening mechanisms in the composite using the information available from digital image correlation. The fracture behaviour of the concrete reinforced with the macro-synthetic fibers is evaluated in terms of the cohesive stress-crack opening relationship. The cohesive stress as a function of crack opening displacement is derived for different volume fractions of fibers

1.2 Objectives

The broad objective of the work reported in this thesis is to investigate the influence of macro synthetic fibers on the mechanical behaviour of concrete. Specific objectives of the thesis include

1. To study the influence of crack bridging on the flexural response of fiber reinforced concrete
2. To evaluate the influence of macro-synthetic fibers on the toughness and ductility of concrete
3. To provide an interpretation for the observed tension response of fiber reinforced concrete in flexure in terms of crack propagation and toughening mechanisms in the composite.
4. To determine the crack bridging stresses contributed by macro-synthetic fibers

1.3 Organization of thesis

This thesis is organized in six chapters. Description of content of each chapter is given below.

Chapter 2

A review of literature on the influence of fibers on the mechanical properties and tension response of concrete is presented. The influence of fiber type and volume fraction on the tensile response of concrete are summarized.

Chapter 3

Details of the experimental program to investigate the tensile behaviour of macro synthetic fiber reinforced concrete are presented in this chapter. The materials, Mix designs and test methods used in the experimental test program are described for macro synthetic polypropylene fiber reinforced concrete (SPFRC) and macro synthetic nylon fiber reinforced concrete (SNFRC).

Chapter 4

Experimental results from flexure tests on notched and unnotched beams for SPFRC and SNFRC at different volume contents of fibers are presented. The standard test measures available from the different standards for evaluating improvements in toughness, ductility and load carrying capacity are calculated.

Chapter 5

The results of the digital image correlation from the notched beams tested in flexure are analysed. The strain distribution information obtained from the DIC is used to study the crack growth in the beams. The relationship between the crack length and crack opening are obtained for SPFRC and SNFRC.

Chapter 6

The results of numerical analysis to obtain the cohesive stress as a function of crack opening within the framework of the hinged crack model are presented. The influence of fibers content on the cohesive crack closing stresses is investigated.

Chapter 2

Review of Standard Test methods and Literature

2.1 Introduction

Fibers have been used as discrete randomly distributed reinforcement to strengthen a material weak in tension. Fibers have been shown to improve the toughness and the post crack ductility in tension, which is achieved by the reinforcement effect across a crack in the material matrix. The use of fibers results in an enhancement in the load carrying ability which is achieved due to stress transfer after cracking. The earliest documented use of fibers has been the incorporation of chopped hay and camel hair in adobe bricks by the Egyptians. Since then different types of fibers have been developed, which can broadly be classified as metallic, synthetic, glass, and mineral. Properties of the different fibers commonly available today are listed in Table 2.1.

Fiber volume content is the primary variable which influences the response of the fiber reinforced composite in tension as shown in Fig 2.1 1. For small volume fraction, after first crack, there is drop in the load. There are a small number of fibers bridging the crack that sustain the load. The capacity provided by the number of fibers crossing the crack is significantly less than the first crack load and load carrying capacity decreases rapidly with increasing deformation. For intermediate volume fraction, after the drop in load associated with the formation of a crack, the load carrying capacity provided by the fibers produces a progressive yet gradual decrease in the load carrying capacity. For high volume fraction, after first crack, there are a large number of fibers bridging the crack and the resistance to crack opening provided by the fibers is larger than the first crack load. As the load increases, more cracks form along the length of specimen.

Table 2.1: Typical Properties of Fibers

Fiber	Diameter	Specific gravity	Tensile strength	Elastic Modulus	Fracture strain
	(um)		(GPa)	(GPa)	(%)
Steel	5-500	7.84	0.5-2.0	210	0.5-3.5
Glass	9-15	2.6	2.0-4.0	70-80	2.0-3.5
Fibrillated Polypropylene	20-200	0.9	0.5-0.75	5-77	8.0
Cellulose		1.2	0.3-0.5	10	
Carbon (high strength)	9	1.9	2.6	230	1
Cement matrix		2.5	3.7×10^{-3}	10-45	0.02

The observed load response at the different volume fractions is associated with the pullout response of steel fibers from the concrete matrix averaged over the crack. The mechanical behaviour of the FRC are influenced by reinforcing mechanisms or the ability of the fibers to transfer stress across the crack. In short randomly distributed fibers at low and intermediate fiber volume fractions (typically up to 2%) the contribution of fibers is after strain localization, which occurs close to the peak tensile load. The tensile strength in these cases is comparable to that of the unreinforced matrix. The strain softening is influenced by the cracking closing pressure provided by the fibers as a function of the crack opening displacement. The toughening provided fibers depends upon the pull out resistance of the fibers embedded in the matrix. During crack propagation, debonding and sliding contribute significantly to the pull out resistance of the fibers and hence to the total energy consumption when a large crack develops in the matrix. Fiber breakage has not been considered to contribute significantly to the energy dissipated during crack propagation in FRC [24]. Several fracture based formulations which consider the debonding behaviour of fibers from the cementitious matrix have been proposed [10].

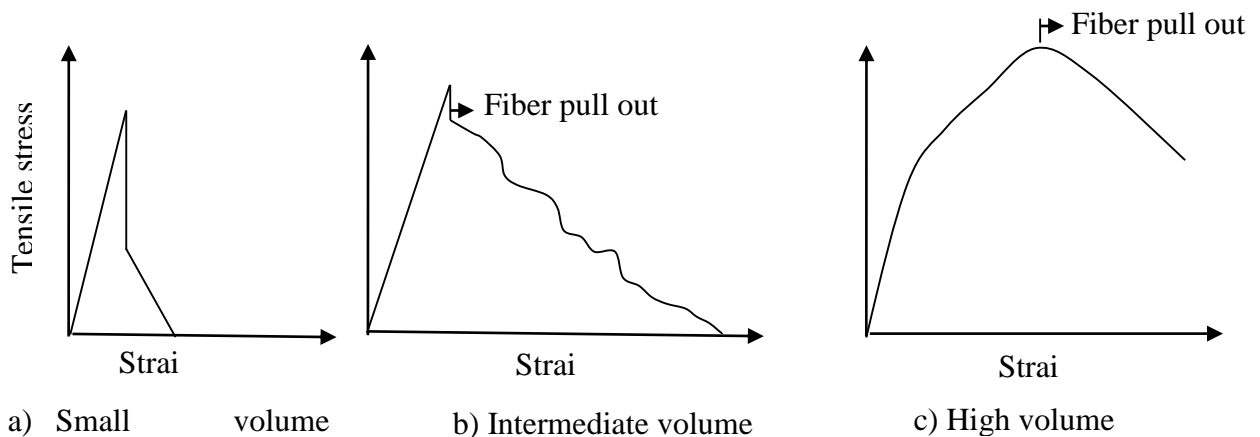


Fig 2.1 1: The composite stress-strain curves for fiber-reinforced brittle matrix

At higher volume fractions, which are usually achieved using special processing techniques, the pre-peak behaviour is fundamentally altered due to stabilization of micro cracking in the matrix. A uniform distribution of micro cracks in the matrix leads to significant enhancement in the strain capacity of the matrix [11]. The load response of such composites exhibits strain hardening response as shown in Fig 2.1 2. There is a point in the load response identified as the bend-over-point (BOP) where the matrix contribution to the tensile load response reaches a maximum. The load response following the BOP is characterized by multiple cracking in the matrix. In this stage the incremental loading of the fibers at the location of the crack is transferred to the matrix through the interfacial bond, which results in a build-up of tensile stress in the matrix. More cracks are produced in the matrix when the tensile stress in matrix reaches the tensile strength of the matrix. Mechanistic and fracture based approaches which consider fiber-matrix interaction in high volume composites where the localization of crack is suppressed is very complex and is still developing.

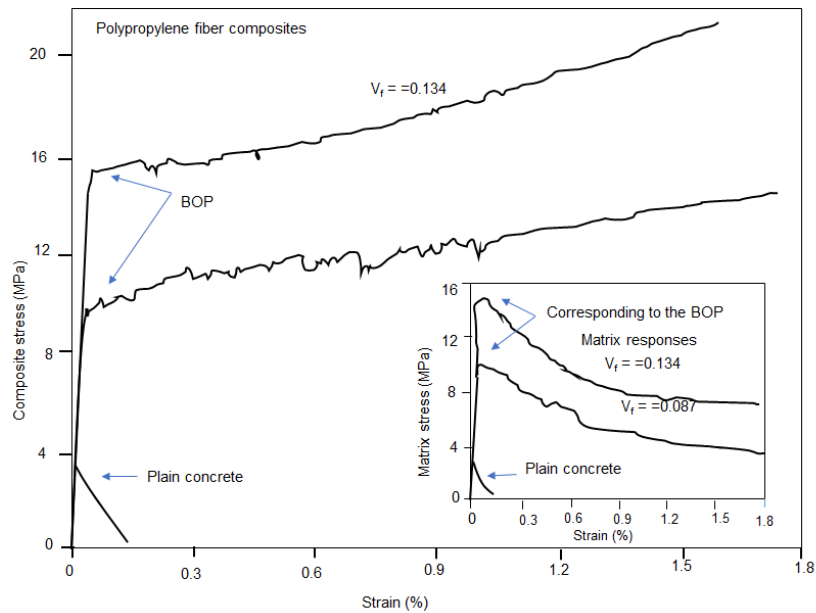


Fig 2.1 2: Strain hardening response of polypropylene fiber composites

The available literature on the behaviour of steel and synthetic fibers is reviewed

2.1.1 Steel Fibers

Steel fibers have a relatively high strength and modulus and are available in aspect ratios ranging from 20 to 100 and length ranging from 6.4mm to 75mm. The process of manufacture varies from cut sheets, cold drawn wires or hot melt extraction and are available in different cross-sections and shapes depending on the method of manufacture and use.

While steel fibers improve the strength of concrete under all load actions, their effectiveness in improving strength varies among compression, tension and flexure. There is an insignificant change in the ultimate compressive strength upon the addition of steel fibers; There is an increase of up to 15 percent for volume of fibers up to 1.5 percent by volume [12] [13]. There is a significant improvement in strength in tension with an increase of the order of 30 to 40 percent reported for the addition of 1.5 percent by volume of fibers in mortar or concrete [14]. Strength data [15] shows that the flexural strength of SFRC is about 50 to 70 percent more than that of the unreinforced concrete matrix in the normal third-point bending test [15, 16].

The ability of steel fibers to serve as reinforcement is determined by the resistance of the fibers to pullout from the matrix resulting from the breakdown of the fiber-matrix interfacial bond. Improvements in ductility depend on the on the type and volume percentage of fibers present [17, 18]. In conventionally mixed SFRC, high aspect ratio fibers are more effective in improving the post-peak performance because of their high resistance to pullout from the matrix. However, at high aspect ratio there is a potential for balling of the fibers during mixing [19]. Techniques such as enlarging or hooking of ends, roughening their surface texture, or crimping to produce a wavy rather than straight fiber profile allow for retaining high pullout resistance while reducing fiber aspect ratio. These types are more effective than equivalent

straight uniform fibers of the same length and diameter. Consequently, the amount of these fibers required to achieve a given level of improvement in strength and ductility is usually less than the amount of equivalent straight uniform fibers [19, 20].

The fiber pullout behaviour is influenced by the type of fiber as seen in the load response obtained from steel fiber reinforced concrete with 50 kg/m^3 fibers in Fig 2.1 3. For hooked end steel fiber, after first crack, there is drop but that drop is less than the other two fibers, deformed end fiber and corrugated fiber. For deformed end fiber and corrugated fiber, after first crack there is a continuous decrease in the load carrying capacity with increasing deformation. Hooked end fibers, which provide the highest pullout resistance from the matrix provide the highest load carrying capacity with increasing deformation after crack formation.

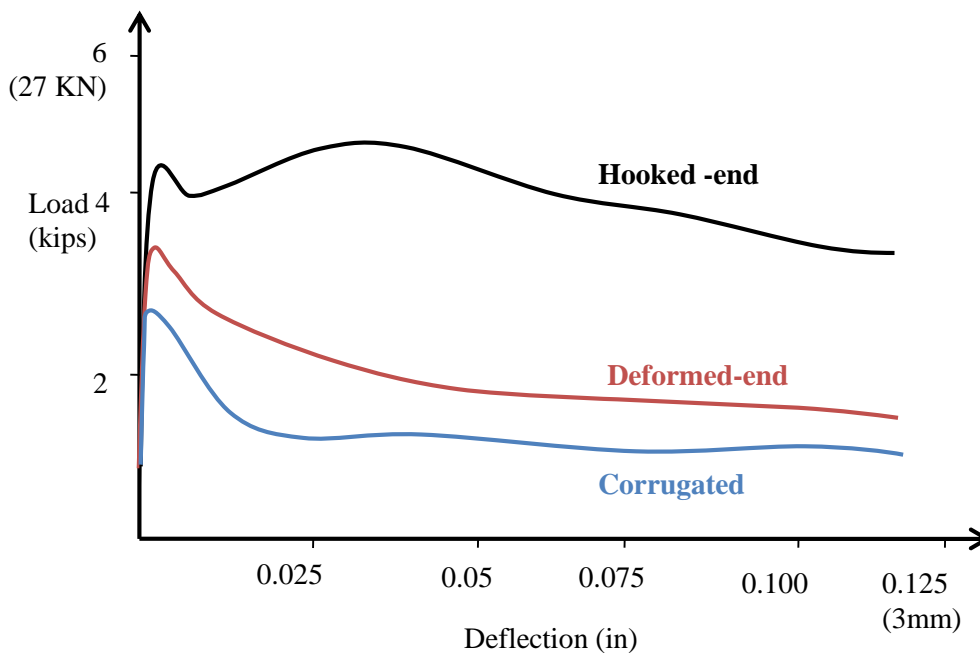


Fig 2.1 3: Effect of steel fiber shape on the load response in flexure

Improvements in post-crack ductility under tension result in significant improvements in flexural response. Ductile behaviour of the SFRC on the tension side of a beam alters the normally elastic distribution of stress and strain over the member depth. The altered stress distribution is essentially plastic in the tension zone and elastic in the compression zone, resulting in a shift of the neutral axis toward the compression zone [21].

2.1.2 Polypropylene Fibers

Polypropylene fibers are available in two different forms; Monofilaments and Fibrillated. Monofilament fibers are single strand of fibers having uniform cross-sectional. Fibrillated fibers are manufactured in the form of films or tapes that are slit in such a way that they have net like physical structure. Most commercial applications of polypropylene fibers have used low volume percentage (0.1 percent), monofilament or fibrillated fibers (in the case of polypropylene). Typical properties of monofilament and fibrillated polypropylene fibers is given in Table 2.2.

Table 2.2: Properties of various types of polypropylene fiber

Fiber type	Length	Diameter	Tensile strength	Modulus of elasticity	Specific Surface	Density
	(mm)	(mm)	(MPa)	(MPa)	(m²/kg)	(kg/cm³)
Mono filament	30-50	0.30-0.50	547-658	3.50-7.50	91	0.9
Micro filament	12-20	0.05-0.20	330-414	3.70-5.50	225	0.91
Fibrillated	19-40	0.20-0.30	500-750	5.00-10.00	58	0.95

These use of these fibers have been restricted to non-structural and non-primary load bearing members. At typical dosages usually employed in the construction industry there is a marginal improvement in the mechanical properties of concrete.

At dosages considered by the industry, of 1.2 kg/m³, PP fibers have been shown to influence the fracture behaviour; the influence of the fibres was especially felt in the tail of the P-d curve, showing a wider softening branch in the case of the FRC mixes, which corresponds to a more ductile behaviour of the concrete. The effect of the fibre is more remarkable in the case of the low strength concrete, where the stresses in the cohesive zone are lower, and the bridge effect of the fibre has a greater effect due to the higher level of deformation. It was shown that the fibres with the highest elongation and lowest strength (i.e. the most ductile fibres) presented the highest values of fracture energy. In the case of high strength concrete the higher level of the cohesive stresses mitigates the bridge effect of the fibres. In low- and normal-strength concrete the main mechanism of failure of the fibres was by pull-out while in high strength concrete it was due to fiber breakage [22].

2.1.3 Macro-synthetic Polypropylene fiber

Structural synthetic fibers are available in different geometries and shapes as shown in Fig 2.1.4. The energy absorption capacities from pullout tests on the different shape synthetic fiber obtained from pullout tests are shown in Fig 2.1.5. [23]. Test results indicate that the crimped-shape structural synthetic fibers exhibit the highest energy absorption capacity.

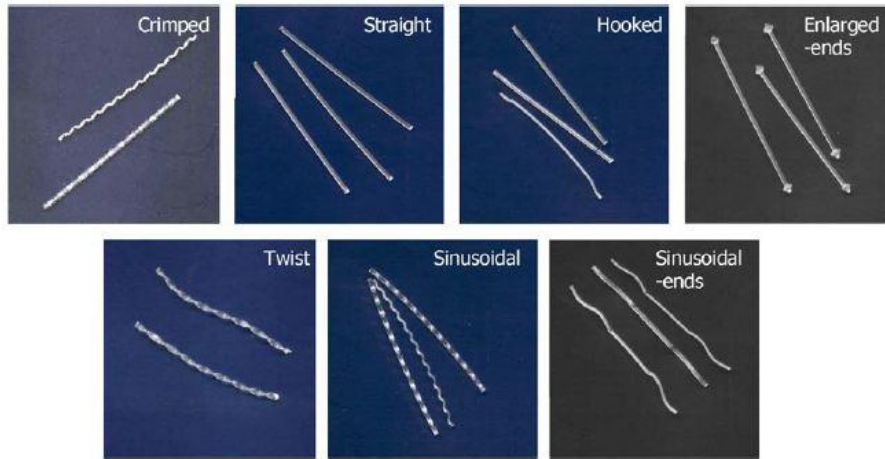


Fig 2.1.4 Various types of synthetic fibers tested in the present study

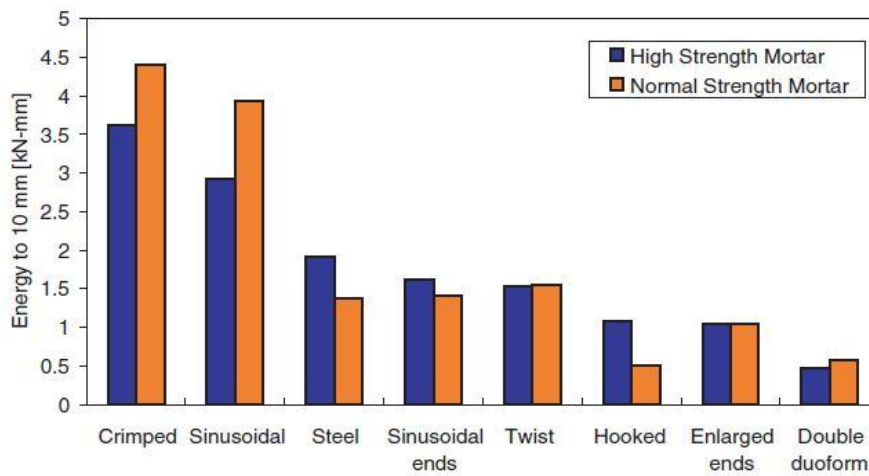


Fig 2.1.5 Comparison of absorbed energies from pullout tests for various fiber types.

The energy absorption capacity and thus the toughening effect of FRC is the result of fiber matrix interactions such as fiber pullout, fiber debonding and also due to fiber rupture. Shukla et al [24] in his investigation to understand the pullout behavior of polypropylene fibers found that the embedded length and interfacial bond affects the pullout of fiber from matrix.

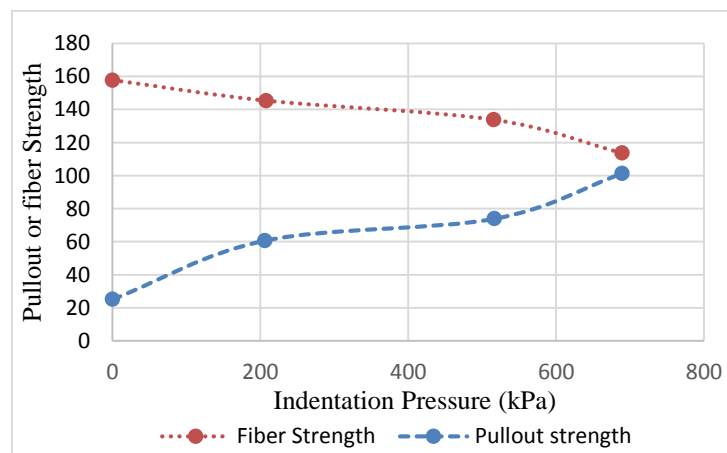


Fig 2.1.6 Pullout/ fiber strength with indentation pressure

A high embedded length and modified fiber for performance showed toughness enhancement. Shukla et al [24] also suggested a method to optimize fibers for performance after investigating the pullout of fibers with various degree of indentation as indentation will increase the bond with matrix compared to that of smooth fiber and the same is shown in Fig 2.1.6

A comparison of the load response in flexure between hooked end steel fibers and synthetic fibers is shown in Fig 2.1.7. Data obtained from [25] are plotted in the Fig 2.1.7. Steel fibers at dosages up to 50 kg/m^3 , show in a drop in load immediately after formation of the crack, followed by a gradual decrease in load carrying capacity. In case of synthetic fiber, at fiber dosage rate 4.6 kg/m^3 , there is sudden drop (that drop decrease in fiber dosage rate 5.3 kg/m^3), after first crack, there is continuously decreasing load and increasing the deflection (slowly fiber pull out start from the matrix).

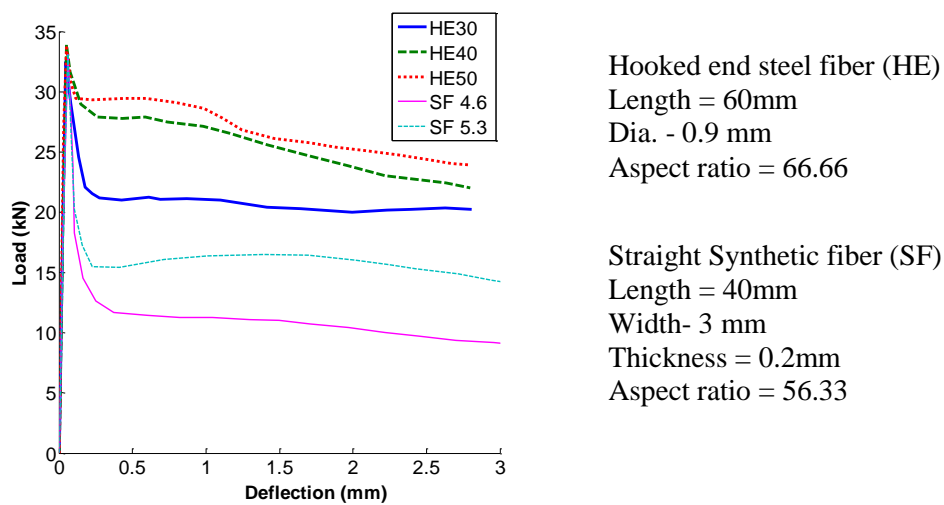


Fig 2.1.7 Load–deflection curves for Hooked end steel fibers and Synthetic fibers.

A comparative study on the mechanical behaviour and fracture properties and fracture behaviour of concrete containing steel fiber and micro-polypropylene fiber (19mm length) was published by Bencardino et al [26]. It was found that while steel fibers had an insignificant influence on the compressive strength of concrete, Polypropylene fibers reduced the compressive strength about 25% and 35% at 1% and 2% fiber volumes, respectively. This was attributed to the low modulus of elasticity of the polypropylene fibers and insufficient dispersion of the fibers in the mixture. The elastic modulus of steel fibers were also shown to influence the fracture properties and behaviour obtained using notched beams tested in three-point bending configuration. The equivalent flexural strength values of SFRC are much higher than the strength at the limit of proportionality, while for polypropylene fibers, the reverse is true. Steel fibers produced an increase in the peak load with increase in the steel fiber volume content when compared with ordinary concrete. The polypropylene fiber reinforced concrete specimens were able to retain peak load values similar to those recorded for the control specimens at 1% fiber volume content. However, at the 2% fiber volume content, these specimens showed a substantial decrease in peak flexural loads compared to those of the control. After reaching the peak load, all the PFRC specimens showed sudden drop in load, about 67% and 40% of the peak load for fiber volume contents of 1% and 2%, respectively. The residual loads after the load drop remained constant with increasing deflection, up to the

end of the test. Macro synthetic fibers were shown to be significantly less effective than the hooked end steel fibers in increasing the fracture energy. However, the low modulus polypropylene fibers were shown to give as much ductility as the steel fibers.

In their study involving a comparison of hooked end steel fibers and macro synthetic (MS) fibers (slightly coiled Polyolefin, hooked Polystyrene, flat polymeric mix), Buratti et al. (2010) [27] also showed that the residual strength for steel fibers (SF) are higher when compared to macro synthetic fibers from notched concrete beams tested in three-point configuration.

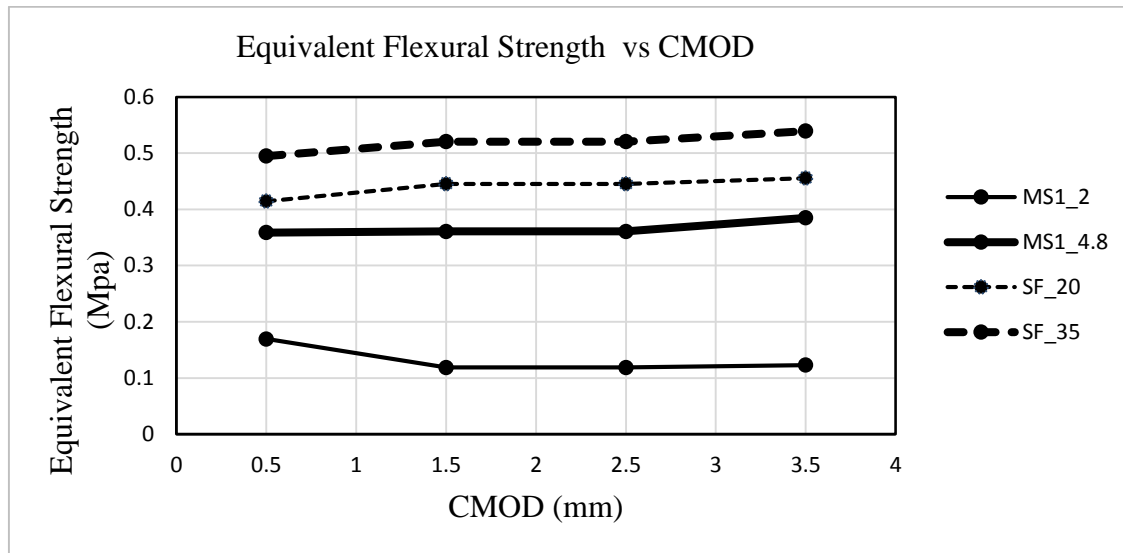


Fig 2.1.8 Equivalent Flexural Strength Ratio of steel and Synthetic fiber

At volume fractions in the range of 0.2-0.5%, the residual strength was found to increase with an increase in the fiber content. The addition of fibres, both steel and macro-synthetic, to the concrete increased its toughness from 5 to 10 times. The results of the experimental investigation revealed that considering the variability of results, the mean values of residual strengths at different CMOD opening normalized to its corresponding flexural strength as shown in Fig 2.1.8., indicate a significant improvement in the performance of the steel fibres when compared with synthetic fibres. If the characteristic residual strengths, which are obtained as the 5 percentile values are used, the benefit given by the steel fibres is reduced. A direct correlation between the statistical distribution of fibers in the crack plane and the residual strength values is also shown for the macro synthetic fibers.

In the study of post cracking inelastic behaviour of Synthetic FRC, Ji Kim et al [23] observed a similar response of an immediate load drop after peak and subsequent increased resistance attributed due to engagement of fibers as shown in Fig 2.1 9. In the same study on crimped structural synthetic fibers [23], it was also observed that higher volume fraction of 1.5 % has enhanced toughening effect than that of with 1.0 % volume of fibers but observed load drop is almost comparable exhibiting the delay in fibers getting engaged in resisting the loads.

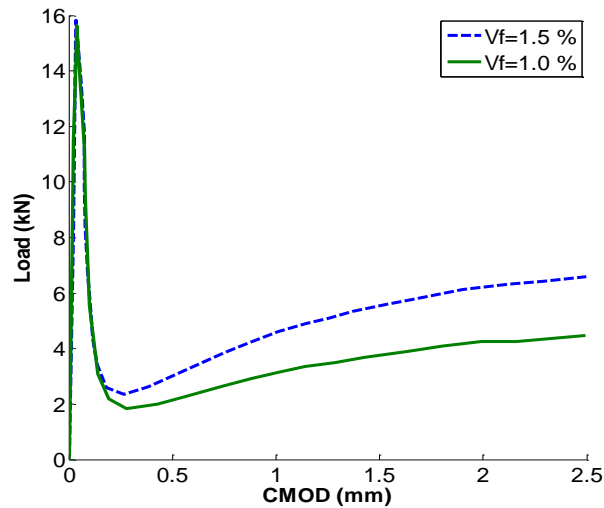


Fig 2.1 9 Load CMOD response of synthetic fiber with varying volume fraction

2.2 Cohesive behaviour

The main aim in development of adding fibers to concrete is to increase its fracture energy of concrete. Influence of fibers on increasing stiffness and strength are also observed at high volume fractions. The increased load carrying ability and energy dissipation is a result of local crack arrest and resistance to crack opening provided by fibers. In the fracture mechanical framework adopted for conventional concrete, the crack bridging effects are represented using a stress crack opening relationship, which is characterized in terms of area under the load deflection curve. A softening curve, which represents the relationship between the crack opening displacement and the decrease in stress after tensile strength is used for simulating tensile cracking in concrete. This approach, known as the cohesive crack model, was adopted from the early fictitious crack approach proposed by Hillerborg in 1976 [28]. The cohesive crack model has been extended for FRC as well.

Conceptually, a crack propagating in concrete is represented by a zone of diffuse micro cracking known as the fracture process zone, and a localized crack [29] as shown in Fig 2.2.1 and Fig 2.2.2. The localized crack can be divided into a part where aggregate interlock is present, and a "true" traction free crack. In the fictitious crack model (FCM), the process zone, localized crack with aggregate interlock and localized stress free crack are modelled by a single crack plane and only crack bridging forces normal to the crack plane are considered. The process zone, together with the part of the localized crack where aggregate interlock is present is referred to as the fictitious crack. The mechanical behaviour of the fictitious crack is characterized by the stress-crack opening relationship, $\sigma_w(w)$, where σ_w is the traction applied to the crack surface as a function of crack opening w . In the FCM approach, stress-singularities are disregarded. A fictitious crack is formed as soon as the largest principal stress reaches the tensile strength. The FCM approach was intended for use in combination with FEM but can also be implemented in numerical and analytical computations.

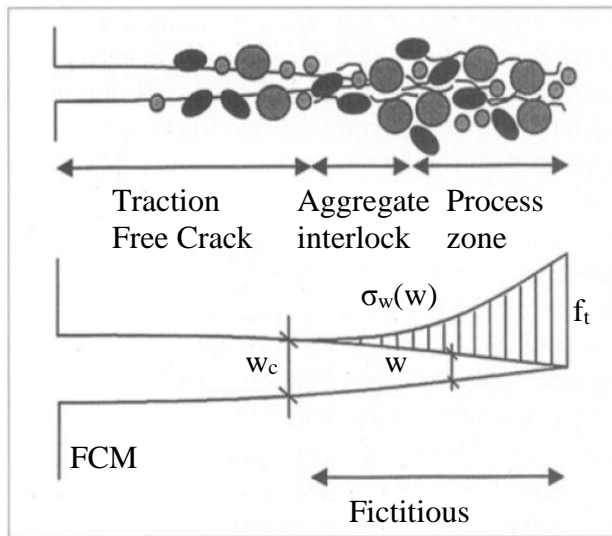


Fig 2.2.1 A crack in plain concrete and the essential features: zone with fiber bridging, the process zone and aggregate interlock together with the FCM.

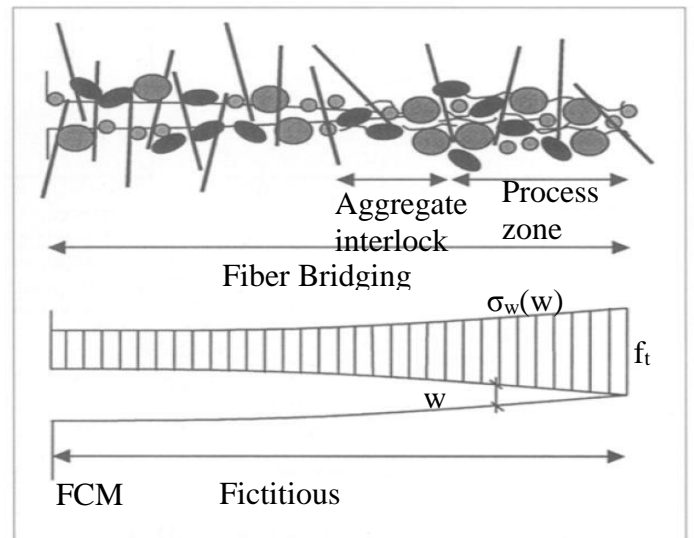


Fig 2.2.2 A crack in FRC and the essential features: zone with fibre bridging, the process zone and aggregate interlock together with the FCM.

The constitutive relation between increasing (localized) material separation w and the traction carried across the cracking material (e.g., in a uniaxial test) is called the stress-separation curve (or the σ_c-w curve). The basic assumption for the existence of the stress-separation curve is that the diffuse damage in a given material localizes into a narrow zone (or a plane on the continuum scale) due to stress concentration associated with material inhomogeneity or structural geometry (such as a notch). This stress singularity assumed in linear elastic fracture mechanics will be absorbed into the inelastic deformation (the process of decreasing traction with increasing opening) in the process zone. Furthermore, the material ahead of the total crack becomes part of the process zone as soon as the (ultimate) tensile strength f_t is reached. Inside the process zone, the stress decays from f_t to zero at the tip of the traction free crack, the rate of decay being consistent with the stress-separation behavior. Thus $\sigma_c = \sigma_c(w)$ for a given material.

Available σ_c-w relationships can be found in [30, 31, 32, 33, 34] for concrete and mortar and for some FRC. Two stress-separation constitutive models, shown in Fig 2.2.3, are used by the analyses. Model 1 is a linear straight line descending from the tensile strength f_t , at zero material separation to zero stress at the critical separation w_c . This linear decay model has been used by Hillerborg [35] to describe the crack formation in plain concrete. Model 2 has a rapid drop in traction transfer σ_c with separation w , followed by a long tail (large w_c). This model provides a better representation of the stress-separation behaviour in concrete and has also been used by Ingraffea and Gerstle [36] to model FRC.

A bi-linear approximation (Shown in Fig 2.2.4) for the stress-separation behaviour of concrete has been proposed and implemented in several finite element and numerical analysis procedures. In the bilinear approximation, there is an initial steep drop followed by a more gradual decrease until complete separation indicated by a critical value of crack separation.

The initial steep part is attributed to localization and the tail part of the response is due to bridging stresses provided by aggregate.

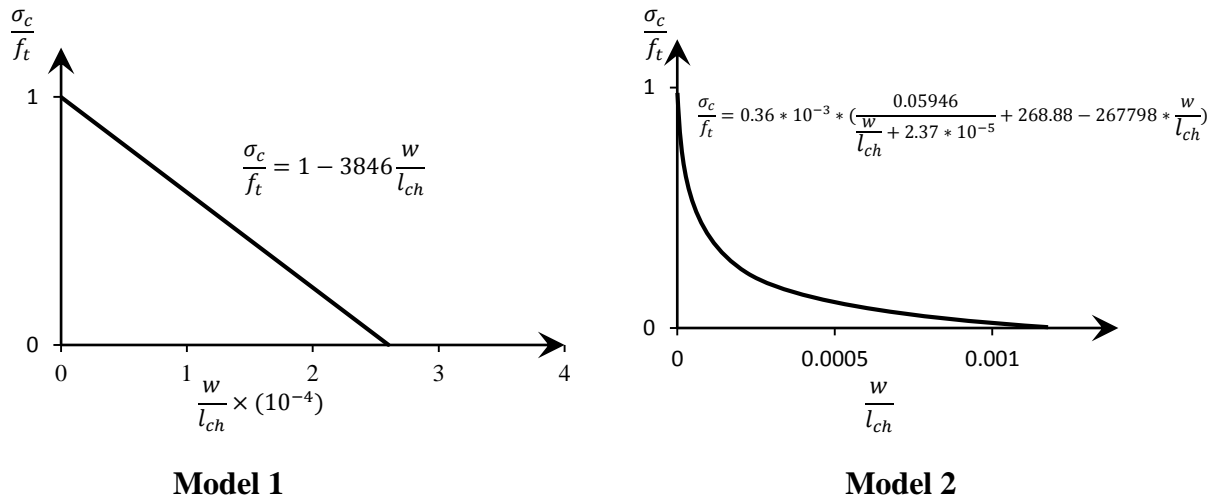


Fig 2.2.3 Stress Crack opening Relationships

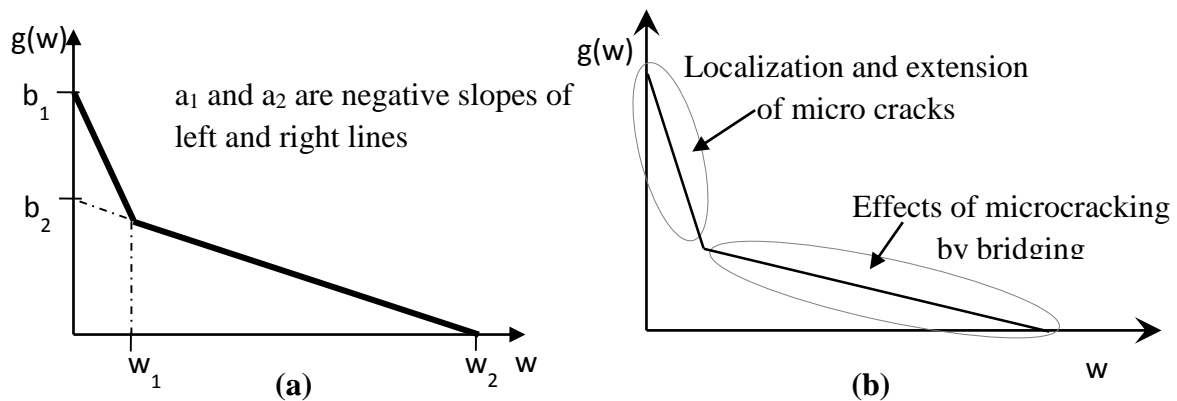


Fig 2.2.4 Bi-linear stress crack opening relationship

Ostergaard et al [37] also assumed bilinear crack stress crack opening relationship to predict load CMOD relationship under wedge splitting tests for early age concrete and he concluded that a_1 has higher values for very early age that is at 10 hours indicating more brittle nature at early age may be due to poor crosslinking between hydration products but for 2-28 days also a_1 is decreasing which is a bit surprising as conventional concrete is brittle after maturity, so it requires further study and interpretation. Assumption of stress crack opening relationship, development of moment curvature relationship and load deflection response was thoroughly discussed in chapter 5.

A tetra linear stress crack opening relationship was obtained for concrete by inverse analysis from experimental response and was found to provide a better representation of the softening behaviour with increasing crack opening displacement [38]. The effect of specimen size on different branches of stress crack opening revealed that the first steep branch of crack opening is not affected by size and geometry of specimen which corresponds to localisation

and extension of micro cracks as shown in Fig 2.2.4(b) but the tail part of crack opening relationship where stress transfer is through bridging is significantly affected by specimen size. The tail in the stress-separation response is shown to increase with increasing specimen size

Though similar in many aspects, the FCM approach for crack initiation, propagation and opening in SFRC differs significantly from the FCM approach to concrete fracture. Since the fibre bridging is closely related to the fibres debonding and pulling out of fibers, the shape of stress crack opening curve gets altered as shown in Fig 2.2.5. The fictitious crack in FRC materials represents the process zone, aggregate interlock as well as the influence of fibre bridging [29]. The contribution of fibers to the total resistance can be significant in the stress-separation curve.

The stress-separation curve must reflect the energy dissipation connected with pull-out of aggregates and or fibers, microcrack branching, tip blunting by voids, and all other possible energy absorption mechanisms. In fact, the area under the stress-separation curve provides a measure of the fracture toughness or the critical energy release rate. G_c is given by the area under the stress-separation curve

$$G_c = \int_0^{w_c} \sigma_c(w) dw$$

It may be expected that fiber types, lengths, cross-sectional geometry, surface treatment, volume fractions, etc., all contribute to affect the stress-separation curve. In general, the bridging action of the fibers in FRC provides a long tail in the stress-separation curve.

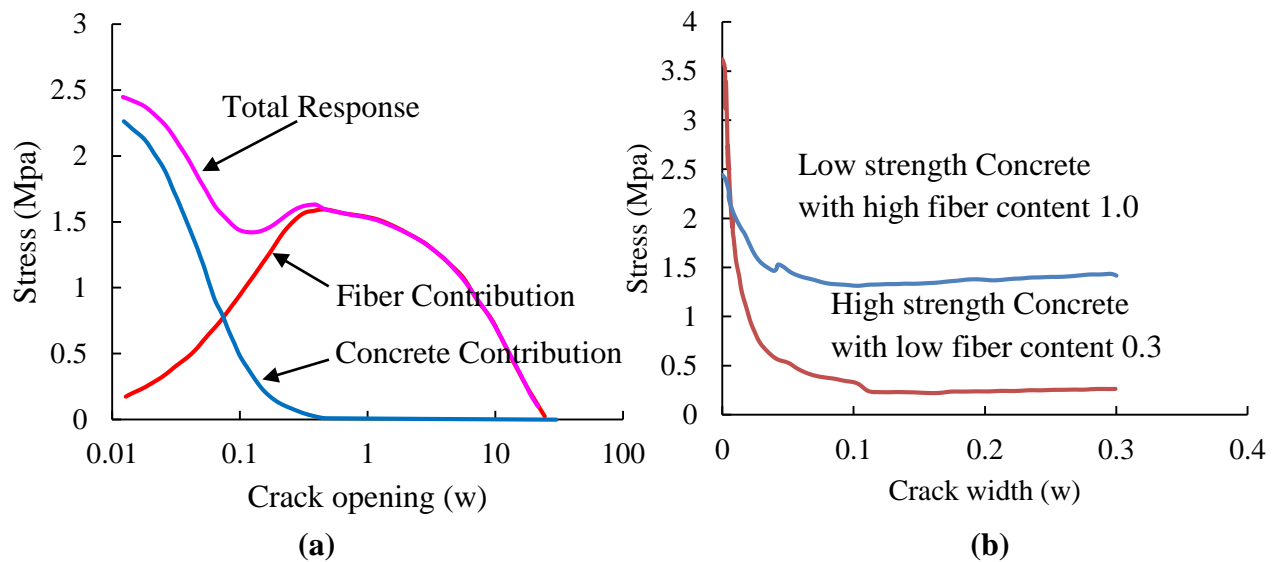


Fig 2.2.5 Typical stress-crack opening relationships

The shape of the stress-crack opening relationship depends heavily upon the type and amount of fibre used. The relationship can be divided into a concrete contribution and a fibre contribution. The concrete contribution is the softening stress-crack opening relationship for the unreinforced concrete, while the fibre contribution consists of a steeply ascending part followed by a slowly descending or softening part. The first part of the resulting relationship - up to crack openings of about 0.1-0.2 mm-is a result of the competing concrete and fibre

contribution, while the relationship for larger crack openings is due mainly to the fibre contribution. The resulting total response consists of first a descending part, then a slowly ascending and finally a descending or softening part [29], see Fig 2.2.5.

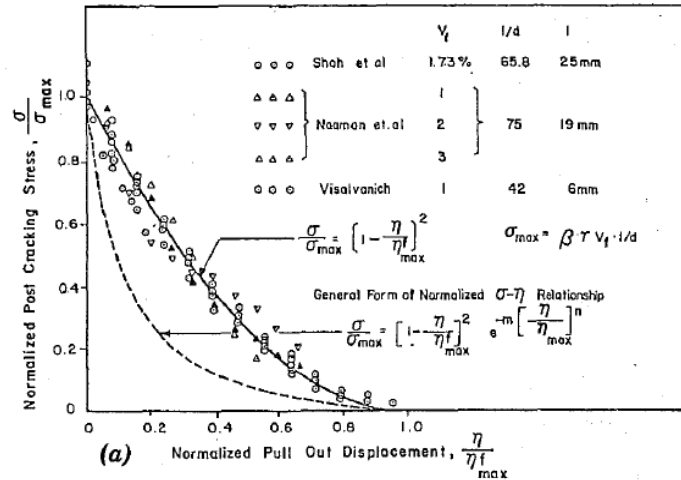


Fig 2.2.6 Stress Crack opening Relationships for Steel FRC

Fig 2.2.6 shows several experimental σ_c-w curves for steel FRC [39] and shows some typical σ_c-w curves for concrete and FRC [35]. The overall mechanical behavior of a concrete or FRC structure could be strongly influenced by the stress-separation constitutive relation.

In order to predict the flexural load response of FRC a numerical approach based on analytical model for a cracked element known as the cracked hinge model was proposed by Olesen (2001) [40]. The crack growth in flexure is modelled using the fictitious crack approach with a bilinear stress crack separation law. The basic idea of this model is to divide the portion of the beam close to the propagating crack in a series horizontal strips, attached at the ends to two rigid boundaries which can translate and rotate so that it is amenable to incorporate with an uncracked beam modelled according to Euler Bernoulli theory. Constitutive behaviour of spring layer is given by

$$\sigma = \begin{cases} E\varepsilon & \text{Precrack State } (w = 0) \\ \sigma_w(w) = g(w) * f_t & \text{cracked State } (w > 0) \end{cases}$$

where, $g(w)$ is a function in terms of crack opening w , normalized such that $g(0)=1$. The cohesive stress-crack opening relationship for concrete reinforced with macrosynthetic fibers was obtained by inversion procedure applied to load response prediction given by the cracked hinge cracked model by Savoia et al [2011] [27].

Earlier in 2006, J C Kim et al [23] adopted an iterative procedure to determine neutral axis by sectional force equilibrium considering exponential softening curve of a single fiber and fiber volume effect by multiplying with number of fiber and their orientation across the section.

JF Olesen et al 2005 [41], assumed poly linear crack opening relationship in their crack hinged model to accurately predict the later hardening effect in load deflection relationship in

their wedge splitting and three point bending tests using finite element tool TNO-DIANA and here the softening parameters are changed manually for each iteration till the result is converged. In their inverse analysis a stepped analysis strategy was adopted for the reason that the earlier part of load response is highly sensitive to tensile strength and crack opening relationship. Single step analysis is often ill posed and is not possible to converge a good solution over the entire load displacement curve.

In predicting the load deflection relationship for hooked end steel fibers Matthys et al [42] adopted a trilinear stress-crack opening constitutive law and iteratively solved for force equilibrium by transforming crack widths into equivalent strains by assuming fictitious length and cross verified results with analytical model based on single fiber pull-out and obtained a reasonably closed match. Barros et al [43] in his study to theoretically correlate experimental data on steel fibers, they performed an inverse analysis numerically by using stress strain relationship [29] and stress crack opening constitutive relationship and derived a statistical relation between strain and crack opening.

2.3 Standard Test Methods

The influence of fibers on overall improvements in ductility and toughness are often interpreted in terms of improvements to fracture behaviour and crack propagation. Quantitative measures which allow for comparison between fibers and assess improvements involve standard test methods and data reduction procedure. The fracture behaviour of fiber reinforced concrete is also investigated using the test configurations and specimens of dimensions specified in standardized test procedures. A review of different standard test is presented first.

Standardized test methods for quantifying improvements in material behaviour and obtaining specific material properties have been developed. In these tests material parameters which quantify ductility and toughness of the material are obtained from measured load response. The quantities derived from these tests allow for comparison of material behaviour. Standard test procedures for evaluating the response of FRC are available in ASTM 1609, UNI 11039-2, ASTM 1018, EN 14651 and JSCE SF 24. Additionally, researchers have proposed methods for obtaining fracture or material parameters from the measured test response from the standardized test procedures. The test procedures and the different data reduction procedures are reviewed in this section

2.3.1 ASTM 1609 test procedure

In ASTM C1609/C1609M-10 a standardized test procedure is available to establish the flexural toughness, the flexural strength and the residual strength factors of the fiber reinforced concrete using beam specimens. The loading and support system capable of applying third point loading the specimen without eccentricity or torque in accordance with ASTM C78-02 is shown in Fig 2.3.1. ASTM test is performed measuring the applied load and the beam net deflection (i.e. the absolute mid-span deflection minus the support deflection) at a constant

deflection rate. The beam midpoint deflection between the tension face of the beam is measured in relation to the neutral axis of the beam at its support.

First peak deflection, toughness and Equivalent flexural strength are derived from the measured response. The standard load-displacement behaviours of fiber reinforced concrete beams are shown in Fig 2.3.2. The peak load is determined as that value of load corresponding to the point on the load-deflection curve that corresponds to the greatest value of load obtained prior to reaching the end-point deflection. The first-peak load (P_1) is defined as that value of load corresponding to the first point on the load-deflection curve where the slope is zero, that is, the load is a local maximum value. In specimens, which exhibit an increase in load after the load drop produced by cracking, the first peak load is the distinctive point in the load response associated with load drop as shown in Fig 2.3.2.

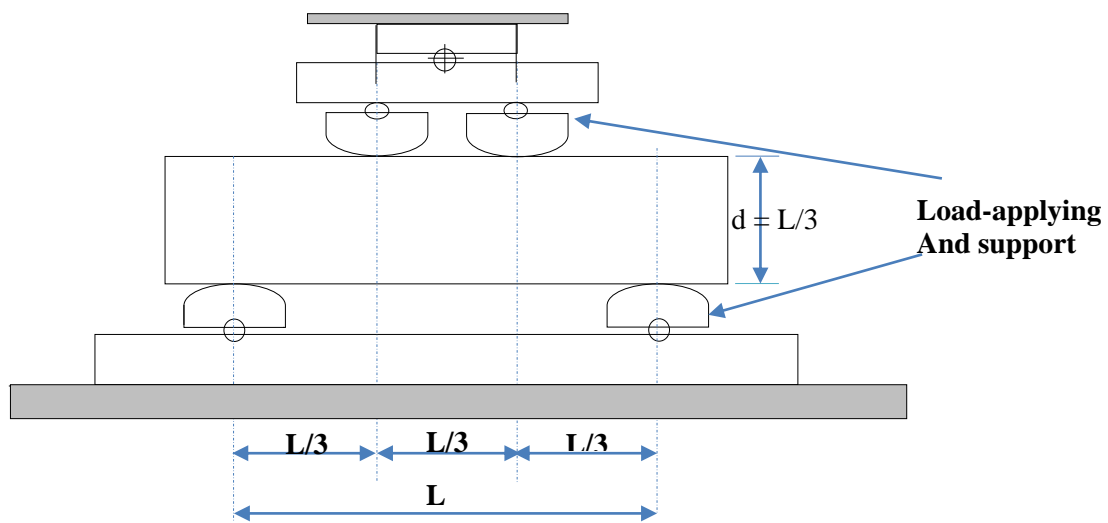


Fig 2.3.1 Diagrammatic View of a Suitable Apparatus for Flexure Test of Concrete by Third-Point Loading Method

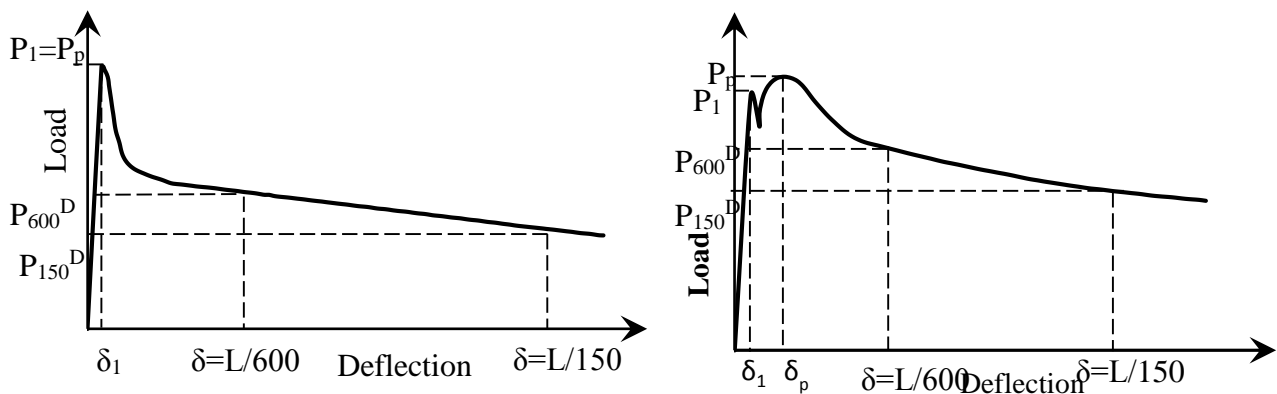


Fig 2.3.2 Example of Parameter Calculations

Strength corresponding to each peak load, f_P is determined following formula for modulus of rupture

$$f = \frac{PL}{bd^2}$$

First-peak deflection for third-point loading is estimated assuming linear-elastic behaviour up to first peak from the equation

$$\delta_1 = \frac{23P_1L^3}{1296EI} \left[1 + \frac{216d^2(1 + \mu)}{115L^2} \right]$$

The residual strengths, f_{600}^D and f_{150}^D are determined from the residual load values, P_{600}^D and P_{150}^D corresponding to net deflection values of 1/600 and 1/150 of the span length.

Toughness T_{150}^D is determined as the total area under the load-deflection curve up to a net deflection of 1/150 of the span length. The equivalent flexural strength ratio, $R_{T,150}^D$ is determined using the first-peak strength determined and the toughness determined. Record the number rounded to the nearest 0.5 % as equivalent flexural strength ratio, as appropriate for the specimen depth.

$$R_{T,150}^D = \frac{150T_{150}^D}{f_1bd^2} 100\%$$

2.3.2 ASTM 1018 test procedure

In ASTM C1018, toughness indices are taken as the area under the load-deflection curve up to certain specified deflection to area under the load-deflection curve up to the first crack as shown in Fig 2.3.3. Three level of deflection 3δ , 5.5δ and 10.5δ . Deflection value greater than 10.5δ can also be chosen for composite that can carry considerable loads at large deflection. The three suggested indices called I_5 , I_{10} and I_{20} are defined by following equations.

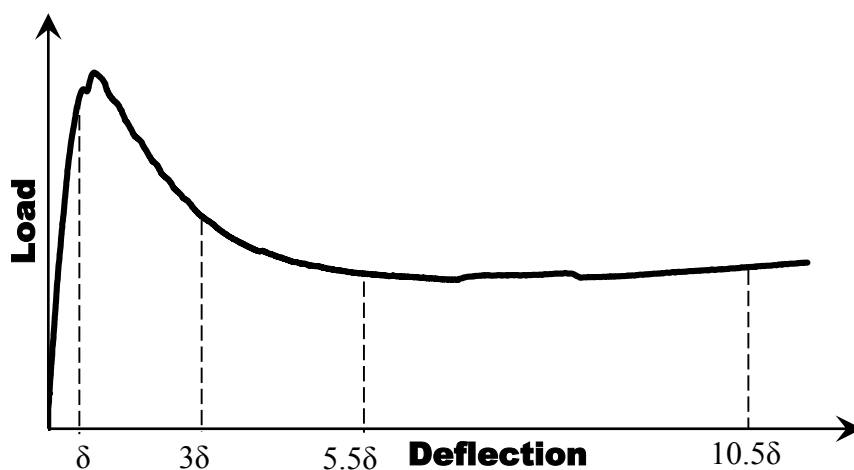


Fig 2.3.3 Important Characteristics of the Load-Deflection Curve

$$I_5 = \frac{\text{Area under the load – deflection curve up to } 3\delta}{\text{Area under the load – deflection curve up to } \delta}$$

$$I_{10} = \frac{\text{Area under the load – deflection curve up to } 5.5\delta}{\text{Area under the load – deflection curve up to } \delta}$$

$$I_{20} = \frac{\text{Area under the load – deflection curve up to } 10.5\delta}{\text{Area under the load – deflection curve up to } \delta}$$

The deflection values of 3δ , 5.5δ and 10.5δ are chosen using elastic perfectly plastic behaviour as the datum as shown in Fig 2.3.4. Residual loads at specified deflections, the corresponding residual strengths and determination of specimen toughness based on the area under the load-deflection curve up to a prescribed deflection and the corresponding equivalent flexural strength ratio are also obtained.

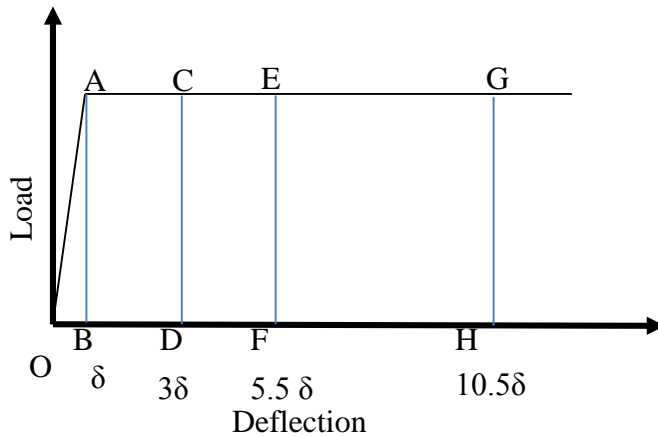


Fig 2.3.4 Definition of Toughness Indices for Elastic-Plastic Material Behaviour

$$I_5 = \frac{OACD}{OAB} \quad I_{10} = \frac{OAEF}{OAB} \quad I_{20} = \frac{OAGH}{OAB}$$

2.3.3 JSCE SF24

Ductility is commonly measured using the Japanese standard test method JSCE-SF4, which used beams in a third-point loading arrangements. The JSCE SF 24 provides a measure of flexural toughness from the measured load-deflection response as shown in Fig 2.3.5. The value of toughness, T_{JSCE} is determined as the area under the load-deflection curve up to a deflection equal to $\text{span}/150$. Toughness factor, F_{JSCE} is derived from the value of toughness. F_{JSCE} has the unit of stress such that its value indicates, in a way, the post-matrix cracking residual strength of the material when loaded to a deflection of $\text{span}/150$. The chosen deflection of $\text{span}/150$ for its calculation is purely arbitrary and is not based on serviceability considerations.

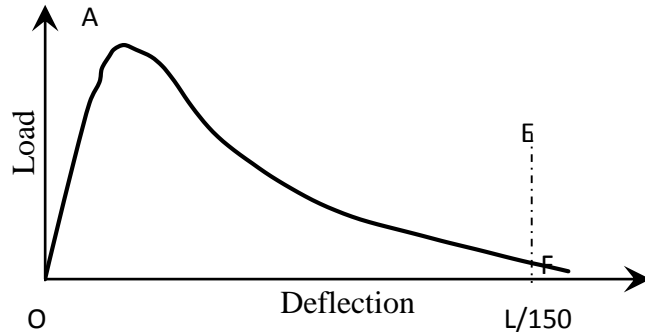


Fig 2.3.5 Definitions of JSCE Toughness and Toughness Factor

Toughness

$$T_{JSCE} = AREA_{OAEFO}$$

Toughness factor

$$F_{JSCE} = \frac{T_{JSCE} L}{BH^2 w_{tb}}$$

where, F_{JSCE} is Toughness factor or Equivalent flexural strength and w_{tb} is averaged over the prescribed deflection.

The equivalent flexural strength as defined by the JSCE-SF4 for a deflection of 3 mm, the $R_{e,3}$ value, a measure of the ductility, is the average load applied as the beam defects to 3 mm expressed as a ratio of the load to first crack. This measure is also known as the equivalent flexural strength as denoted as $f_{e,3}$ has been calculated as

$$f_{e,3} = \frac{P_{mean,150} \times l}{bd^2}$$

where $P_{mean,150}$ is the area under the load-deflection curve divided by the limit deflection of 3 mm and l , b and d are the span, width and depth of the prism, respectively (i.e. 450 mm, 150 mm and 150 mm, respectively).

2.3.4 RILEM TC 162-Test Procedure

Centre point bend tests are performed on notched specimens with a nominal size (width and depth) of 150 mm and a minimum length of 550 mm. Net deflection at mid-span excluding extraneous deformations is increased at a constant rate of 0.2 mm/min.

This test method is used to determine the limit of proportionality, equivalent flexural tensile strength, residual flexural strength which identify the material behaviour at selected deflection or CMOD.

Limit of proportionality

$$f_{ct,fl} = \frac{3F_L L}{2bh_{sp}^2}$$

where,

$f_{ct,fl}$ is the LOP (N/mm²)

F_L is the load corresponding to LOP (N)

L is span of specimen (mm)

b is the width of specimen (mm)

h_{sp} is the distance between the tip of notch and top of the specimen (mm)

Residual flexural Tensile Strength

$$f_{R,i} = \frac{3F_i L}{2bh_{sp}^2}$$

Where,

$f_{R,i}$ is residual flexural Tensile Strength corresponding with $CMOD = CMOD_j$ or $\delta = \delta_i$ (i= 1, 2, 3, 4) (N) and F_i is the load corresponding to with $CMOD = CMOD_j$ or $\delta = \delta_i$ (i = 1,2,3,4)

2.3.5 UNI 11039-2 Test Procedure

UNI 11039-2 bending test is a four-point loading test on a prismatic beam. UNI test specifically prescribes the specimen absolute dimensions. The UNI [44] test employs a notched beam with a specimen which is 150 mm deep, 150 mm wide and the span length is 450 mm. It is sawed at mid-span with a depth equal to 0.3 times the overall specimen depth (0.3d). The test is performed measuring the load P and the Crack Tip Opening Displacement (CTOD), at a rate of increase of the Crack Mouth Opening Displacement (CMOD), equal to 0.05 ± 0.01 mm/min. A schematic diagram of the UNI test setup is shown in Fig 2.3.6.

The first-crack load which required subtracting the contribution due to matrix cracking is obtained by determining the value of CTOD corresponding to the peak load value obtained by performing four-point bending tests on plain concrete beams is determined ($CTOD_0$). The value of $CTOD_0$ can be assumed equal to 25 μ m.

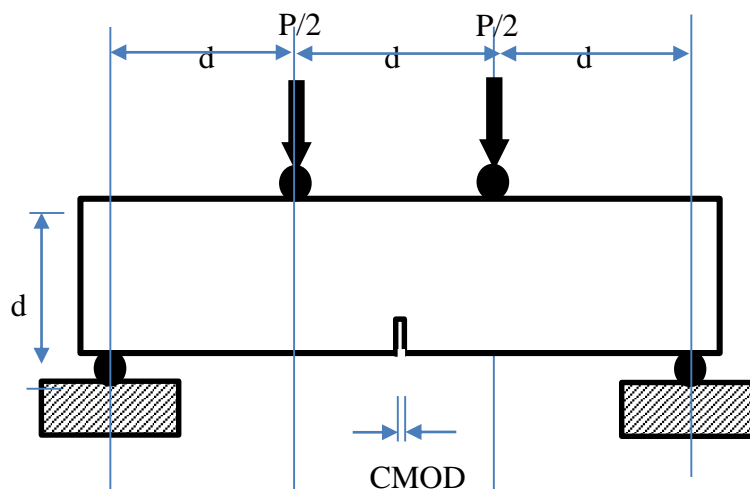


Fig 2.3.6 Schematic diagram of the UNI 11309 four-point bending test setup

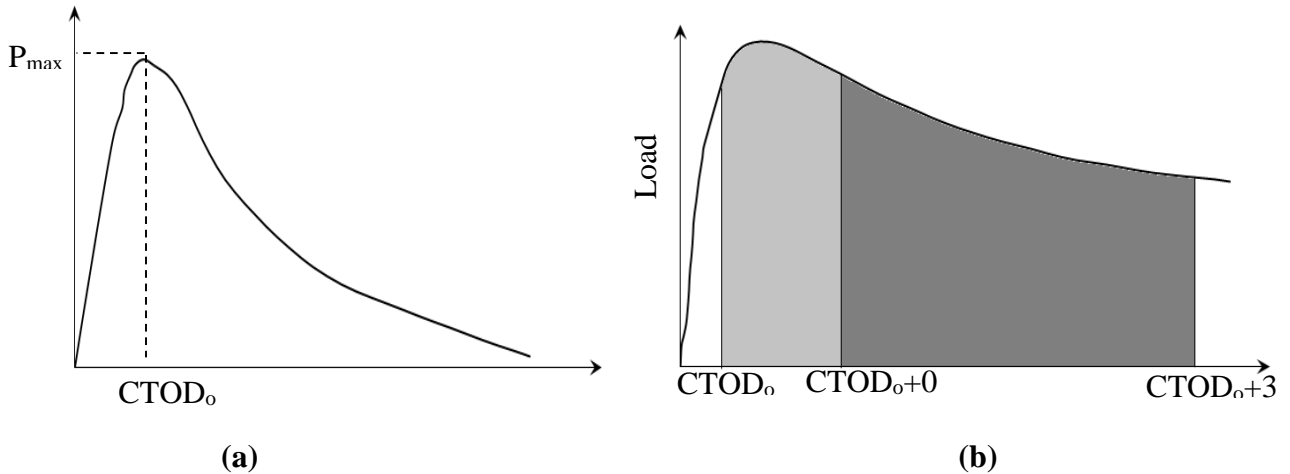


Fig 2.3.7(a) Basic concrete load-CTOD, (b) Load-CTOD

The first-crack flexural strength is determined, according to UNI 11039, as follows:

$$f_{lf} = \frac{P_{lf}L}{b(h - a_0)^2}$$

where

L (mm) = span between supports;

b (mm) = specimen width (equal d);

h (mm) = specimen depth (equal d);

a₀ (mm) = notch depth;

P_{lf} (N) is the load value corresponding to CTOD₀ for the FRC specimen.

The **first** and **second Material's ductility** indexes D₀ and D₁, according to UNI 1039 [11] by means of the equivalent flexural strengths $f_{eq(0-0.6)}$ and $f_{eq(0.6-3)}$ (MPa), which denote SFRC ductility in a defined range of crack mean opening displacement. Ductility indexes D₀ and D₁ were derived by means of the following equations:

$$D_0 = \frac{f_{eq(0-0.6)}}{f_{lf}} \qquad D_1 = \frac{f_{eq(0.6-3)}}{f_{eq(0-0.6)}}$$

where $f_{eq(0-0.6)}$ is the equivalent strength (MPa) is calculated when the mean crack opening value is included between 0 and 0.6 mm, $f_{eq(0.6-3)}$ is the equivalent strength (MPa) calculated when the mean crack opening value is included between (0.6 and 3) mm, derived from the following relationships:

$$f_{eq(0-0.6)} = \frac{l}{b(h-a_1)} \cdot \frac{U_1}{0.6} \qquad f_{eq(0.6-3)} = \frac{l}{b(h-a_1)} \cdot \frac{U_2}{2.4}$$

where U_2 and U_3 (10^{-3} J) are the area under load - $CTOD_m$ curve for $CTOD_{net}$ intervals equal to 0-0.6 mm and 0.6-3 mm respectively. Such area are approximately proportional to the energy dissipated in the mean crack opening intervals considered.

2.3.6 EN 14651 Test Procedure

Centre point bend tests are performed on notched specimens with a nominal size (width and depth) of 150 mm and a length L so that $550 \text{ mm} < L < 700 \text{ mm}$. Test is performed by increasing the $CMOD$ at a constant rate of 0.05 mm/min up to a $CMOD$ value of 0.1 mm and at a rate of 0.2 mm/min up to a $CMOD$ value of 4 mm.

This European standard specifies a method of measuring a flexural tensile strength of metallic fibered concrete on moulded test specimen. The methods provided for the determination of the limit of proportionality (LOP) and of a set residual flexural tensile strength values. Arrangement as per EN14651 is shown in Fig 2.3.8

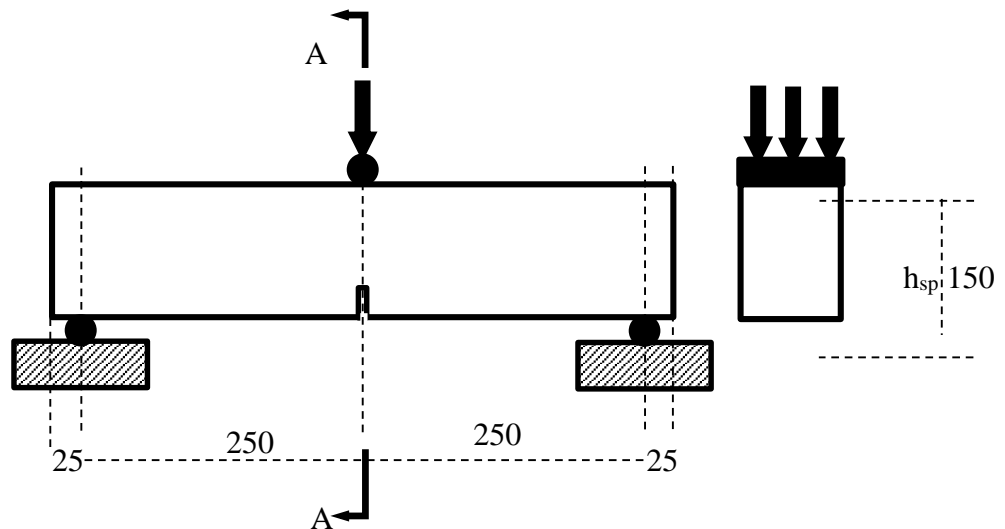


Fig 2.3.8 Typical arrangement of measuring CMOD

Limit of proportionality

$$f_{ct,fl} = \frac{3F_L L}{2bh_{sp}^2}$$

Where,

$f_{ct,fl}$ is the LOP (N/mm^2)

F_L is the load corresponding to LOP (N)

L is span of specimen (mm)

b is the width of specimen (mm)

h_{sp} is the distance between the tip of notch and top of the specimen (mm)

Residual flexural Tensile Strength

$$f_{R,i} = \frac{3F_iL}{2bh_{sp}^2}$$

Where,

$f_{R,i}$ is Residual flexural Tensile Strength corresponding with $CMOD = CMOD_j$ or $\delta = \delta$ ($i= 1.5, 2.5, 3.5, 4.5$ mm) (N) where $CMOD_j$ corresponds to $CMOD$ at j mm and F_i is the load corresponding to with $CMOD_j$ as shown in Fig 2.3.9.

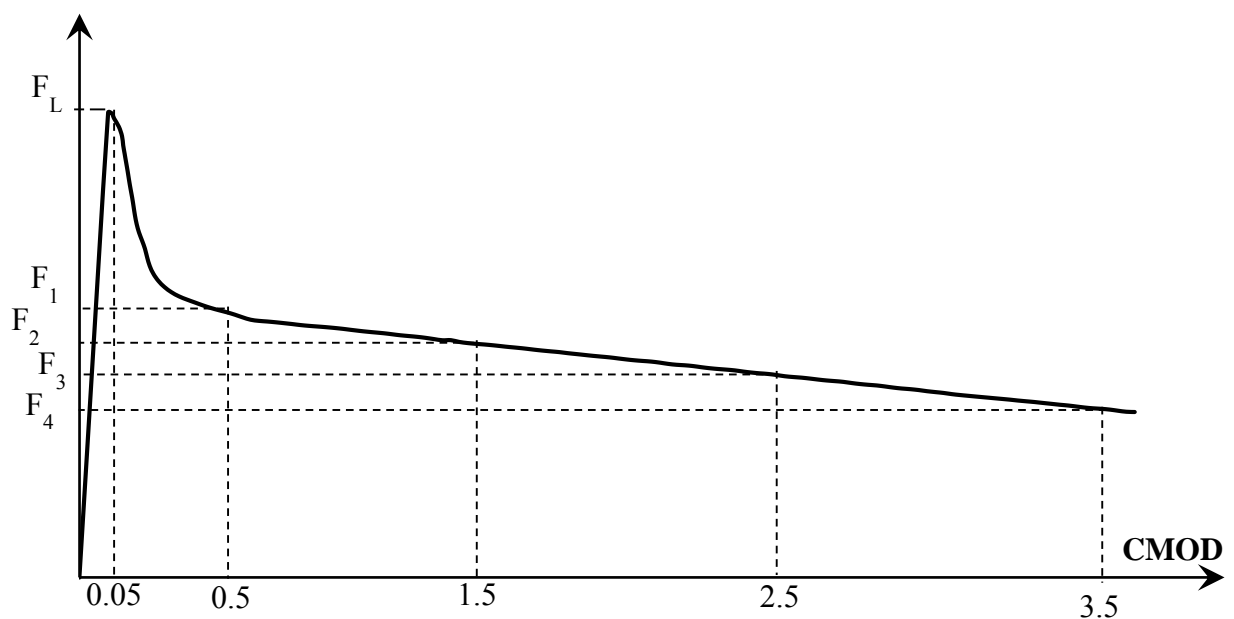


Fig 2.3.9 Load-CMOD and F_j ($j=1.5, 2.5, 3.5, 4.5$)

Toughness index is used to measure the energy absorbed in deflecting a beam at specified amount, being the area under a load–deflection curve in three-point bending. A measure of toughness index from the results of the EN 14651 test has been proposed as the ratio of the area under the force-CMOD curve up to CMOD of 4 mm for the FRC specimen over that for the plain-concrete specimen

Chapter 3

Materials and Methods

3.1 Introduction

This section presents the details of materials and experimental methods used in the study. The types of specimens, mix proportions and test methods employed are presented.

3.1.1 Cement

In the present investigation, commercially available 53 Grade ordinary Portland cement was supplied by ACC Cement with Specific Gravity of 3.1 and Fineness modulus of 325 m²/kg was used for all concrete mixtures.

3.1.2 Fly Ash

Fly ash conforming to the requirements of IS 3812 and IS 1727 (1967) supplied by NTPC with Specific gravity of 2.5 and fineness modulus of 320 m²/kg was used as supplementary cementitious material in concrete mixtures.

3.1.3 Aggregates

Crushed sand with a specific gravity of 2.67 and fineness modulus of 2.83 was used as fine aggregate and crushed granite of specific gravity of 2.63 was used as coarse aggregate. Two different classes of coarse aggregate fractions were used: 10-4.75 mm and 20-10 mm.

3.1.4 Synthetic Fibers

FibreTuff™ Monofilament structural polypropylene fibers of 60 mm length manufactured by Bajaj Reinforcements were used in this study. The fibers are made of a modified polyolefin and have a modulus of elasticity between 6 GPa to 10 GPa and tensile strength between 550 and 640MPa. The fibers are continually embossed surface anchorage mechanism to enhance bond. A photograph of the fibers used in this study is shown Fig 3.1.1.



Fig 3.1.1 FibreTuff™ Monofilament structural polypropylene fiber

Nylon fibers with 50 mm length and 22.9 μm diameter supplied by Brug Contec will be used. Fibers have tensile strength around 0.97 GPa and Elastic modulus about 5.2 GPa.

3.1.5 Admixture

Super plasticizer (Glenium) was used to increase the workability of freshly prepared fiber reinforced concrete.

3.2 Experimental program and Mix Proportions

Concrete mix design for the mix design procedure given in IS: 10262 was followed with minor modification for M35 grade. For a target mean strength of 43 MPa, two different water/cement ratios equal to 0.48 was considered (from Fig 2, curve E IS 10262-1982 for 53G). Taking into considerations, the minimum requirements for cement content in kg/m^3 of concrete for M35 as per IS 456-2000 as $300 \text{ kg}/\text{m}^3$, cementitious content was fixed at $340 \text{ kg}/\text{m}^3$. Using this, the water content was determined. In the concrete mixture fine aggregate were taken as 45% of the total aggregate volume fraction. The weights of fine and coarse aggregate were then calculated considering the specific gravities of coarse and fine aggregate.

The Concrete mixtures were produced at a constant water/Cement ratio of 0.48 and one control mixture and three different mixtures with different dosage of fiber were prepared. The control mixture contained no fiber. Concrete mixtures labelled PF3, PF4 and PF6 were produced with different dosage of polypropylene fiber $3 \text{ kg}/\text{m}^3$, $4 \text{ kg}/\text{m}^3$ and $6 \text{ kg}/\text{m}^3$ by volume. The final batch weights of the different mixes for one cubic meter of concrete are presented in Table 3.1.

Table 3.1 Summary of weight proportion of the various mixes

Materials(kg/m³)	C1	PF4	PF6	PF8	NF4	NF6	NF8
Polypropylene fiber	-	4	6	8	4	6	8
OPC 53 grade cement	200	200	200	200	200	200	200
Fly ash(pozzocrete 60)	140	140	140	140	140	140	140
Water/Cement Ratio	0.48	0.48	0.48	0.48	0.48	0.48	0.48
Admixture (%)	0.65	0.65	0.65	0.65	0.65	0.65	0.65
20 mm aggregates	508	508	508	508	508	508	508
10mm aggregates	508	508	508	508	508	508	508
Fine aggregates(robo sand)	823	823	823	823	823	823	823
Water	163	163	163	163	163	163	163

3.2.1 Casting and Curing of Specimens

IS standard 150mm Cubes, 150mm X 300mm cylinder and 150 X 150 X 500 beams were cast from each mixture to evaluate compressive strength and toughness and ductility gain. Concrete was prepared using a drum mixer with a capacity of 0.25 m³. The ingredients were put into the mixer in the decreasing order of their sizes starting from 20mm aggregate to cement. Dry mixing of the aggregates and cement was done for two minutes and then water was added gradually in the rotating mixer and allowed to mix for 15 minutes. During the mixing process, the walls and bottom of mixer were scraped well to avoid sticking of mortar. After mixing, the slump was checked and noted down to ascertain the effects of differently proportioned blends on workability of concrete. Finally the fresh concrete was placed in oiled moulds and compacted properly in three layers, each layer being tamped 35 times using a tamping rod. After the initial setting of concrete, the surface of the specimen was finished smooth using a trowel. Immediately after casting, all specimens were covered with plastic covers to minimize moisture loss. The specimens were stored at room temperature about 25°C. Specimens were demoulded 24 hours after casting and kept in curing water tank.

3.3 Test Methods

An experimental program was designed to study the influence of fiber on the toughness and ductility. Each concrete mixture was evaluated with respect to Slump, compressive strength, and flexural tensile Strength of fiber reinforced concrete.

3.3.1 Slump

Slump was used to find the Workability of fresh concrete where the nominal maximum size of aggregate does not exceed 38 mm. slump cone was used to find the slump of the concrete as per the requirements of IS 1199-1959.

3.3.1.1 Procedure

Oil was applied on the base plate and interior surface of the slump cone. After that, Slump cone was attached to a base plate with screws and finally kept on the levelled surface. Immediately slump cone was filled with fresh concrete approximately one-quarter of height of the cone, each layer was tampered with the tampered rod 25 times. After compacting the top layer, mould and the base plate was cleaned with the clothes. Slump cone was Unscrewed from the base plate and removed immediately from the concrete by raising it slowly and carefully in a vertical direction. Finally slump cone of the base plate kept reverse position, height between the top of the mould and highest point of the concrete was measured with the scale. This height indicated the slump of the concrete.

3.3.2 Compression Strength Testing

For cubes 2000kN digital compressive testing machine was used for determine the compressive strength of hardened concrete as per the requirements of IS 516-1959. For cylinders servo hydraulic closed-loop test machine was used.

3.3.2.1 Procedure

For cubes, before starting the test the weight of the sample was recorded. The plates of the machine were cleaned and the specimen was kept centrally between the two plates. Load was applied gradually on the specimen at a load rate of 5.2 kN/s up to failure. Once the sample was failed, the failure pattern was recorded and the compressive strength was calculated from the maximum load recorded in the test.

For cylinder, cylinders loaded uniaxially on servo hydraulic closed-loop test machine was used. The displacements were increased at a rate of 0.05 mm/min. Two LVDTs with a gauge length of 60 mm were used to measure the displacement on the cylindrical specimens. They were mounted at circular tie placed on the specimen surface at 120 mm from the top of the specimen. A second tie was placed on the specimen at 120 mm from the bottom and provided the reaction frame for the two LVDTs. Each tie was made of two aluminum rings connected by springs. These aluminum ties were able to support the measuring devices, to allow lateral deformations when they occurred, and did not confine the specimens. The data acquisition and signal control were carried out using control unit.

3.3.3 Four-point-bending test

Flexural testing machine with servo hydraulic closed-loop test machine was used to determine the toughness and ductility as per ASTM C1609-M10 and EN 14651.

3.3.3.1 Procedure

This test method utilizes 150 x 150 x 500 mm beams tested on a 450 mm span. The testing was done using a servo-controlled test machine where the net deflection of the centre of the beam is measured and used to control the rate of increase of deflection. Testing was done

as per ASTM C1609 to capture the portion of the load-deflection curve immediately after the first-peak. The loading and specimen support system applied third-point loading to the specimen without any eccentricity or torque. The fixtures used in the testing allowed free rotation on their axes. Linear variable displacement transducers (LVDT) were used to ensure accurate determination of the net deflection at the mid-span. Rectangular jig, surrounding the specimen was clamped to it at mid-depth directly over the supports. Two displacement transducers were mounted on the jig at mid-span, one on each side, to measure deflection through contact with appropriate brackets attached to the specimen. The average of the measurements represented the net deflection of the specimen exclusive of the effects of seating or twisting of the specimen on its supports. The loading was applied such that the net deflection of the specimen increased at a constant rate of 0.04 mm/ min up to a net deflection of $L/900$. Thereafter, i.e., beyond $L/900$ and up to a deflection of $L/150$, loading rate was kept constant at 0.08 mm/min. Beyond $L/150$ and up to the end point deflection, the rate of loading was kept constant at 0.16 mm/min. The testing was continued till the specimen fails.

3.3.4 Three-point-bending test (For notch beam)

The test procedure adopted was consistent with the guidelines given by EN 14651:2005 and 150 X 150 X 500 (height X width X length) mm³ prismatic specimens were tested in the three-point bending configuration. A notch of 25mm depth was introduced at the mid-span using a circular saw as per the guidelines given in EN 14651:2005. The flexure test was conducted in crack mouth opening displacement control by increasing the CMOD at a prescribed rate. The corresponding deflection of the beam was measured using the rectangular jig clamped to the specimen at mid-depth directly over the supports. The testing machine had sufficient stiffness to avoid unstable unloading phenomena in the softening branch of the load-CMOD curve. The notched beam was tested with a span equal to 450 mm during the tests, the rate of increase of the CMOD was controlled in two stages, at 0.05 mm/min for CMOD less than 0.1 mm and at 0.2 mm/min for CMOD greater than 0.1 mm. All the tests were ended at 30 when the CMOD reached a value of 4 mm.

Chapter 4

Experimental Results

4.1 Introduction

The evaluation of the properties of FRC composites is of prime importance for these composites to be used effectively and economically in practice. Fibers are known to contribute to improvements in properties such as toughness, ductility, load carrying capacity, crack control. Improvements in the properties of concrete are primarily attributed to the ability of the fibers to function as discrete reinforcement bridging cracks. Improvements in mechanical properties on using fibers are a result of crack closing stresses provided by fibers and the improvements depend upon the crack closing stresses generated by the fibers as a function of crack opening. The efficiency of fibers depend the ability of fibers to contribute during localization and propagation of a crack. For a given fiber type, fiber volume fraction is a primary variable which controls the properties of the composite. Standard test procedures, which provide measures of specific properties derived from the mechanical response of specimens tested in flexure have been developed. These test measures allow for comparing different fiber types and for assessing the improvement provided by fibers as a function of volume fraction.

The results of an investigation into the influence of the macro synthetic fibers on the fresh and hardened properties of concrete are presented in this chapter. Results of compression tests of cube and cylinder at 28 and 90 days respectively, and results of beam flexural tests at 28 days are presented. The results of the flexural response are interpreted in terms of the influence of fibers on crack propagation in fiber reinforced concrete.

4.2 Compressive strength

The mean 28 day and 90 day compressive strength from standard 150 mm cubes for control and synthetic FRC obtained are tabulated in Table 4.1 and Table 4.2, respectively. The compressive strengths and weights of the individual cubes are listed in Annexure III. The observed standard deviation in the compressive strength values from the same batch are the expected variations produced by sample preparation, and to variations in the actual air contents of the hardened concrete and the differences in their unit weights. While there is an increase in the compressive strength, the variation of compressive strength with fiber content does not show a clear trend with fiber volume fraction. At 28 days of age, the compressive strengths obtained from Synthetic Polypropylene Fiber reinforced concrete (SPFRC) at 4 and 8 kg/m³ and control mixture are comparable and the variation in the compressive strength is within the range of experimental scatter evident within the batch. While the mean compressive strength at a fiber volume content of 6 kg/m³ is higher than the mean compressive strength of the control

mix, the associated increase in the standard deviation at this fiber volume fraction does not permit for a making an inference about statistical significance of the observed increase in strength. Thus it may be concluded that there is no statistically significant change in the 28-day compressive strength in SPFRC for fibers at quantities up to 8 kg/m³. These results are in agreement with the observation from fibrillated polypropylene fibers [6].

In Synthetic Nylon Fiber Reinforced Concrete (SNFRC) there appears to be an increase in the mean compressive strength at all fiber volume fractions, and the increase is higher than the standard deviations of strengths from within one batch. The increase in the compressive strength using synthetic Nylon (SNFRC) fibers in both 28-day and 90-day strengths when compared to the corresponding control and SPFRC mixtures may be attributed to a change in the batch of fly ash and aggregate used in for SNFRC specimens. While the control and the SPFRC specimens were cast using aggregate and fly ash procured from one source, aggregate and fly ash were procured from a different for SNFRC specimens. The same control was used for both SPFRC and SNFRC specimens. The observed improvements in the compressive strength observed in SNFRC when compared with the control mixture may therefore be attributed to a change in the materials. The variations in both 28-day and 90-day compressive strengths at the different fiber volume fractions however, are not significant, suggesting that the compressive strength does not depend on the fiber volume content for volume greater than 4 kg/m³.

Table 4.1 28- Day Compressive strength results

Specimen	Mean Compressive Strength (MPa)	Std. Deviation (MPa)
Control	34.6	1.05
PP (4 kg/m ³)	34.4	0.82
Nylon (4 kg/m ³)	40.4	1.88
PP (6 kg/m ³)	38.0	2.27
Nylon (6 kg/m ³)	39.4	1.28
PP (8 kg/m ³)	35.6	0.54
Nylon (8 kg/m ³)	40.5	0.12

Table 4.2 90-day compressive strength results

Specimen	Mean Compressive Strength (MPa)	Std. Deviation (MPa)
Control	43.6	2.72
PP (4 kg/m ³)	48.5	1.92
Nylon (4 kg/m ³)	53.7	2.04
PP (6 kg/m ³)	50.4	1.32
Nylon (6 kg/m ³)	49.4	0.43
PP (8 kg/m ³)	43.6	1.07
Nylon (8 kg/m ³)	48.2	0.90

Standard 150 mm diameter cylinders with aspect ratio equal to two were tested in compression in displacement control at 50 days of age. The stress-strain response of the concrete obtained from the measured deformations of the central portion of length 60 mm is shown in Fig 4.1. It was observed that the fibers were not playing a significant role initially but at higher displacements the cylinders with higher fiber volume possessed higher residual strength. The addition of synthetic fibers had a significant effect on the mode and mechanism of failure of concrete cylinders in the compression test. The fiber reinforced concrete failed in a more ductile mode, whereas plain control concrete cylinders typically failed in a brittle manner close to the peak load. The fiber reinforced cylinder also possessed structural integrity even at high compression displacement. Fig 4.2 (a) shows the effectiveness of fibres in holding the concrete together and, Fig 4.2 (b) depicts the same during real-time testing.

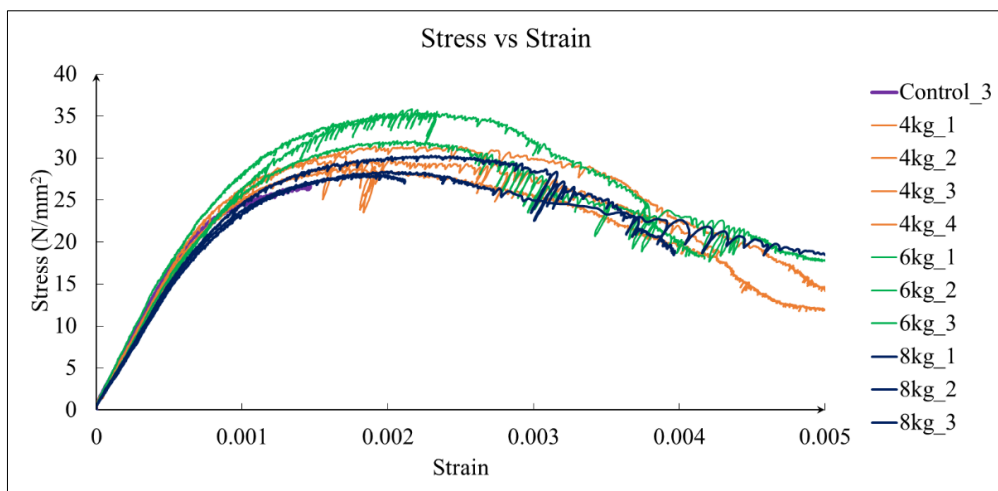


Fig 4.1 Compressive Stress vs Strain of Cylinders

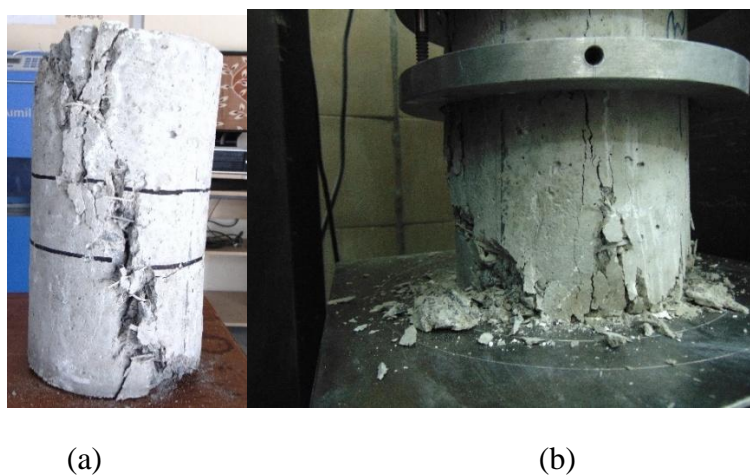


Fig 4.2 Failure in fiber reinforced concrete specimens; (a) cylinder; (b) cube

4.3 Flexural Testing as per ASTM C1609 (Unnotched Beams)

The load-deflection responses of control and SPFRC beams with 4, 6 and 8 kg/m³ in flexure are shown in Fig 4.3, 4.4, 4.5 and 4.6, respectively. The load response up to a deflection of 0.3 mm is shown in the insets for clarity. Failure in both control and SPFRC beams were due to the formation of a single crack in the constant moment region. All beams, both control and SPFRC exhibit nonlinearity in the load response before peak load following the initial linear response. Following the peak load, which is associated with the localization of a single crack, while the control beams show a monotonic and rapid decrease in the load with increasing deflection, the SPFRC beams exhibit significant load carrying ability even at large deflection. In all SPFRC beams, there is an initial decrease in the load with increasing deflection immediately after peak. Following the load drop, the beams exhibit a load recovery, where the residual load carrying capacity increases with increasing deflection. One control beam failed suddenly in a brittle manner, which resulted in splitting the specimen into two pieces immediately following peak load. The load response in the post peak could not be obtained in a controlled manner. The lack of control was due to inability of the control algorithm to compensate for sudden load drops associated with abrupt crack advance.

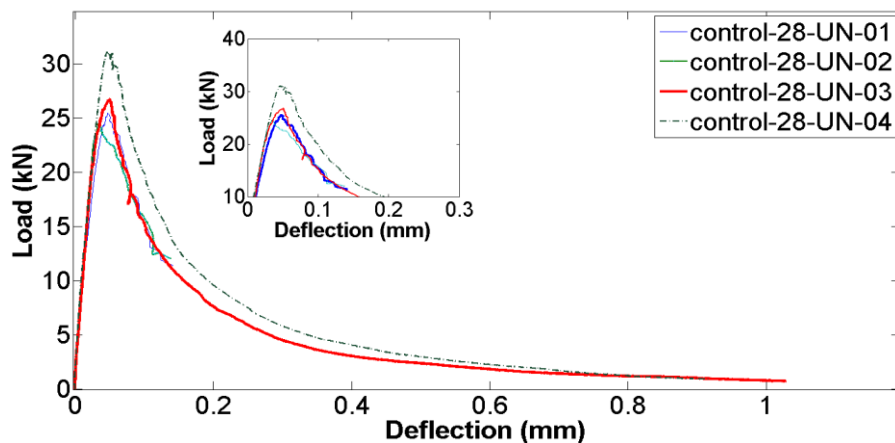


Fig 4.3 Load deflection response control specimen

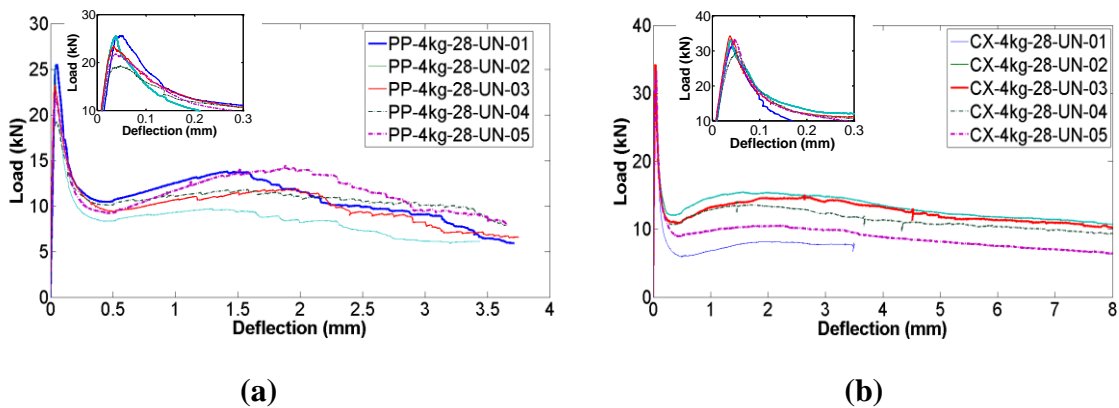
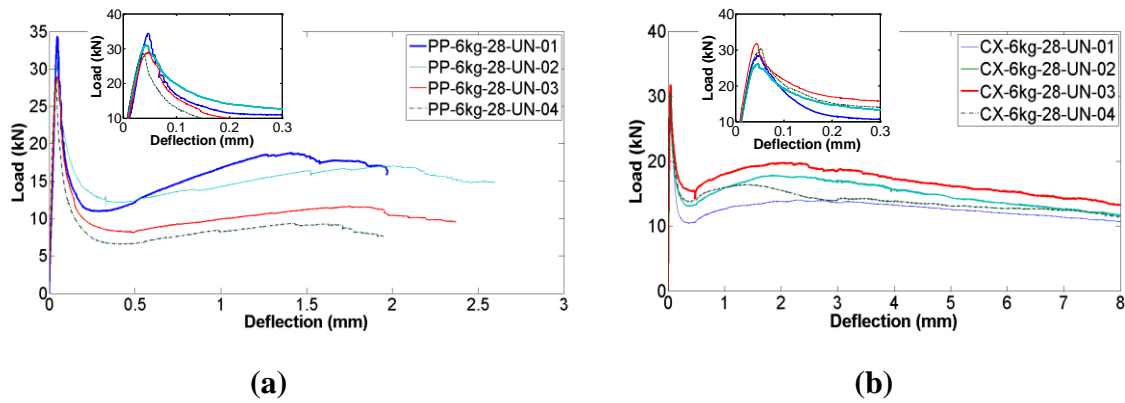
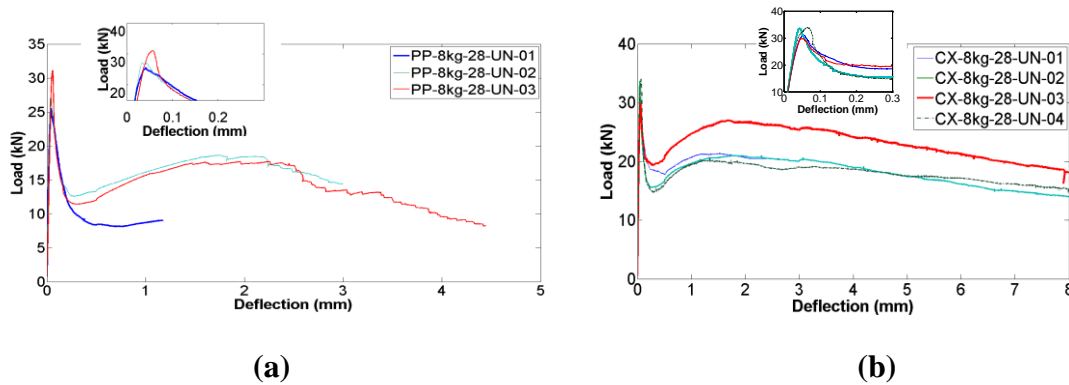


Fig 4.4 Load deflection response from flexure test for 4 kg/m³

(a) SPFRC; and (b) SNFRC



**Fig 4.5 Load deflection response from flexure test for 6 kg/m³
(a) SPFRC; and (b) SNFRC**



**Fig 4. 6 Load deflection response from flexure test for 8 kg/m³
(a) SPFRC; and (b) SNFRC**

A comparison of load responses from SPFRC and SNFRC specimens reinforced with 4, 6 and 8 kg/m³ fibers is shown in Fig 4.7 and Fig 4.8, respectively. The response of SPFRC and SNFRC beams under flexure are nominally similar. There is clearly an increase in the post-peak load carrying capacity with the addition of fibers. The beams with 6 and 8 kg/m³ show a prominent load recovery, where the load carrying capacity increases with increasing deflection following the initial drop after the peak load. All SPFRC beams indicate residual load carrying capacity up to a deflection 2 mm and all SNFRC beams up to a deflection of 3 mm. Further, the maximum load recovery following the initial load drop in the post peak occurs at deflection greater than 1.5 mm. The maximum point in the load recovery occurs at a larger deflection for higher fiber content.

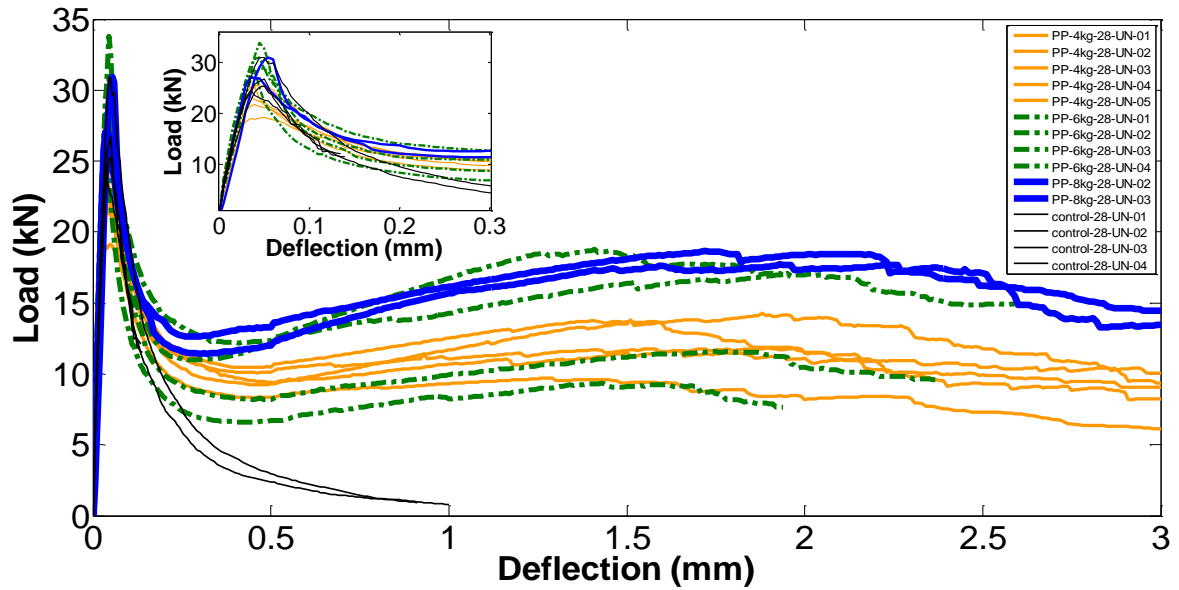


Fig 4.7 Load deflection response of SPFRC at 28 days

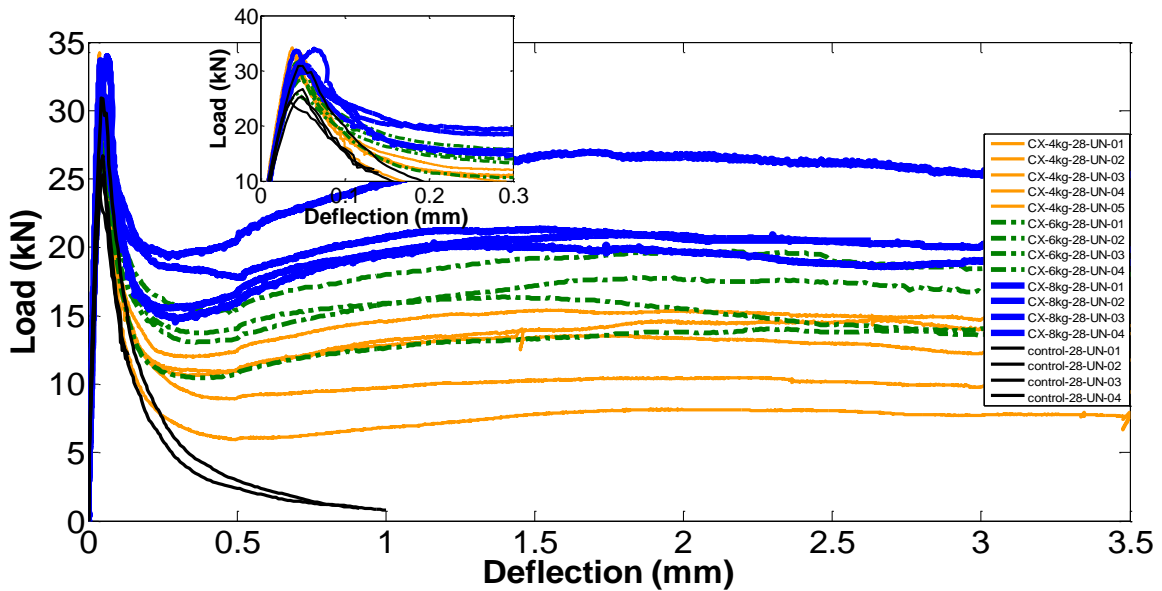


Fig 4.8 Load deflection response of SNFRC at 28 days

The load response obtained from the flexure from both SPFRC and SNFRC can be idealized as shown in Fig 4.9. Key features in the load response identified from the common aspects of load responses from the different fiber types and volume fractions are identified in the idealized response. The peak load and the corresponding displacement are identified as P_u and δ_u . The lowest point in the load response in the immediate post-peak following the load decrease are identified with P_{crit} and δ_{crit} . The load recovery in the flexure test is observed on increasing the deflection beyond δ_{crit} . To understand the influence the type of fiber on the observed trends in the load response, statistics related to points on the load response are

compiled from all the specimens tested and tabulated in Table 4.3 and Table 4.4. The individual values for each specimen tested are listed in Annexure III.

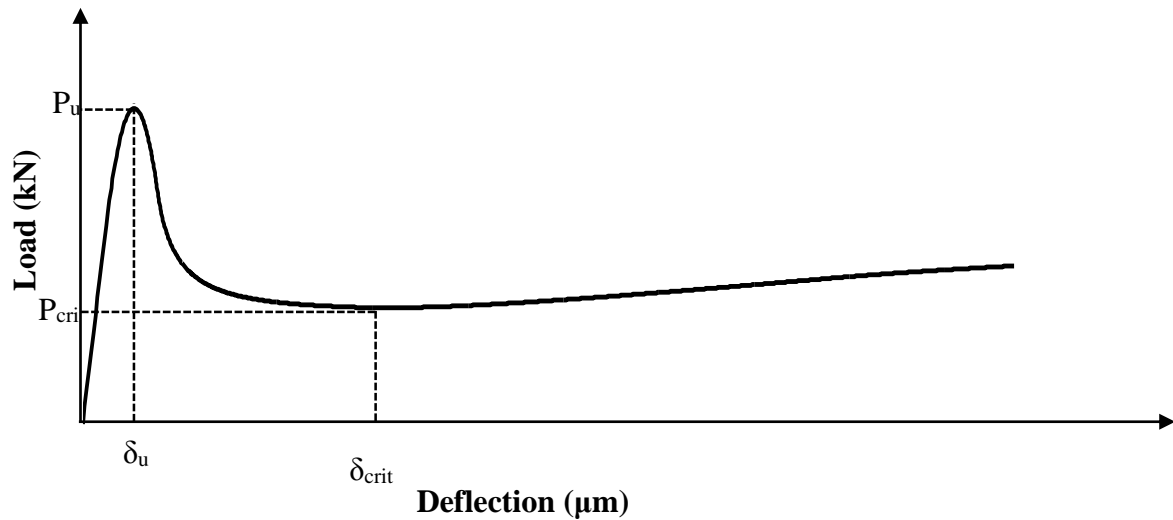


Fig 4.9. Idealized load response for beams tested in flexure

Table 4.3 Key Parameters in the flexural load response of SPFRC

Fiber Volume (kg/m ³)	Mean P _u (kN) (stdev)	Mean δ _u (μm) (stdev)	Mean P _{crit} (kN) (stdev)	Mean δ _{crit} (μm) (stdev)
4	23.1 (2.40)	42.1 (7.15)	9.5 (0.74)	468.3 (24.21)
6	30.8 (2.29)	44.2 (3.39)	9.4 (2.09)	386.9 (80.38)
8	27.9 (2.34)	44.2 (9.57)	10.7 (1.89)	441.7 (216.21)
Control	27.0 (2.51)	44.7 (5.73)		

Table 4.4 Key Parameters in the flexural load response of SNFRC

Fiber Volume (kg/m ³)	Mean P _u (kN) (stdev)	Mean δ _u (μm) (stdev)	Mean P _{crit} (kN) (stdev)	Mean δ _{crit} (μm) (stdev)
4	32.3 (1.63)	44.4 (6.50)	9.7 (2.11)	417.0 (74.20)
6	29.2 (2.11)	47.9 (3.36)	12.8 (1.45)	393.5 (47.63)
8	32.2 (1.72)	51.2 (8.05)	16.8 (1.87)	328.8 (102.48)
Control	27.0 (2.51)	44.7 (5.73)		

Comparing the P_u and the corresponding δ_u from the different specimens, it can be seen that there is no statistically significant improvement in peak strength and the corresponding deflection. The variation in the mean strength obtained from both SPFRC and SNFRC is within the range of scatter indicated by the standard deviation. Thus it may be concluded that both Polypropylene and Nylon fibers do not influence the peak load for fiber dosages up to 8 kg/m³. The values of P_{crit} and δ_{crit} are comparable for SPFRC and SNFRC at 4 kg/m³. In SPFRC, there is no significant change in P_{crit} and δ_{crit} with increase in fiber volume content. There is however

a significant increase in the P_{crit} values and a corresponding decrease in δ_{crit} with increasing fiber content in SNFRC.

Comparing the response of SPFRC and SNFRC and by observing peak load values from Table 4.3 and 4.4, it is seen that the variations in the peak load were found to be within the range of experimental scatter for each fiber volume content suggesting that the fibers do not influence the peak load. The pre-peak behavior of both macro-synthetic fibers at the three fiber dosages is similar to that for the control. The pre-peak non-linearity, which is associated with the initiation of crack formation indicates that fibers do not play role before localization of crack. After peak load, in case of control specimens, the mechanism of crack bridging provided by aggregate produces a continuous decrease in load with increase in deflection, which makes obtaining the controlled post-peak behavior difficult. Immediately after peak load, there is progressive decrease in the load with a small corresponding increase in deflection. The early part of the post-peak responses (shown in Fig 4.7 and 4.8) for the three fiber dosages is nominally similar, which suggests that this part of the response is not significantly influenced by fiber content. Thus, the load decrease in the post-peak response immediately after the peak is dominated by crack propagation in the matrix and stiffness contribution of fibers is insignificant compared to the contribution of aggregates. The load which can be safely supported decreases with an increase in the crack length. The propagation of the crack in the matrix results in an increase in the compliance of the beam, which produces a rapid increase in deflection accompanied by a decrease in the load. In fiber reinforced beams, following an initial load decrease associated with crack propagation in the matrix, the load starts to increase with increasing deflection due to contribution of fibers. The fibers over the depth of the beam at the location of crack provide additional crack bridging forces. The load recovery and hence the increase in the load carrying capacity with increasing deflection increases with an increase in fiber content. There is considerable recovery in the load carrying capacity in 8 kg/m^3 . For both macro synthetic fibers at 8 kg/m^3 , because the number of fibers that come into play to across the crack surface are significantly larger than the 4 kg/m^3 , the post peak load decrease is arrested earlier. While this is clear in the case of SNFRC, the trends in SPFRC are not clear. It can be observed from Table 4.4 that the load at which drop is arrested at a higher fraction of the peak load with an increase in fiber volume and also the corresponding deflection at which load recovery starts, decreases with an increase in fiber volume. This indicates that the contribution of fibers to the load response is initiated earlier during the post-peak load drop at higher fiber volume. Further, on increasing the deflection, the increase in load carry capacity of the beam suggests an increase in the tensile resistance provided by the fibers crossing the crack. The increase in the total tensile resistance after the attaining a minimum can be attributed to the increased resistance provided by additional fibers across the crack face with an increase in crack length and the additional stress due to increased resistance to pullout of individual fibers. The increased resistance from crack bridging which results in arrest of the load drop load after the initial post-peak load drop is also reflected in the increased residual strengths with increasing deflection.

4.4 Flexure Testing on Notched Specimens (EN 14651).

The load-CMOD response of control and the fiber reinforced specimens with 4, 6 and 8 kg/m³ of fibers is shown in Fig 4.10, 4.11, 4.12 and 4.13 respectively. The variations in the peak load were found to be within the range of experimental scatter for each fiber volume content suggesting that the fibers do not influence the peak load. Further, the immediate post-peak softening response after peak load is also nominally identical for control and fiber reinforced specimens. The initial drop in the load in the post-peak softening is not influenced by the presence of fibers. For each of the three fiber contents used in this study, 4, 6 and 8 kg/m³, the load at which the fibers contribute to crack bridging can be identified from the observed deviation from the response of the control specimen. Available data indicates that there is no significant deviation from the response of the control specimen up to a CMOD value of 0.3 mm for 4 kg/m³ and 6 kg/m³. For the 8 kg/m³ fiber content, the influence of larger number of fibers across the crack results in a deviation from the load response with increasing CMOD, before a CMOD value of 0.3 mm, when compared with the control specimens. The crack bridging provided by the fibers contribute to increasing load carrying capacity with increasing CMOD.

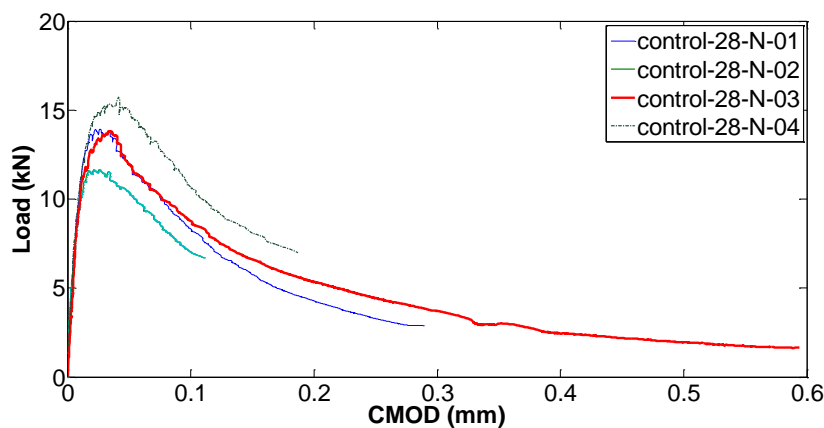


Fig 4.10 Load CMOD response of control at 28 days

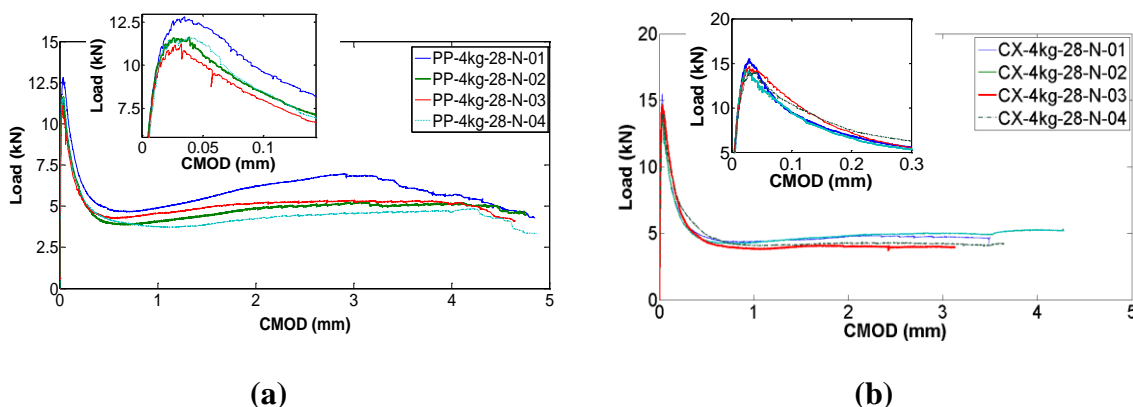


Fig 4.11 Load CMOD response of 4 kg/m³ at 28 days (a) SPFRC and (b) SNFRC

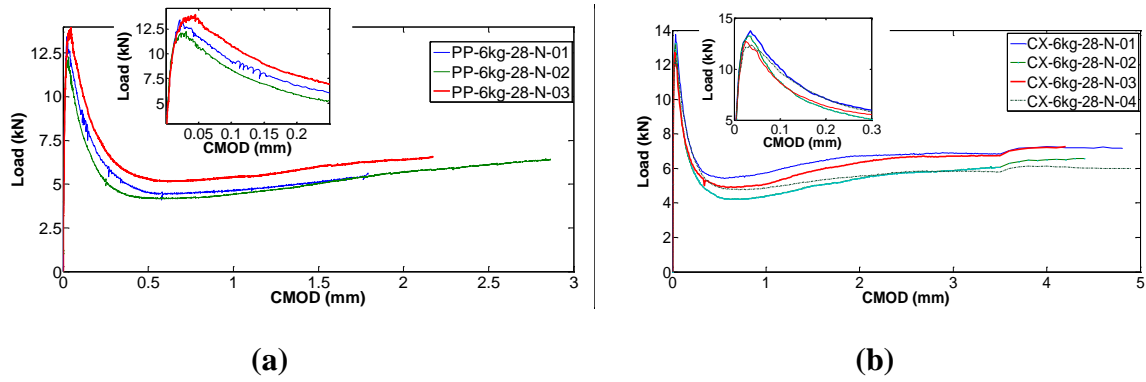


Fig 4.12 Load CMOD response of 6 kg/m³ at 28 days (a) SPFRC and (b) SNFRC

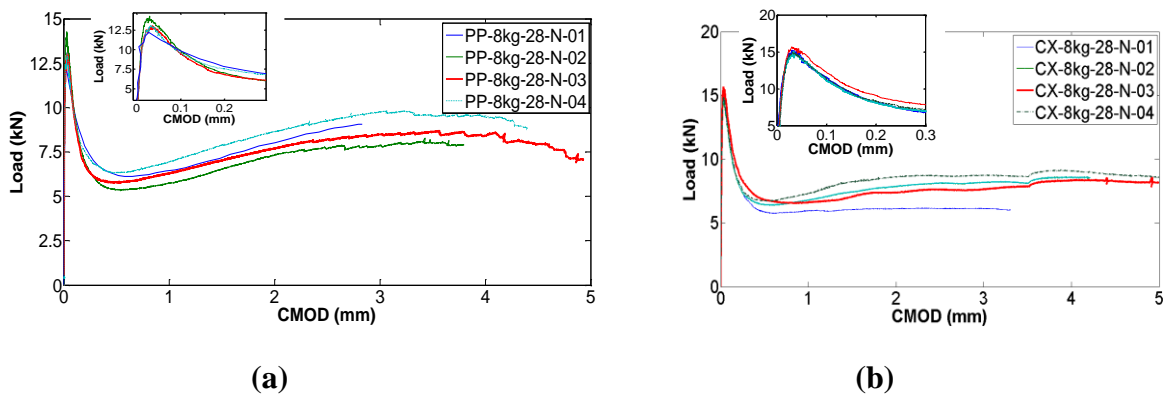


Fig 4.13 Load CMOD response of 8 kg/m³ at 28 days (a) SPFRC and (b) SNFRC

A comparison the load-CMOD responses for the different fiber volume contents are shown in Fig 4.14 and Fig 4.15 for SPFRC and SNFRC, respectively. The presence of fibers results in an increase in the load carrying capacity with increasing crack opening after an initial load drop in the immediate post-peak load response following the peak load. While the fiber volume content does not appear to influence the peak and the immediate post-peak load response on increasing crack opening, the influence of the fiber volume is evident at a smaller value of crack opening displacement where the load recovery starts. The larger fiber volume produces a load recovery at a smaller value of crack opening. There is also a higher load achieved during the load recovery on increasing the fiber volume.

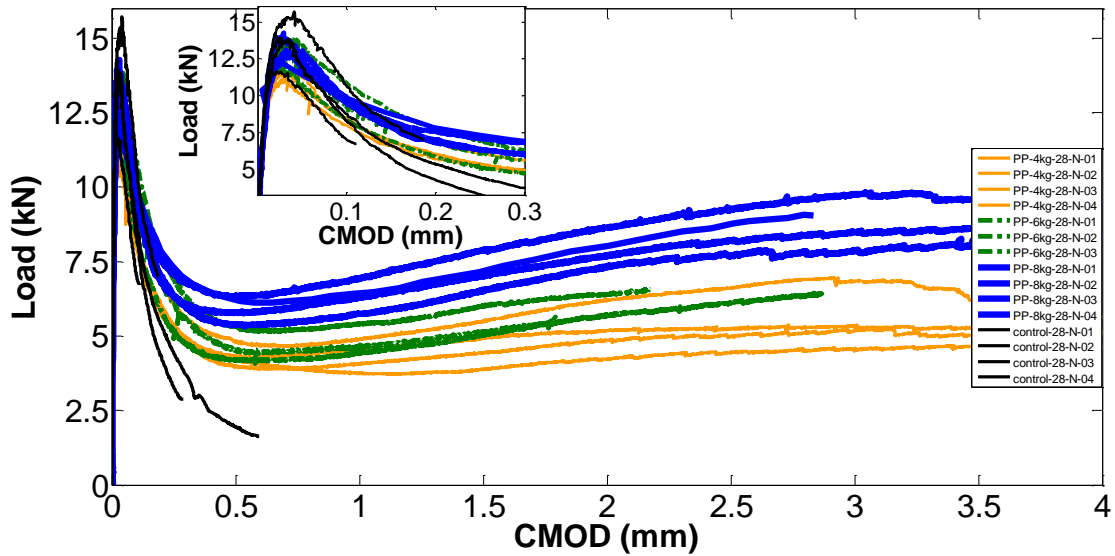


Fig 4.14 Load CMOD response SPFRC at 28 days

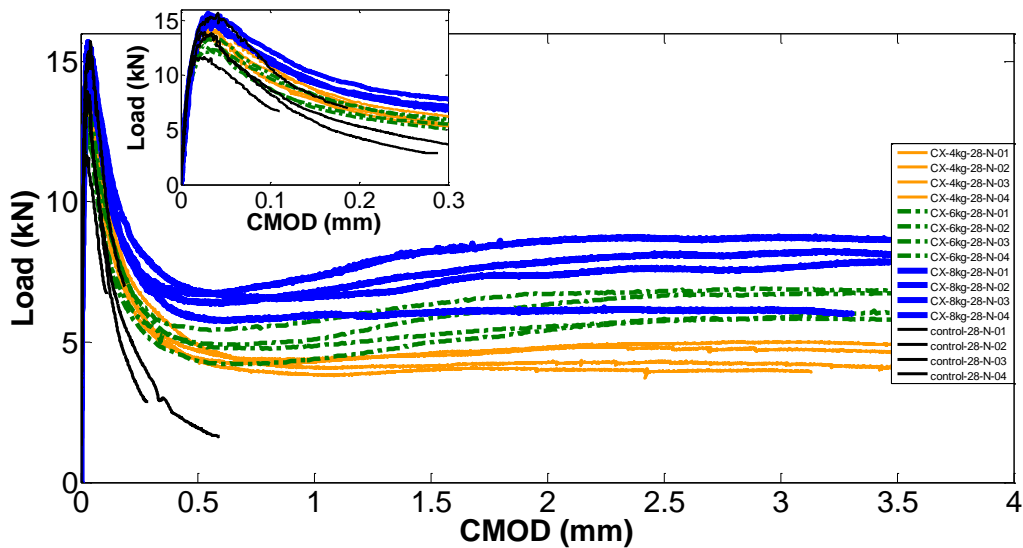


Fig 4.15 Load CMOD response SNFRC at 28 days

Following a procedure similar to that adopted for the analysis of the flexural test response from the unnotched specimens an idealization similar to Fig 4.9 was also adopted for the test response from the notched tests. It can be observed that for both SPFRC and SNFRC the trends in the peak load and the corresponding CMOD do not indicate any statistically significant change. There is not systematic change with the increase in fiber content and the observed change in the mean values is within the range of scatter obtained from one batch. There is however a significant increase in P_{crit} , and a corresponding decrease in the CMOD on increasing the fiber volume. This suggests that increasing the fiber volume, increases the

resistance to crack opening, thereby provides an earlier deviation from the descending portion of the load response seen in control specimens. Thus at larger volume fractions, the fibers are effective at a smaller crack opening.

Table 4.5 Key Parameters in the flexural load response of SPFRC from notched beams

Vol. Fibers (kg/m ³)	Mean Pu (kN) (stdev)	Mean CMOD _u (μm) (stdev)	Mean CTOD _u (μm) (stdev)	Mean P _{crit} (kN) (stdev)	Mean CMOD _{crit} (μm) (stdev)	Mean CTOD _{crit} (μm) (stdev)
4	11.8 (0.60)	35.9 (2.52)	24.0 (3.93)	4.1 (0.35)	731.1 (154.62)	537.2 (23.98)
6	13.2 (0.71)	32.9 (9.54)	27.2 (8.55)	4.5 (0.49)	606.2 (21.54)	531.5 (32.88)
8	13.5 (0.56)	32.2 (2.43)	23.8 (1.31)	5.8 (0.40)	526.9 (12.56)	429.5 (7.09)
control	13.8 (1.44)	31.9 (6.37)	21.5 (6.54)			

Table 4.6 Key Parameters in the flexural load response of SNFRC from notched beams

Vol. Fibers (kg/m ³)	Mean (kN) (stdev)	Mean (μm) (stdev)	Mean (μm) (stdev)	Mean (kN) (stdev)	Mean (μm) (stdev)	Mean (μm) (stdev)
4	14.6 (0.56)	31.2 (7.17)	18.1 (10.18)	4.1 (0.19)	929.0 (86.55)	616.8 (263.10)
6	13.1 (0.61)	32.9 (4.36)	25.2 (4.4)	4.8 (0.43)	529.5 (112.75)	439.2 (87.61)
8	15.2 (0.29)	31.4 (1.12)	17.7 (4.30)	6.3 (0.36)	616.2 (139.48)	495.8 (95.36)
control	13.8 (1.44)	31.9 (6.37)	21.5 (6.54)			

4.5 Analysis of Data

The response of the SPFRC and SNFRC beams under flexure was analyzed in compliance with ASTM C1609, ASTM C1018, JSCE SF4 for unnotched beams and EN14651 for notched beams and corresponding parameters are graphically shown in Fig 4.16, 4.17, 4.18, 4.19 and 4.20. The residual Strength at span/600 (0.75 mm deflection) is observed to increase with increase in fiber volume. While there is a nominal increase in residual strength with fiber content in SPFRC beams, the increase is significant in SNFRC. The values for the residual strength are comparable at 4 kg/m³ for both SPFRC and SNFRC. However, the trends from SPFRC do not indicate any significant improvement on increasing the fiber volume content. Comparing with the deflection at the critical point, δ_{crit} (in Table 4.5 and 4.6), it can be seen that the deflection corresponding to span/300 is in the load recovery portion of the load response. This indicates that the Nylon fibers contribute more significantly in the early part of the post-peak load recovery and the contribution of the fibers in influencing the early part of the post-peak response is more significant at higher fiber content. Similar trends in residual strength with fiber volume are also observed in SNFRC at span/150 (3 mm deflection). All beams exhibit considerable amount of residual strength even at 3 mm deflection. There is

however considerable improvement in the residual flexural strength with fiber content at span/150 deflection in SPFRC.

Equivalent flexural strength ratio also increases with an increase in the fiber volume indicating that more energy is required to break the specimen with higher fiber volume. It is observed that there is 75% enhancement in flexural strength ratio in SNFRC beams from 4 to 8 kg/m³ and 20% in SPFRC beams.

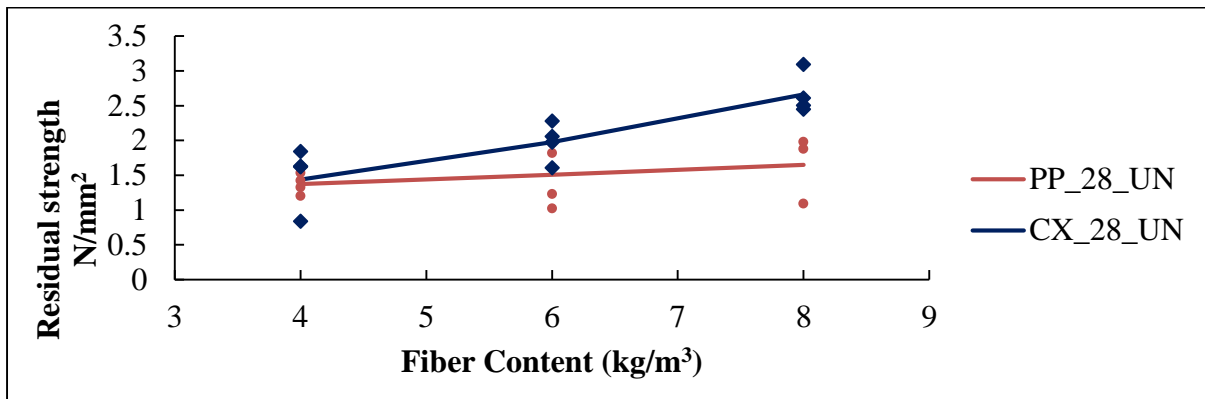


Fig 4.16 Residual Strength at L/600 as per ASTM C 1609

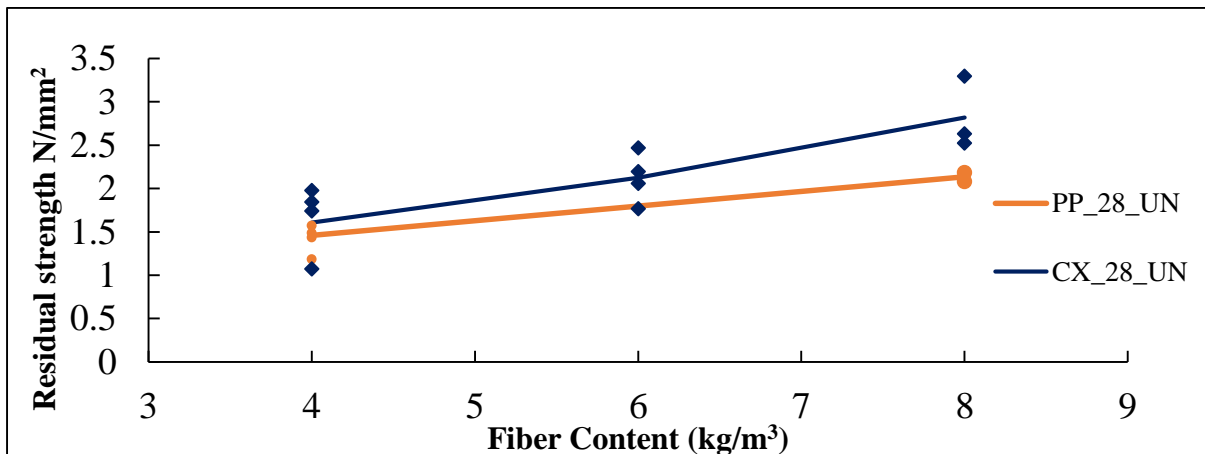


Fig 4.17 Residual Strength at L/150 as per ASTM C 1609

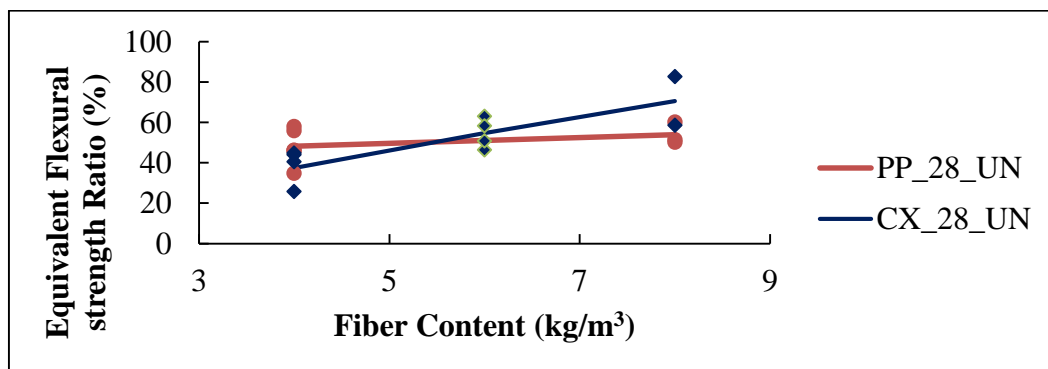


Fig 4.18 Equivalent Flexural strength Ratio as per ASTM C 1609

Toughness factor calculated as per JSCE standard 4 is shown in Fig 4.19. The toughness factor is observed to increase with fiber volume indicating the enhancement in energy absorption capacity of beam. The increase in toughness factor is 60 to 70 percent for both types of fibers as fiber volume is increased from 4 to 8 kg/m³.

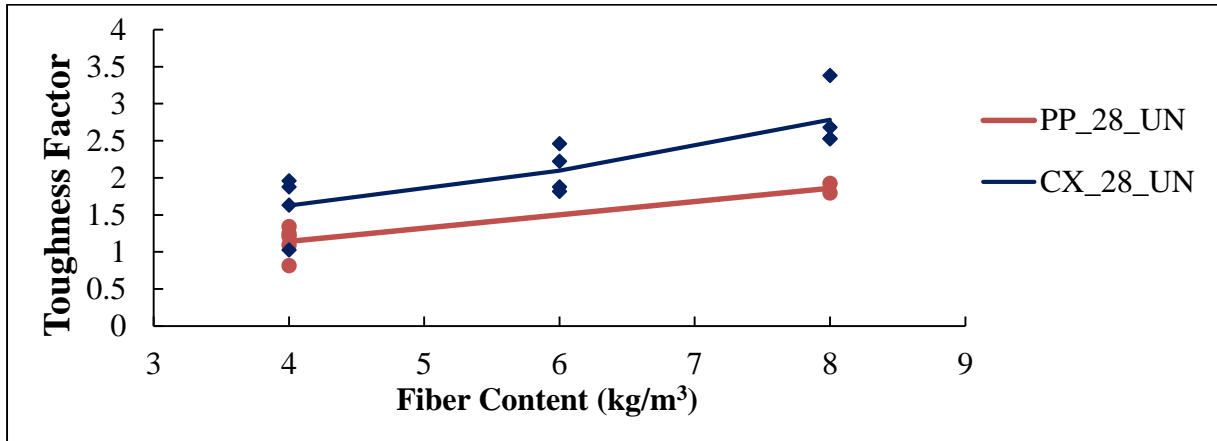


Fig 4.19 Toughness factor as per JSCE 1609

The residual flexural strength calculated as per EN14651 from the test response of notched specimens tested in CMOD control are shown in Fig 4.20 and 4.21 for SPFRC and SNFRC, respectively. The residual flexural strength provides a measure of effectiveness in providing crack closure. Flexural strength remaining constant implies as the crack opens the load carrying capacity of the beam remains constant. In SPFRC beams it can be observed that the Flexural strength increases for all volume fractions with increasing CMOD beyond 0.5 mm. This indicated that the polypropylene fibers are more effective in providing crack closing stresses. At any value of CMOD greater than 0.5 mm the flexural strength increase with an increase in the fiber volume. In SNFRC the increase in flexural strength beyond a CMOD of 0.5 mm seems to be nominal.

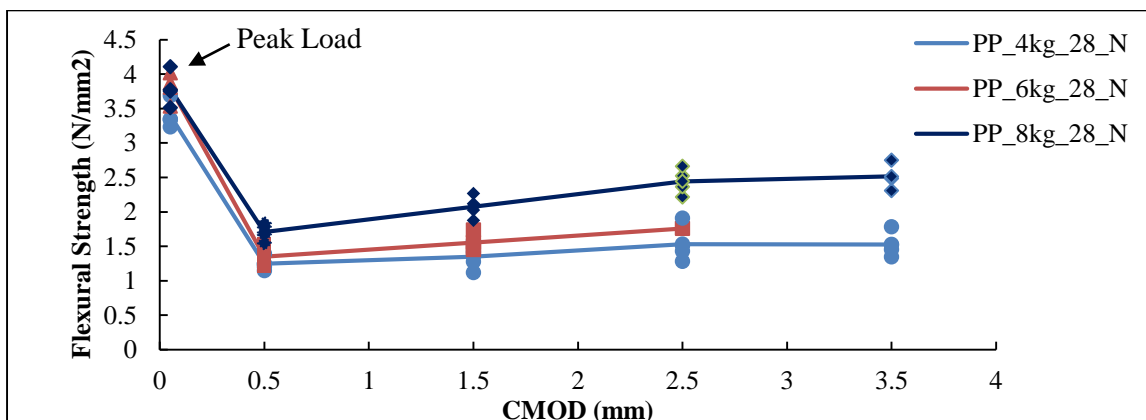


Fig 4.20 Residual Flexural Strength of SPFRC as per EN14651

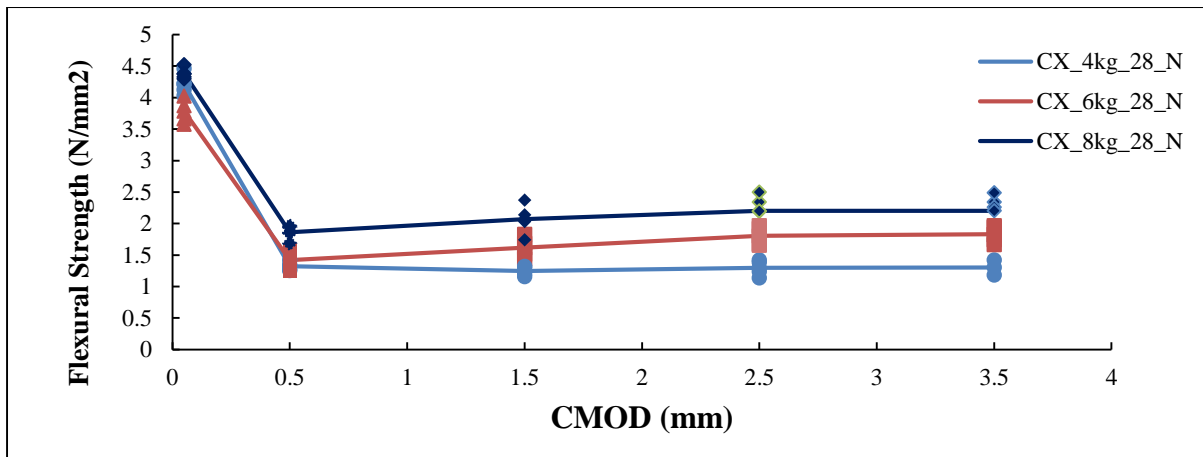


Fig 4.21 Residual Flexural Strength of SNFRC as per EN14651

On comparison with $CMOD_{crit}$ of Table 4.5 and 4.6 it can be observed that 0.5 mm CMOD occurs before the load recovery is initiated and all other $CMOD_j$ lie in the post load recovery portion of the response. From Fig 4.20 and 4.21, we can observe there is strength enhancement at a CMOD of 0.5 mm with volume fraction which indicates that increasing the fiber content influences the load at which recovery is initiated and hence the role of fibers is significant at a lower value of crack opening.

4.6 Summary of Findings

The results of the experimental investigation reveal that both polypropylene and Nylon macro synthetic fibers provide substantial residual load carrying capacity at large deflections. The macro synthetic fibers have an elastic modulus in the range of 10 GPa, while the elastic modulus of mature concrete is expected to be higher than 20 GPa. Therefore, at volumes up to 8 kg/m^3 , which corresponds to approximately 1% of the volume, these fibers do not significantly influence the elastic, pre-peak and early part of the load response. The measures obtained from standard tests also do not indicate any significant improvement in the peak strength in flexure tests. The failure in both notched and unnotched specimens was observed to be produced by a single crack in the constant moment region. Following localization, the crack propagates through the cementitious matrix with little or no resistance from the fibers. The involvement of fibers is seen only at large crack openings. The load drop in the post peak is accompanied with an increasing deflection, which is indicative of increasing compliance produced by the crack propagating along the height of the beam. The influence of the soft fibers is experienced in the post-peak load response after the crack propagates to an extent that the decrease in stiffness of the cracked portion is comparable to the stiffness provided by the fibers. The contribution of the fibers is therefore experienced in the later part of the post-peak load response. The displacement or the crack opening at which the fibers start influencing the load response depends on the volume fraction of the fibers. Following the initial load drop, the load response obtained from the fiber reinforced specimens exhibit a load recovery associated with the crack closing stresses provided by the fibers bridging the crack. The fiber bridging the crack provides a significant load carrying capacity with increasing deflection. Considerable enhancements in the composite fracture energy and toughness are obtained

Chapter 5

Digital Image Correlation Results

5.1 Introduction

Digital image correlation (DIC) is a full-field optical technique which provides spatially continuous measurement of displacements across the surface of the specimen. Compared with other optical techniques, DIC is a very robust measurement technique which does not require the use of lasers. It provides reliable measurements without the requirement of any special vibration isolation, which allows the use of this technique during a mechanical test. The technique relies on a random sprayed-on speckle and a digital camera for image acquisition. With the advent of digital cameras, which provide increased resolution, the accuracy obtained from the technique has increased allowing for the use of the technique in applications which required measurements at a higher resolution. DIC has been used to determine the stress concentration produced by a stress riser such as a crack and for stress distribution due to damage. Application of the technique have included determining the stress concentration for evaluating fracture parameters in composite and metallic specimens [45, 46, 47]. Successful application of DIC in concrete specimens include determination of the strain profile associated with cohesive stress transfer produced with debonding of FRP composite laminates and to derive the cohesive stress-crack separation relationship [48].

DIC measurements were performed on notched specimens tested as per EN 14651. A speckle pattern was created in a region close to the notch. While the available resolution from the technique considering the area of measurement does not allow for determining fracture parameters, the information from the surface displacements and strains obtained using DIC are used for evaluating the crack propagation. The surface displacements and strains were analysed for evaluating the crack growth in concrete in relation to the observed load response in flexure and to compare with measurements obtained from other instrumentation. The observed relationship between crack opening and crack depth as a function of the load supported by the specimen was determined from the DIC results. The effectiveness of fibers in providing crack bridging was evaluated from the observed relationship between crack tip opening and crack depth.

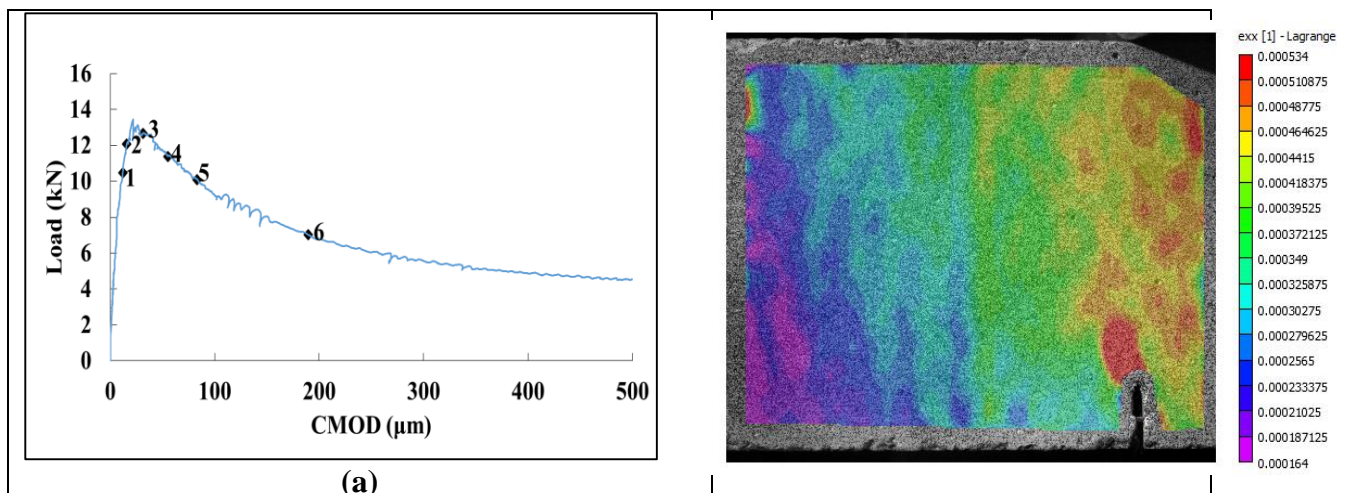
5.2 Background

DIC relies on correlation of the random pattern of speckles between images of the deformed and reference (undeformed) configurations of the specimen within small neighbourhoods called subsets [Sutton et al. (1983, 1988)]. The speckle pattern represents a random pattern, which gives a unique distribution of pixel grey level values in each subset. A two-dimensional displacement field was obtained for all points on the surface from cross-correlating the image of the deformed specimen with the image of the specimen in the reference

configuration. A subset size equal to 35x35 pixels was used for the correlation. In a given image, the pixel grey value in each subset associated with the random sprayed-on pattern forms a unique grey-level distribution, which differs from grey-level distribution of another subset. In the analysis, positions within the deformed image were mapped on to positions within the reference subsets using second-order, two-dimensional shape functions. Spatial domain cross-correlation was performed to establish correspondence between matching subsets in images of the reference and deformed states. Quintic B-spline interpolation of the grey values was used to achieve sub-pixel accuracy. The cross correlation analysis of the digital images was performed using the VIC-2D™ software, which maximizes the correlation coefficient between grey levels in the subsets in the reference and deformed images. Surface displacements and displacement gradients at each loading stage were calculated at each subset centre, by evaluating the shape functions and their partial derivatives at the subset centre. For the setup used in this study, the random error in the measured displacement is in the range of 0.002 pixels. Strains were computed from the gradients of the displacements. A conservative estimate of the resolution in strain obtained from the digital correlation was 10 $\mu\epsilon$ [Bruck et al (1989), Schreier (2002)].

5.3 Results

Typical load-CMOD response of an SPFRC beam with 6 kg/m³ tested CMOD control is shown in Fig 5. 1. The strain in the X-direction (ϵ_{xx}) at distinct point on the load response of the specimen (shown marked on the load response) are also plotted. It can be observed that strain localization is initiated close to the peak load and leads to the formation of single crack emanating from the notch. The growth of the crack can clearly be identified with softening in the post peak load response. Correspondingly there is also an increase in the CMOD. The results indicate that the localization close to the peak load, results in an increase in the crack opening. As the crack propagates, there is a steady increase in the crack opening and an associated drop in the load.



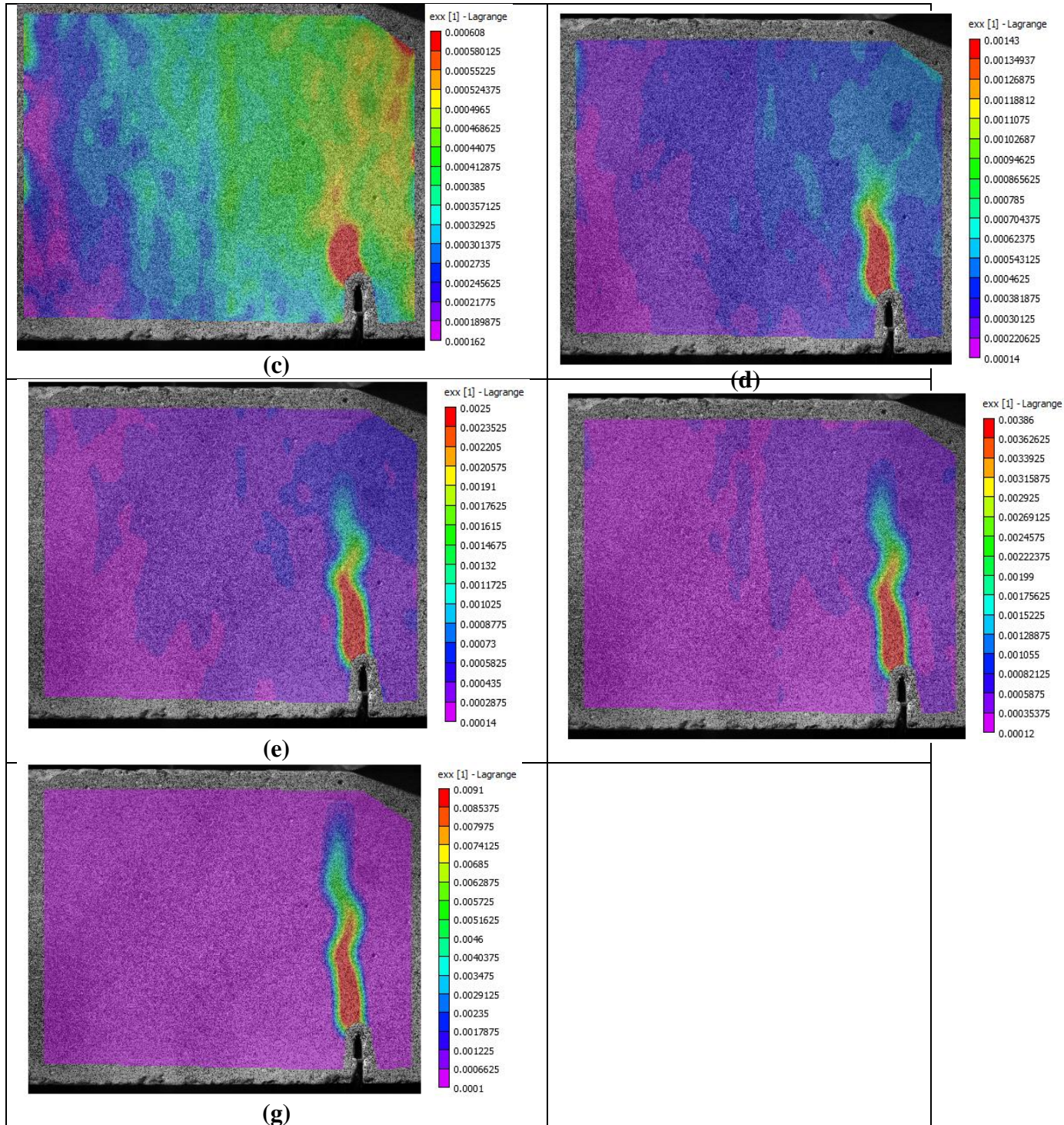


Fig 5. 1: (a) Load-CMOD of plot of SPFRC specimen with 6kg/m^3 fibers. The CTOD measured during the test is also shown in the Figure; (b) ϵ_{xx} at 10.5 kN (pre-peak); (c) ϵ_{xx} at 12.1 kN (prepeak); (d) ϵ_{xx} at 12.7 (postpeak); (e) ϵ_{xx} at 11.4 kN (postpeak); (f) ϵ_{xx} at 10.1 kN (postpeak); and (g) ϵ_{xx} at 7 kN (postpeak)

The variation in ϵ_{xx} at different heights along the depth of the beam are analysed at distinct points in the load response for both control and synthetic fiber reinforced concrete are analysed. Five locations at fixed heights above the notch were selected for evaluating the variation in the strains due to crack propagation. At each location the displacement and strain

relative the centreline of the notch was evaluated to determine the variation as a function of depth. The location of the lines are given in Table 5.1 and shown in Fig 5.2. The variation in displacement, u and strain ϵ_{xx} along line 1, located just above the notch at distinct point in the load response for control, 4 kg/m³, 6 kg/m³ and 8 kg/m³ are shown in Fig 5.3, 5.4, 5.5, 5.6, 5.7, 5.8 and 5.9 respectively.

Table 5.1 Locations of lines

Line No	Depth From Crack Tip (mm)
1	5-10
2	40
3	62.5
4	90
5	105-115

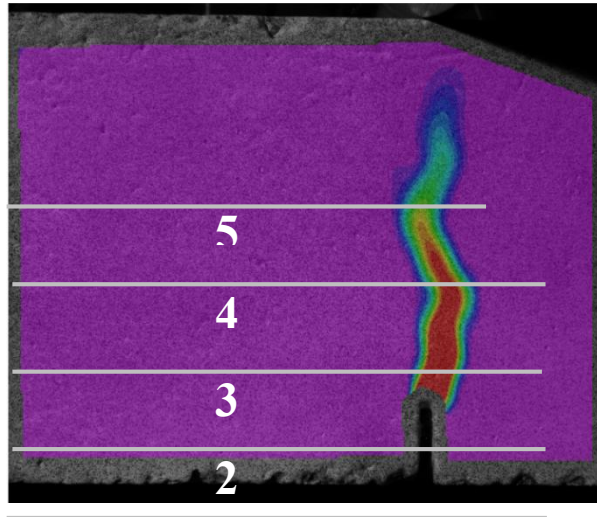


Fig 5.2 Horizontal strips for strain computations

A region of finite length associated with very rapid increase in displacement is observed in the displacement profile along line 1. The region associated with the rapid gradient in displacement is broadly centred on the notch. Within this region, the displacements sharply rise above the linear trend with a gradual slope away from the notch. The size of the region associated with the rapid increase in displacement remains relatively constant with increasing deflection of the beam.

The increase in strain along line 1 close to the notch is indicative of strain localization, which is centred over the notch. The strain localization is noticed over a finite width, along the line. The width associated with localization appears to remain constant during the immediate post peak softening load response following the peak load. This indicates that strains in a finite region close to the crack plane are influenced by the crack. The available data indicates that the strain profile in the immediate post-peak for Polypropylene and Nylon with 4, 6 and 8 kg/m³ is identical to the control specimen.

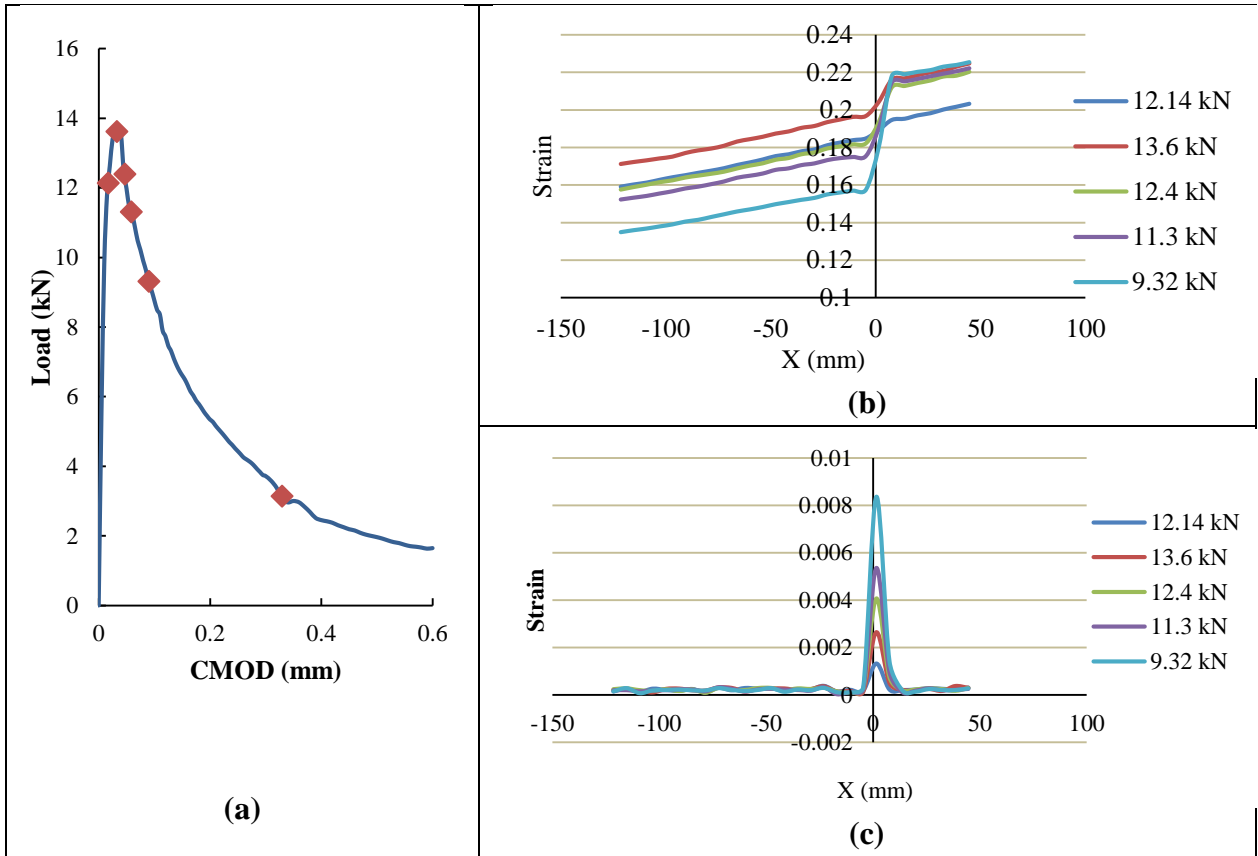


Fig 5.3: (a) Typical load response of control; (b) displacement profile at line 1; (c) strain profile at line 1 at distinct load points

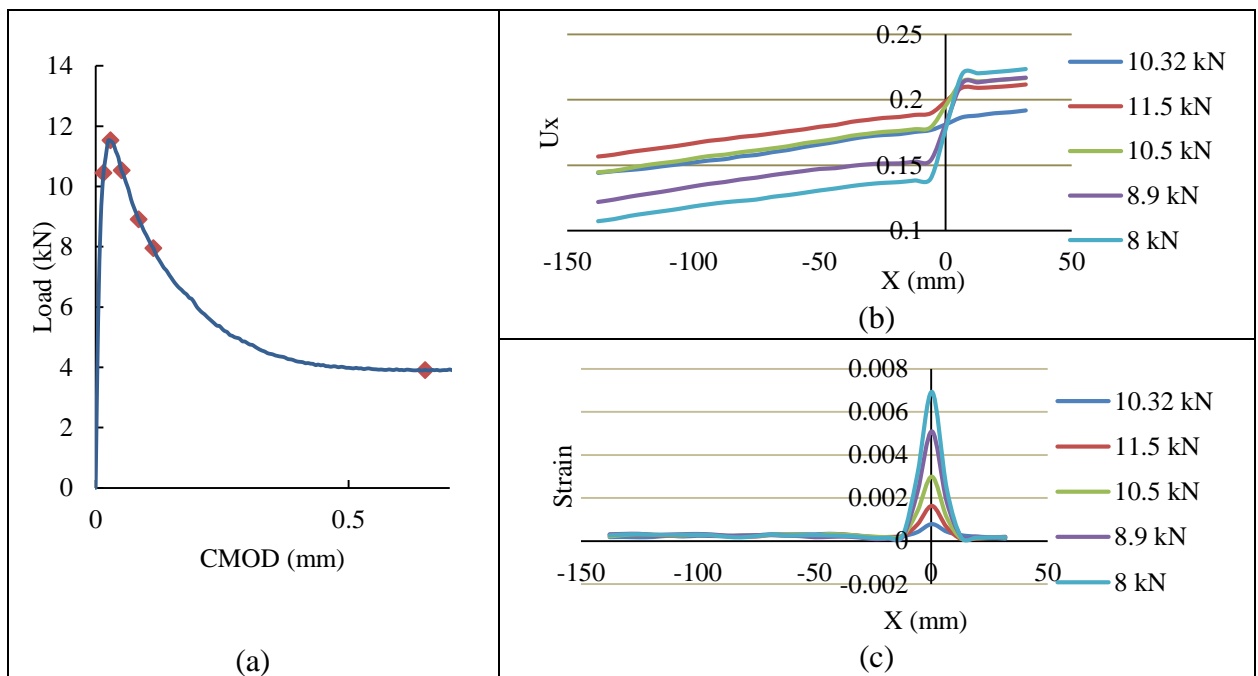


Fig 5.4: (a) Typical load response of 4 kg/m³ Polypropylene fibers; (b) displacement profile at line 1; (c) strain profile at line 1 at distinct load points

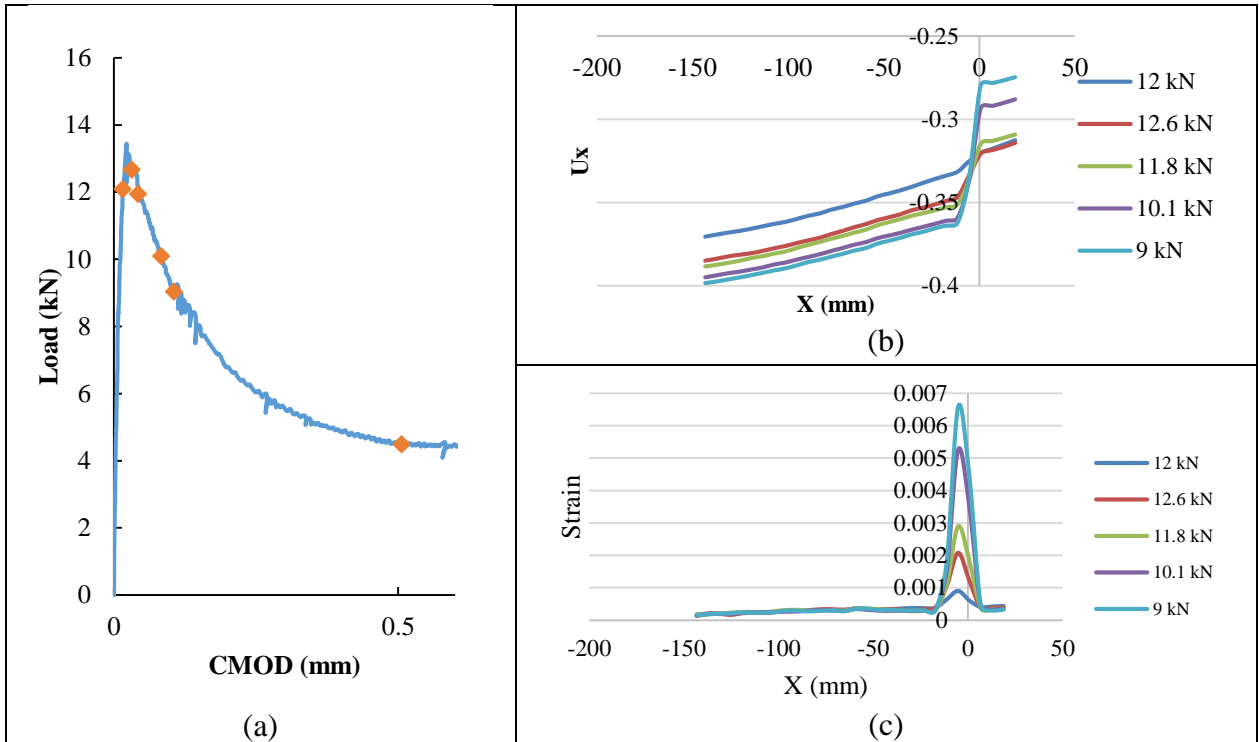


Fig 5.5: (a) Typical load response of 6 kg/m³ Polypropylene fibers (b) displacement profile at line 1; (c) strain profile at line 1 at distinct load points

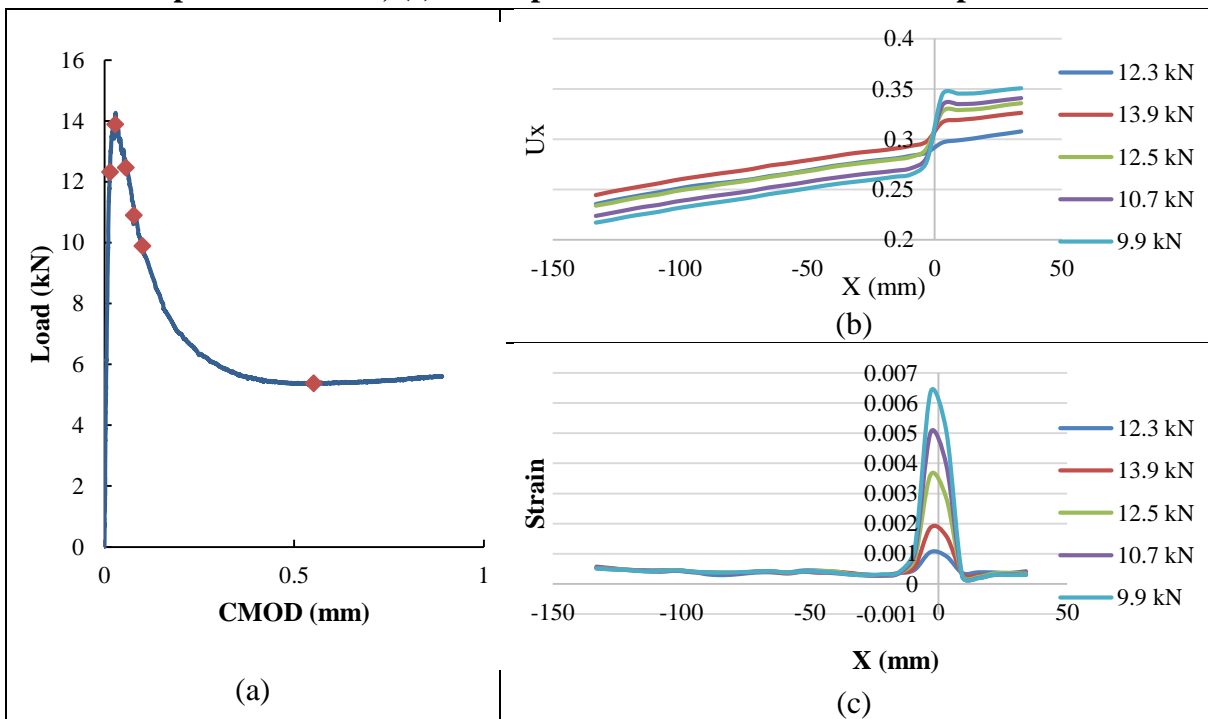


Fig 5.6: (a) Typical load response of 8 kg/m³ Polypropylene fibers (b) displacement profile at line 1; (c) strain profile at line 1 at distinct load points

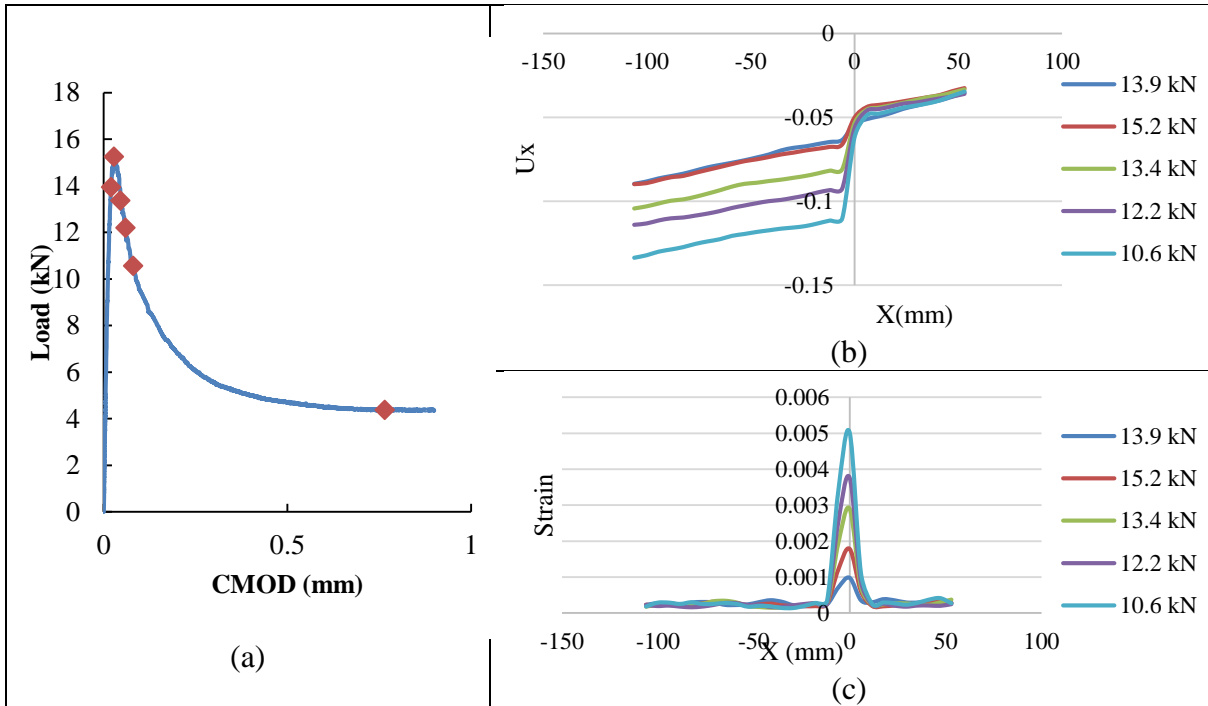


Fig 5.7: (a) Typical load response of 4 kg/m³ Nylon (b) displacement profile at line 1; (c) strain profile at line 1 at distinct load points

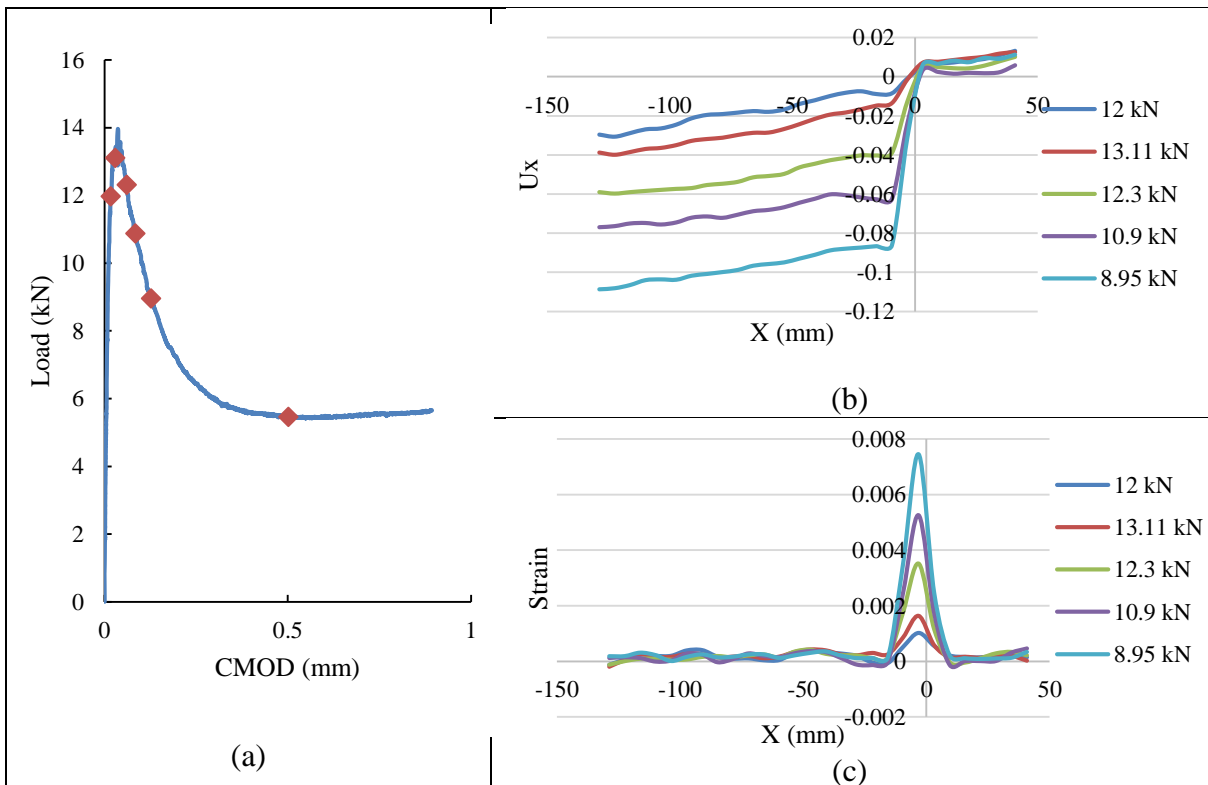


Fig 5.8: (a) Typical load response of 6 kg/m³ PP; (b) displacement profile at line 1; (c) strain profile at line 1 at distinct load points

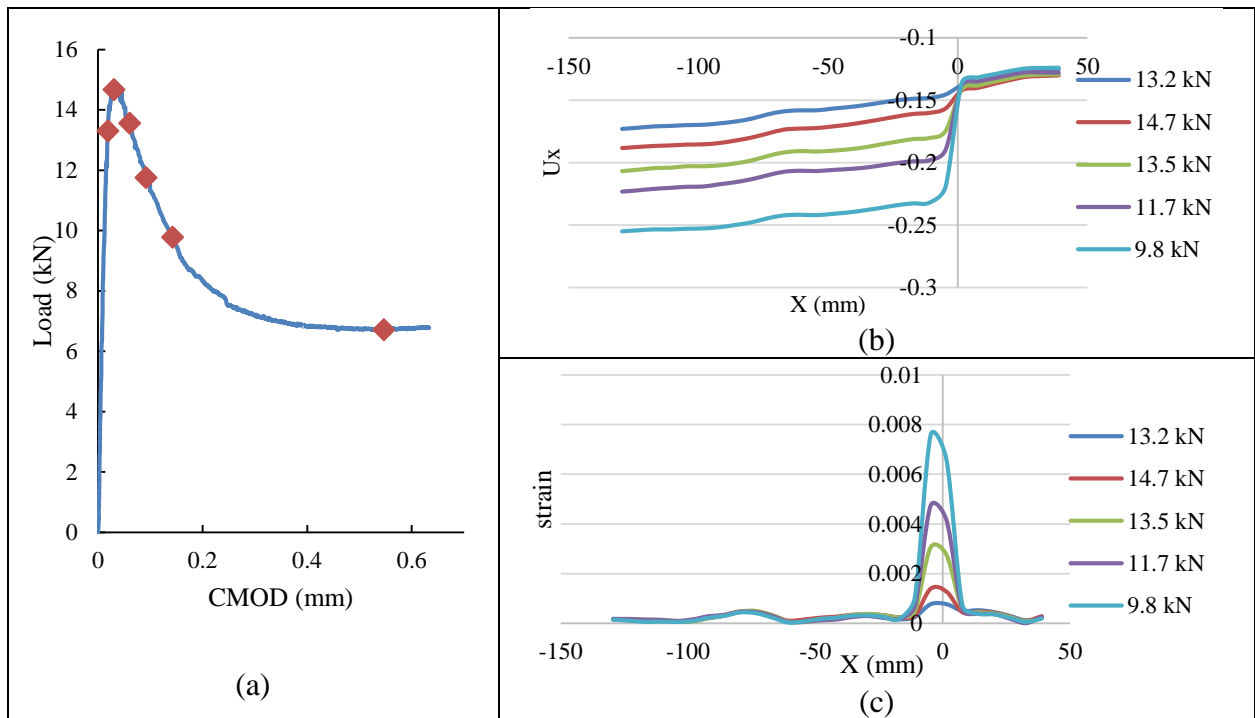
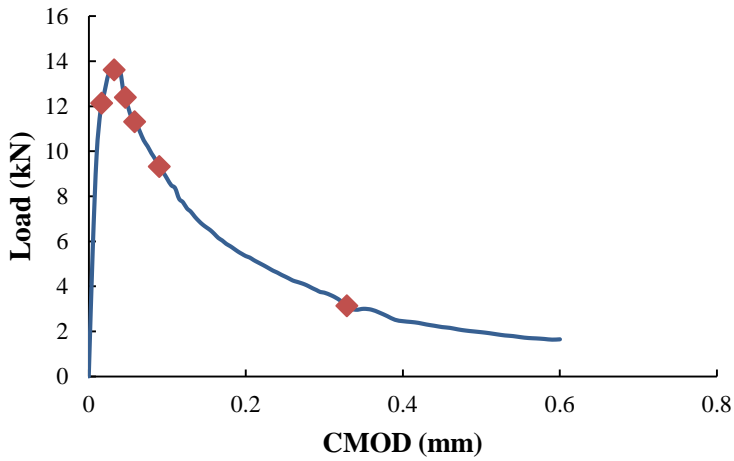


Fig 5.9: (a) Typical load response of 8 kg/m³ Nylon (b) displacement profile at line 1; (c) strain profile at line 1 at distinct load points

Typical result showing strain in the x direction (ϵ_{xx}) at five distinct point on the load response of specimen in the pre peak, close to the peak and in the post peak are shown in Fig 5.10 and 5.11 for 5 lines located at different depths relative to the notch. The respective loads are given in figure for control and specimens with 6 kg/m³ fibers. The distances of the lines above the bottom face of the beam are tabulated in the figure. The extent of crack propagation and the strain profiles associated with the crack are nominally identical for the control and fiber reinforced concrete. The propagation of crack in the material can be traced from the depth at which strain localization is observed. The results clearly indicate that in both control and synthetic fiber reinforced concrete even in the post peak, when the load drops by about 30-40% of the peak load, the crack does not propagate up to line 5 and the same can be observed in Fig 5.10 (e) and Fig 5.11 (e). The strains at line 5 even at load 5 are very small in magnitude and there is no indication of strain localization along the line. This suggests that the crack propagation in control and fiber reinforced concrete is nominally identical in the immediate post-peak associated with load drop after peak load.



Line No	Depth from Crack Tip (mm)
1	7.8
2	40
3	62.5
4	90
5	107

(a) Load CMOD of Control

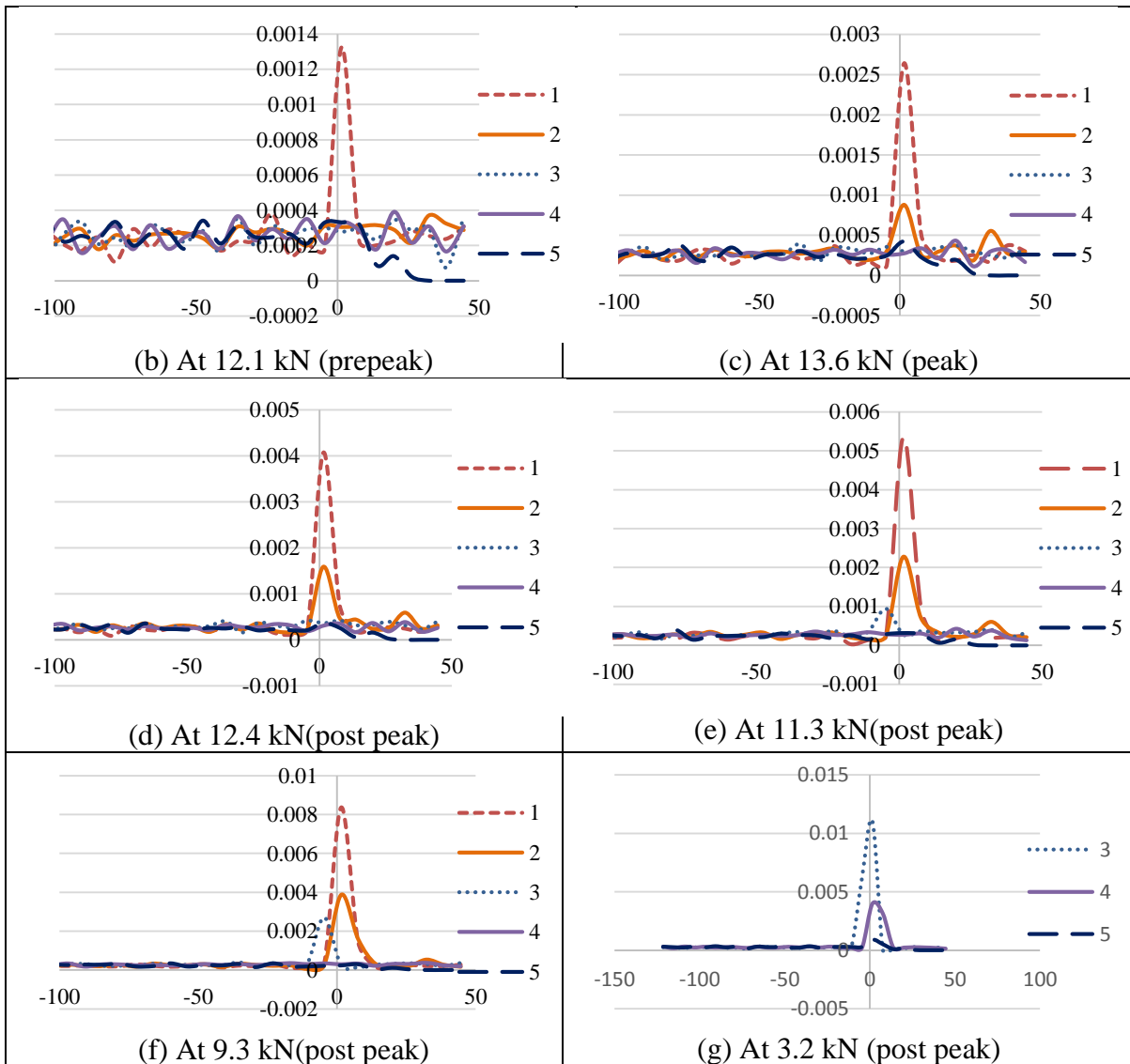
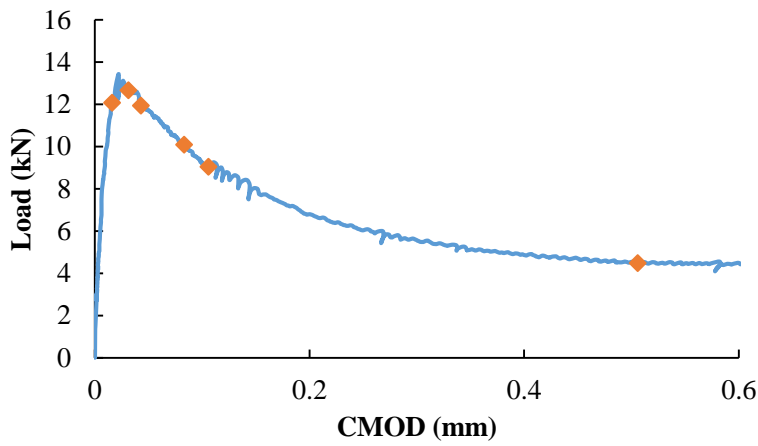


Fig 5.10 Variation of Strain value (ϵ_{xx}) on lines along the depth of section at distinct loads for control Specimen



Line No	Depth from Crack Tip (mm)
1	9
2	40
3	62.5
4	90
5	110

(a) Load CMOD of PP 6kg/m³

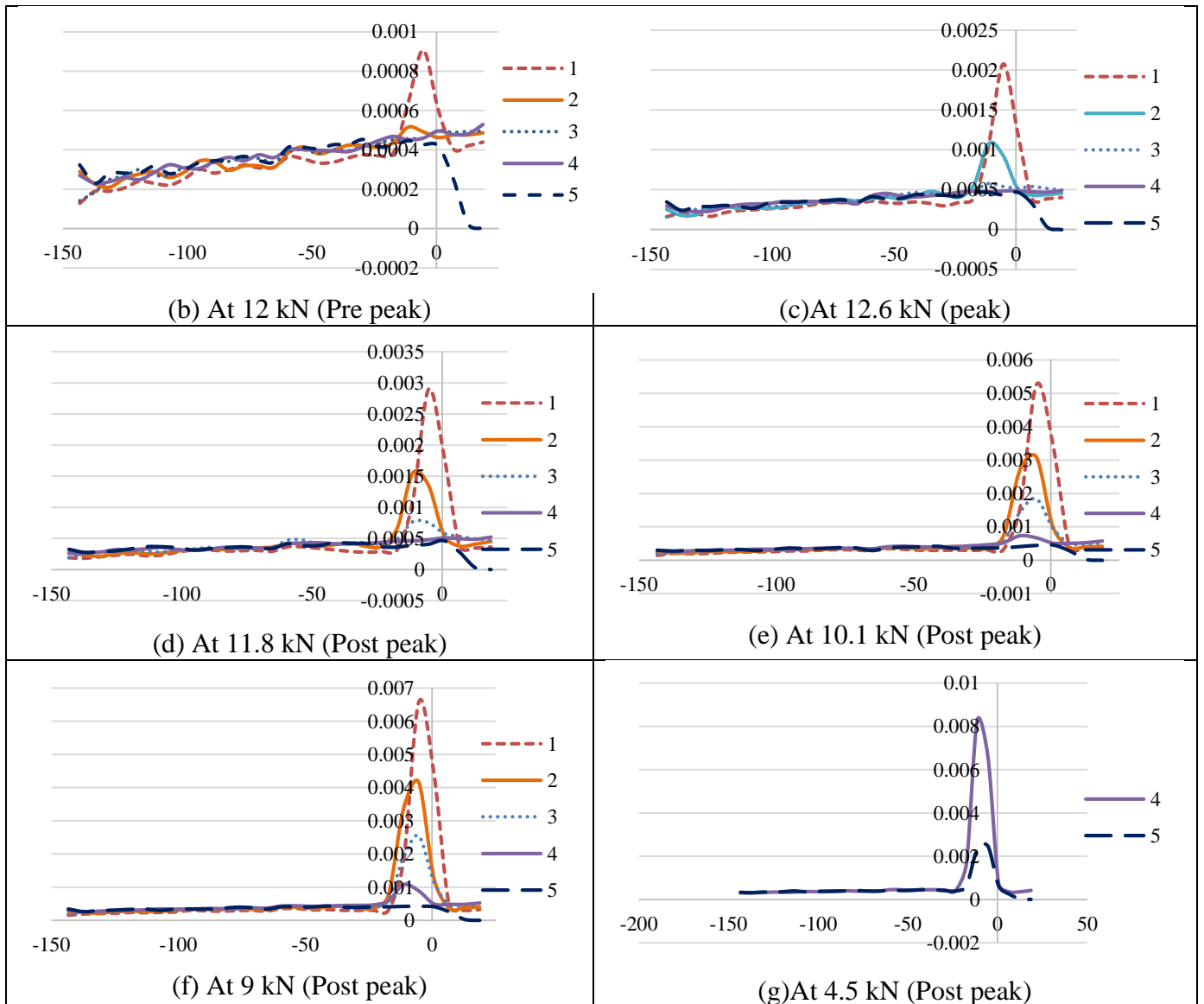


Fig 5.11 Variation of Strain value (ϵ_{xx}) on lines along the depth of section at distinct loads for polypropylene with 6 kg/m³ volume.

Differences in the crack propagation between control and FRC specimens are observed at larger CMOD openings. In the fiber reinforced concrete specimens, at a CMOD opening of 0.5 mm, strain localisation is evident at line 5. At the corresponding CMOD, the strain in line 5 in control specimens indicated very high values which were larger than 0.01.

5.4 Analysis of Results

The contribution of fibers result in the load arrest after an initial load drop in the immediate post-peak response. The increase in the total tensile resistance can be attributed to the increased resistance provided by additional fibers across the crack face with an increase in crack length and the additional stress due to increased resistance to crack opening displacement. An analysis of the influence of fibers on providing control of crack opening as the crack propagates into the matrix was performed by combining the results from DIC with the measured crack tip opening displacement (CTOD) obtained from a surface mounted gage at the tip of the notch. The depth of crack at any load was established from an analysis of ϵ_{xx} along horizontal lines located at different heights above the notch. The depth of the crack was established as the line at which the strain deviation produced by the observed localization exceeded by three standard deviations above the background trend. Plots of the crack depth estimated from strain analysis of DIC images and CTOD for the control and fiber reinforced concrete beams with 4, 8 kg/m³ are shown in Fig 5.12. The general trend in crack propagation for increasing crack opening indicates that initially there is very large increase in crack depth for a small increase in CTOD. Subsequently, the crack depth essentially does not increase significantly for large change in CTOD. This indicates that initially there is a crack propagation, while subsequently, there is opening of the crack. There are also significant differences in the crack depth for a given crack opening between control and fiber reinforced concrete. At small values of CTOD, there is significantly higher crack propagation in control specimens then in fiber reinforced specimens. This suggests that fibers influence the propagation of crack, wherein for a given crack opening, there a smaller crack in the fiber reinforced concrete.

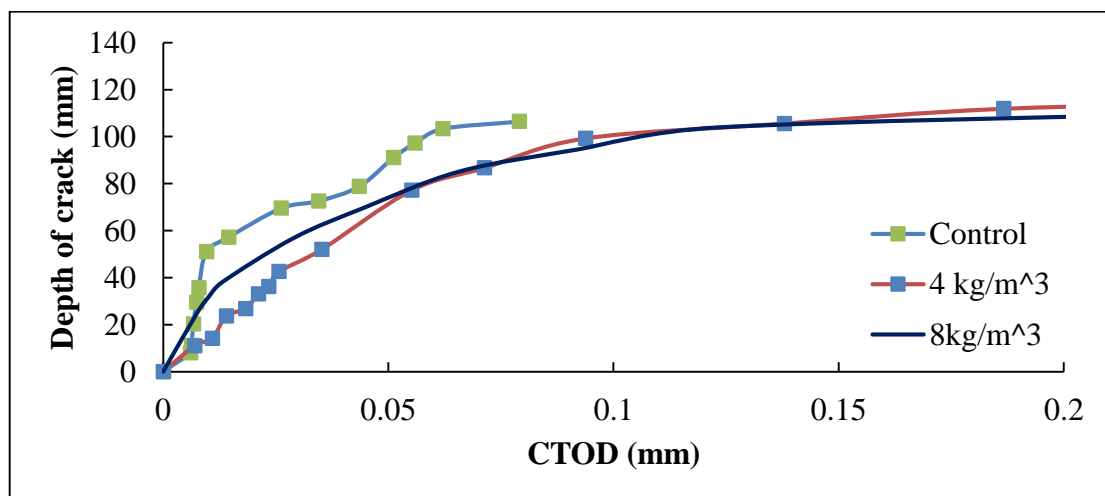


Fig 5.12 Crack Depth vs CTOD of typical SPFRC beams and control

The resistance to crack opening comes from either pull out of the fiber from the matrix or fiber extension which could ultimately lead to fiber fracture. The crack opening displacement at which the resistance to crack opening provided by the fibers provides additional crack bridging stresses, depends on the fiber content.

Examination of the failed surface revealed few fibers which exhibited breakage in addition to fibers pulled out from the matrix. The post-peak load response at the different volume fractions is associated with both breakage and pullout response of fibers from the concrete matrix averaged over the crack. During crack propagation, debonding and sliding contribute significantly to the pull out resistance of the fibers and hence to the total energy consumption when a large crack develops in the matrix. Fiber breakage is also observed to contribute to the energy dissipated during crack propagation.

5.5 Summary and Findings

The results of the experimental investigation reveals that at low volume fractions, up to 8 kg/m^3 , once the matrix has cracked, initial part of the load response is controlled by crack propagation. In the initial softening part of the load response, there is very rapid increase in crack length for a small change in the crack opening. This part of the load response is identical for control and the fiber reinforced concrete specimens and there is little or no influence of fibers. On increasing the deflection, the load response in fiber reinforced beams exhibits a load recovery. The deviation from the softening response of control beams and the load recovery response is influenced by the fiber volume fraction. In the load recovery part of the load response, the crack growth is arrested by the fibers. There is a small increase in crack length as the crack opening continues to increase. The post-cracking resistance is primarily attributed to fiber pull-out.

Chapter 6

Analytical Model

6.1 Introduction

The bending failure of concrete beams may be modeled by the development of a fictitious crack in an elastic layer with a thickness proportional to the beam depth. A brief review about use of various types of stress crack opening (σ - w) relationship was presented in section 2.2. The cracked hinge model proposed by Olesen [12] was used for development of analytical model. The basic idea of the cracked hinge is to model a part of the beam close to the propagating crack as a layer of independent spring elements. These spring elements are formed by incremental horizontal strips, and are attached at each end to a rigid boundary (Fig 6.1). In this way the disturbance of the strain field, caused by the presence of the crack, is confined to take place between the rigid boundaries. Each rigid boundary may translate and rotate such that it may be joined with an uncracked beam modeled according to the classical beam theory. The constitutive relation of the spring layer is the same as that of the FRC, and according to the fictitious crack method, given by

$$\sigma = \begin{cases} E\varepsilon & \text{Precrack State } (w = 0) \\ \sigma_w(w) = g(w) * f_t & \text{cracked State } (w > 0) \end{cases}$$

where E = elastic modulus; ε = elastic strain; $\sigma_w(w)$ denotes the stress-crack opening relationship; and f_t = uniaxial tensile strength. The shape of the stress-crack opening relationship is defined by some function $g(w)$ of the crack opening w , normalized such that $g(0)=1$.

For FRC materials the stress crack open relationship is rather complex. It depends on amount, type of fibers, and age of matrix and pullout of fibers. The hinge model by Olesen starts by adopting a nonlinear hinge with finite length ‘ s ’ usually a factor of depth as shown in Fig 6.1 within which the stress transfer through fibers is assumed to be taking place.

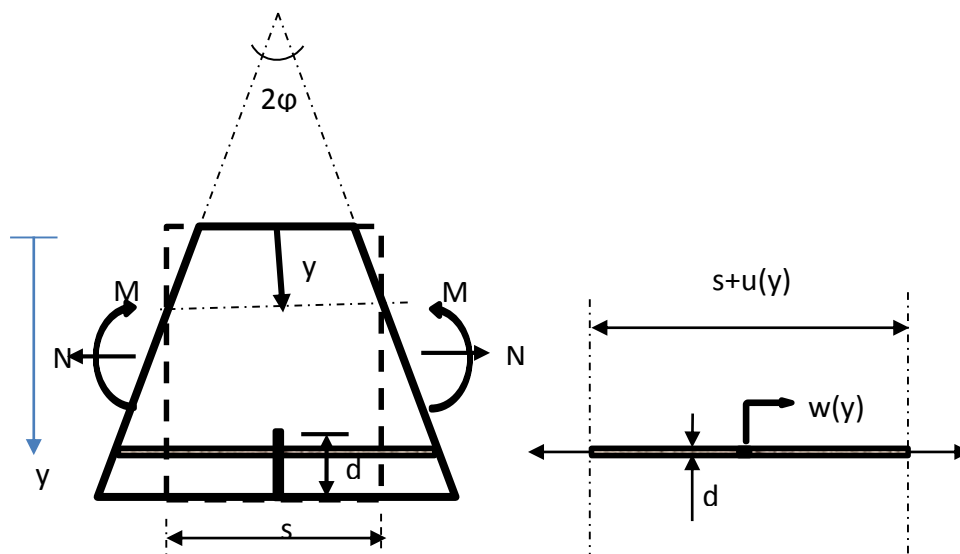


Fig 6.1 Geometry, Loading, and Deformation of Cracked Incremental Horizontal Strip of Hinge

The deformation of the hinge is described by half the angular deformation and the depth of the neutral incremental strip y_0 . It proves convenient to introduce the mean values of the curvature and the distribution of longitudinal strains κ^* and ε^* , respectively given by

$$\kappa^* = 2\phi/s \text{ and } \varepsilon^*(y) = (y-y_0)\kappa^*. \quad (5.1)$$

The deformation of an incremental strip is given by $u(y) = s + \varepsilon^*(y)$, in the case where the strip has cracked the deformation, $u(y)$ may also be obtained as the sum of the elastic deformation of the strip and the crack opening

$$u(y) = s\varepsilon^*(y) = s \frac{\sigma_w(w(y))}{E} + w(y) \quad (5.2)$$

From the equations 5.1 and 5.2 it can be written as

$$\sigma_w(w(y)) = (2(y - y_0)\phi - w(y)) \frac{E}{s} \quad (5.3)$$

The bilinear stress crack model assumed by Olesen is shown in Fig 6.2 and the shape of the stress-crack opening relationship is defined by some function $g(w)$ of the crack opening w with slopes of lines and their offsets on ordinate axis which represent normalised tensile strength.

$$g(w) = b_i - a_i w = \begin{cases} b_1 - a_1 w & 0 \leq w < w_1 \\ b_2 - a_2 w & w_1 \leq w \leq w_2 \end{cases} \quad (5.4)$$

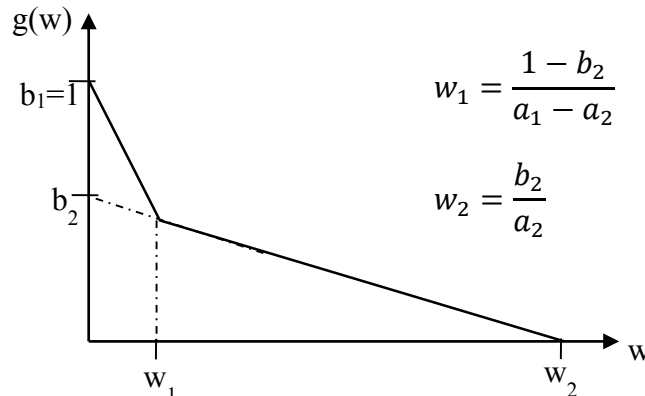


Fig 6.2 Definition of Parameters of Bilinear Stress-Crack opening relationship

From equation 5.3 and 5.4 $w(y)$ and $\sigma_w(w(y))$ for each value of i , the following solutions are obtained:

$$w(y) = \frac{2(y-y_0)\phi - \zeta_i}{1 - \beta_i} \quad (5.5a)$$

$$\sigma_w(w(y)) = \frac{\zeta_i - 2(y-y_0)\phi \beta_i}{1 - \beta_i} \frac{E}{s} \quad (5.5b)$$

where

$$\beta_i = \frac{f_t a_i s}{E}; \quad \zeta_i = \frac{f_t b_i s}{E} \quad i \in 1,2$$

The solutions given in (5.5) establish in analytical form the crack opening profile $w(y)$ and the stress distribution in the cracked part of the hinge $\sigma_w(w(y))$ as functions of the hinge deformations w and y_0 . As the crack propagates from the bottom of the hinge, the Stress distribution changes through three distinct phases (Fig 6.3). The crack-opening profile is divided into different intervals of i .

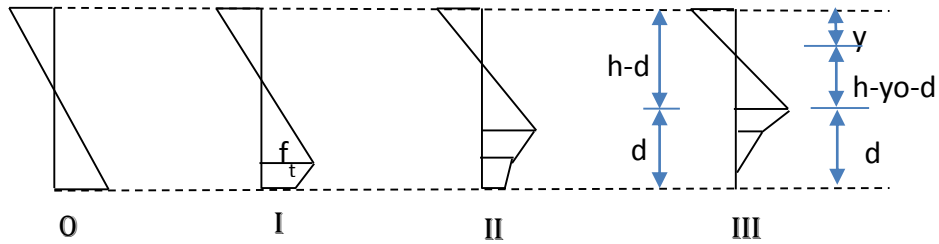


Fig 6.3 Distinct Phases of Stress Distribution during propagation of the crack in the section

Now complete stress distribution for all phases of pre and post cracking was established where phase 0 representing pre crack stress state and others post crack stress states. Now by equating sectional stresses with external applied force N , a relation between moment and curvature was established in the form of closed form equations. To make the derivation simple, following normalisation were introduced.

$$\mu = \frac{6M}{f_t h^2 t} \quad \rho = \frac{N}{f_t h t} \quad \theta = \frac{hE}{s f_t} \varphi \quad \alpha = \frac{d}{h} \quad (5.6 \text{ a-d})$$

The explicit equations for moment rotation with derivations are given in annexure I.

6.2 Load deflection curve from moment curvature analysis

Load-deflection curve can be calculated from given moment rotation relationship. Consider a beam with rectangular cross-section with depth h , width t and span L . The span of the beam is divided into three parts with a centre nonlinear hinge and elastic beam on the either side of the hinge as shown in Fig 6.4. The deflection v is calculated as a sum of elastic deflection and crack deflection (i.e. $v = v_e + v_c$.)

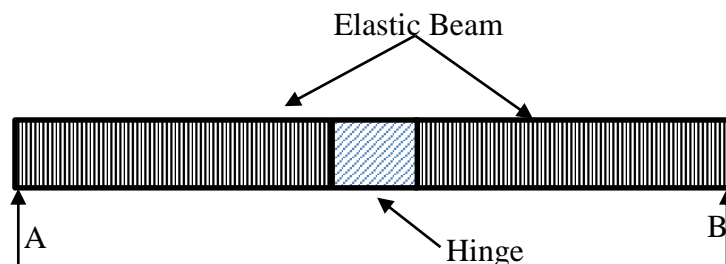


Fig 6.4 Model representation of simply supported beam after cracking

As per classical beam theory, the elastic deflection v_e is given by equation 5.7 (a) and deflection from the nonlinear hinge can be considered as rigid body rotation and is given by equation 5.7(b) but the hinge deflection is sum of deflection due to crack and elastic deformation of hinge, hence to get deflection from crack only elastic deformation should be subtracted from hinge deflection and is given by equation 5.7(c)

$$v_e = \begin{cases} \frac{ML^2}{12EI} & \text{for centre point loading} \\ \frac{ML^2}{9EI} & \text{for third point loading} \end{cases} \quad (5.7a)$$

$$v_h = \phi * L/2 \quad \text{and} \quad (5.7b)$$

$$\phi_c = \phi - \phi_e \text{ where} \quad (5.7c)$$

Equation (5.7) upon normalisation as shown in Eq (5.8a) the normalised elastic deflection and crack deflection is be given by equations 5.8b and 5.8c

$$\delta = \frac{2v}{L} \frac{hE}{sf_t} = \frac{2v}{L} \frac{\theta}{\phi} = \delta_e + \delta_c \quad (5.8a)$$

$$\delta_e = \begin{cases} \frac{L}{3s} \mu(\theta) & \text{for centre point loading} \\ \frac{4L}{9s} \mu(\theta) & \text{for third point loading} \end{cases} \quad (5.8b)$$

$$\delta_c = \theta_c = \theta - \mu(\theta) \quad (5.8c)$$

Total deflection is then given by

$$\delta = \delta_c + \delta_e = \begin{cases} \theta + \left(\frac{L}{3s} - 1\right) \mu(\theta) & \text{for centre point loading} \\ \theta + \left(\frac{4L}{9s} - 1\right) \mu(\theta) & \text{for third point loading} \end{cases} \quad (5.9)$$

Load is calculated for the given loading type from the known moment from equation

$$P(\theta) = \begin{cases} \frac{2}{3} \frac{f_t h^2 t}{L} \mu(\theta) & \text{Centre point loading} \\ \frac{f_t h^2 t}{L} \mu(\theta) & \text{Third point loading} \end{cases} \quad (5.10)$$

The load deflection curve obtained for a beam with adopted parameters (indicated in plot) is shown in figure 5.2.2.

From Fig 6.5 the following inferences can be drawn. The response of the member becomes nonlinear after cracking but still the load continues to increase. The peak load of the member is influenced by a_1 which is clear from Fig 6.5(a) and (b) unless the value of b_2 is very high such that fibers start resisting loads immediately after cracking may be a situation related to higher volume fraction of fibers. From Fig 6.5 (c) it is evident that a_2 has no influence on peak and initial post peak slope rather it has influence over the slope after the initial drop in the post peak load response.

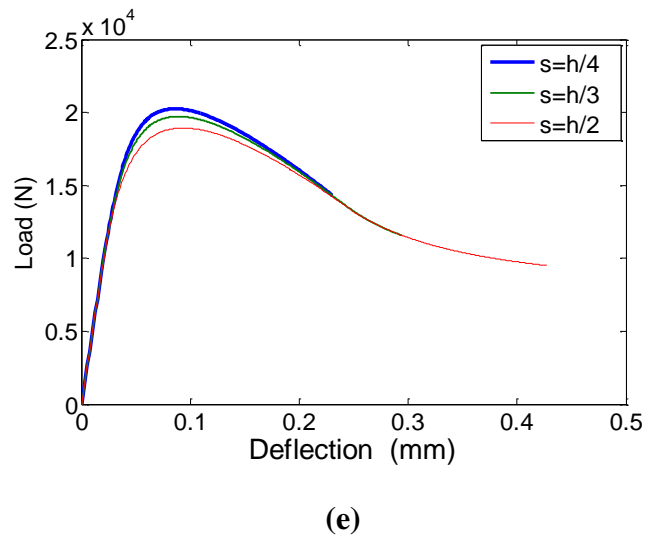
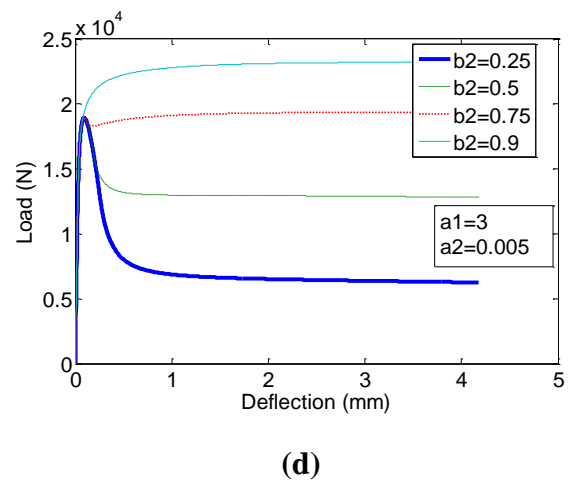
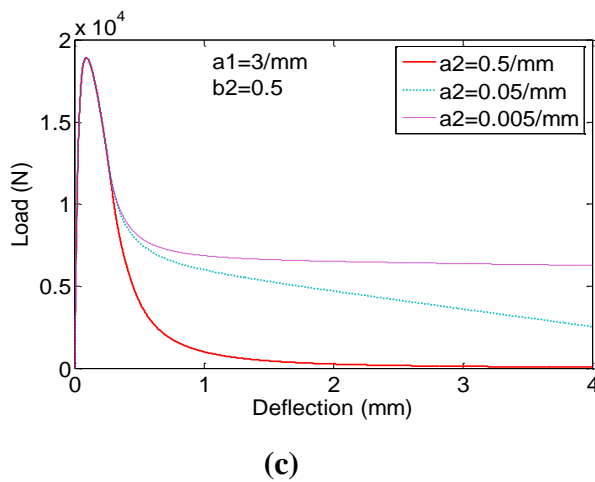
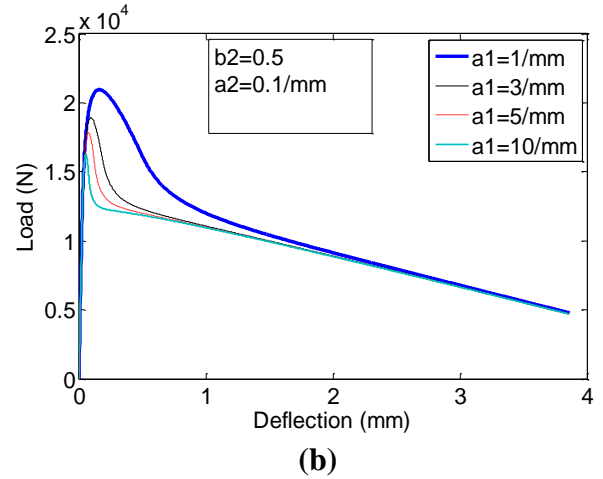
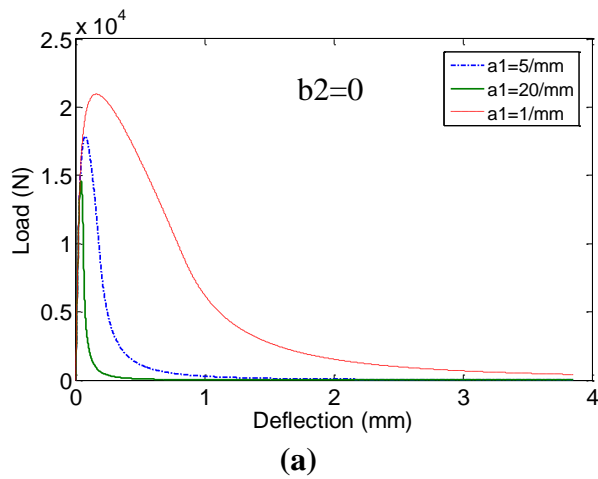


Fig 6.5 Load deflection curves by using bilinear stress crack opening relationship

From Fig 6.5(d) we can conclude that b_2 regulates the drop in load after peak. Fig 6.5 (e) shows the effect of hinge length. As the hinge length increases the nonlinearity after cracking also increases but peak load is reduced.

Results indicate that the choice of a bilinear stress crack opening relationship is able to predict both a drop in load after peak load and a strain hardening type load response depending on the choice of parameters associated with the idealized stress crack opening relationship. In the cases where the load response exhibits either a monotonic decrease following a distinctive peak, the predicted load response exhibits a rapid decrease initially following the peak load followed by a more gradual rate of decrease in load with increasing deflection. In the case of hardening response, the load carrying capacity essentially remains constant after peak.

The assumed bilinear idealization of the cohesive model does not allow for predicting the load recovery after the initial load drop in the post-peak, which is observed in SPFRC specimens (Fig 6.6); the observed experimental response shows a load recovery after the initial drop. Prediction of the observed experimental response therefore requires a multi-linear stress-crack opening relationship.

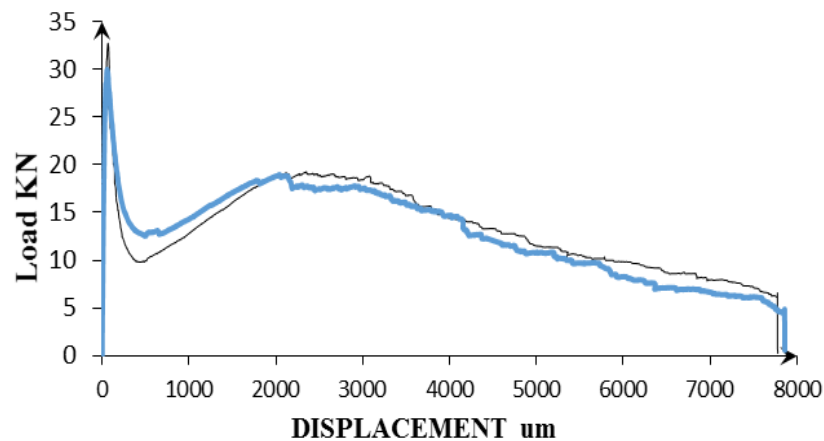


Fig 6.6 Experimental Load deflection curves

6.3 Proposed Analytical Formulation for multi-linear softening

In order to capture the load recovery and a second peak (or subsequent peak points) after initial post-peak softening, a multi linear stress crack opening is required. Unlike the bilinear case, the multi-linear stress crack opening relationship may not be readily amenable to deriving closed form solutions. In order to simplify the algorithm, the formulation and definition of stress crack opening relationship has been modified keeping the background mechanism and assumptions identical to the Olesen model. Multi linear Stress crack opening relationship can be described with coordinates as shown in Fig 6.7, where b axis is described as a fraction of f_t (such that b values will be always less than 1) and corresponding stress will be b times f_t , the stress distribution for the given relationship is shown in Fig 6.8.

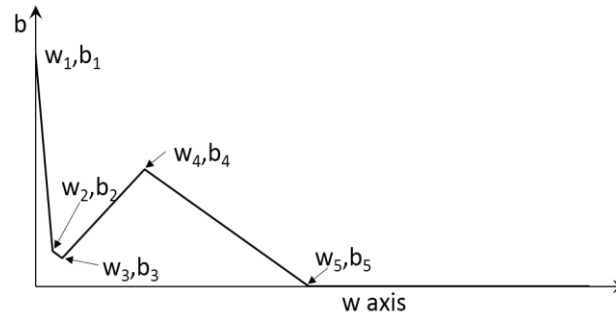


Fig 6.7 Definition of Parameters of Multi linear Stress-Crack relationship

A procedure for obtaining the moment-curvature relationship considering the multi-linear stress-crack opening relationship is presented below. The stress distribution in a section of height h , with crack tip located at a depth d , is shown in Figure 5.3.2. The stress distribution in the cracked portion reflects the multi-linear cohesive stress-crack opening relationship shown in Figure 5.3.1.

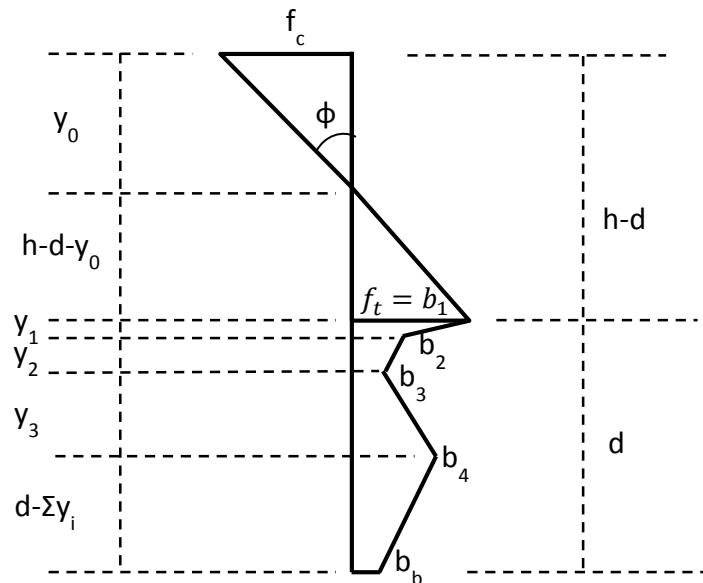


Fig 6.8 General Stress distribution for multi linear case

From compatibility relationship,

$$f_c = \frac{f_t \cdot y_0}{h-d-y_0} \quad (5.9)$$

At the crack tip, the response is elastic (the strain should be elastic) and stress will be equal to tensile strength (i.e. $\sigma_w = f_t$). Therefore, keeping y as $h-d$ and $\sigma_w = f_t$ in equation 5.3 gives

$$d + y_0 = h - \frac{s \cdot f_t}{2\phi \cdot E} = h - \frac{h}{2\theta} \quad (5.10)$$

For a given stress crack opening relationship, using equation 5.3 at start point and end point of a line and their difference gives a relation between k_i and normalised rotation as follows. (See Annexure III for detailed derivation).

$$k_i = (b_{i+1} - b_i) + (w_{i+1} - w_i) \frac{E}{s f_t}, \quad (5.11)$$

where $k_i = \frac{2\theta y_i}{h}$

Slope of the lines are given by

$$m_i = \frac{b_{i+1} - b_i}{w_{i+1} - w_i} \in i = 1 \text{ to } n - 1 \quad (5.12)$$

where 'n' represents number of coordinates

In the Equation 5.11, k_i is normalised y_i , which is independent of rotation. Then all transitions rotations (θ_i) are found by force equilibrium as depth, now can be expressed as summation of y_i and is given as in equation 5.12 where transition rotation is rotation at which the slope of line changes.

$$\theta_i = \frac{1}{2} \left[\left(1 + \sum k_i \right) + \left(1 + \sum (k_i (b_{i+1} + b_i)) \right)^{1/2} \right] \quad (5.13)$$

After evaluating transitions the normalized rotation is gradually increased, when $\theta < 1$ (pre crack state), $\mu = \theta$ and for $\theta > 1$, if we observe Fig 6.8 for a given rotation, stresses distribution above the crack can be expressed in terms of α using equations 5.9 and 5.10. Stress distribution below the crack is known except in the bottom $d - \sum y_i$ portion. Stress at bottom (b_b) is expressed in terms of α using equation 5.3 by substituting $y=h$ and calculating width at bottom by using slope of the corresponding line given by equation 5.12.

$$b_b = \frac{(1+2\alpha\theta) + j_i(b_i - m_i w_i)}{1 + j_i} \quad \text{where } j_i = \frac{E}{m_i s f_t} \quad (5.14)$$

The requirement of force equilibrium (the total force on the section is zero) results in a quadratic equation in terms of α , the depth of crack. The depth of neutral axis is obtained from equation 5.10. Moment of stresses is used to calculate the normalised moment. The moment curvature relationship is obtained by repeating the exercise for different values of curvature. (See Annexure II for detailed derivation).

The accuracy of the proposed methodology and ability of the numerical procedure to predict the moment curvature relationship of a cracked beam was evaluated by comparing with the predictions obtained from the Olesen model using the bi-linear stress-crack opening relationship. Fig 6.9 shows an exact match between the moment-curvature relationships for the bilinear stress crack opening relationship parameters predicted by the closed-form analytical formulation given by Olesen and the current formulation.

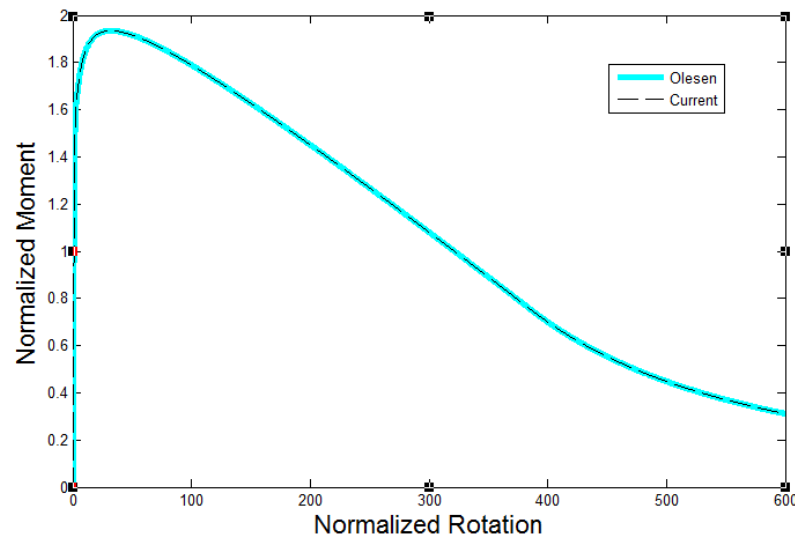


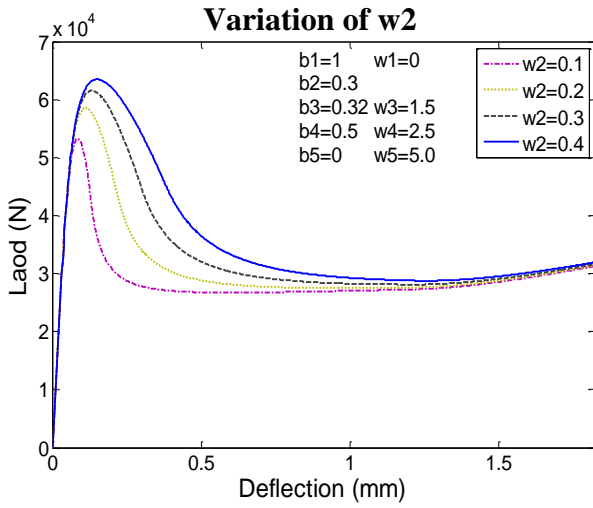
Fig 6.9 Comparison of Moment Rotation relationship for Olesen formulae and current formulae

The influence of various stress crack opening parameters by considering a tetra linear stress crack opening relationship as shown in Fig 6.7 with 5 points (ten parameters) was studied. Out of ten parameters initial coordinate is fixed with crack opening as zero units and stress equals to tensile strength. The ordinate value of last point is set to zero and remaining seven parameters are varied and their influence was plotted in Fig 6.10.

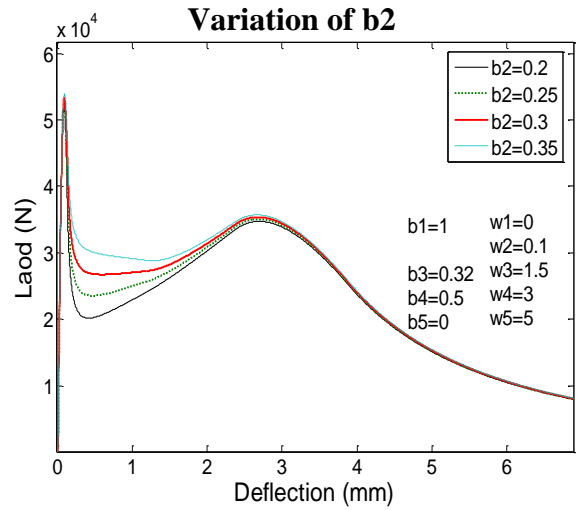
From Fig 6.10(a) and (b) it is clear that coordinate defined with b_2, w_2 has effect on peak load, post peak load drop and post peak slope of load deflection response. w_2 seems to have more influence on peak load and post peak slope whereas b_2 is playing major role in regulating load drop.

From Fig 6.10 (c) and (d) it is evident that coordinate defined with b_3, w_3 has no effect on peak load, load drop and initial post peak slope of load deflection response rather w_3 offsets the commencement of load recovery as we can observe in figure 5.3.4 (c) and b_3 influences recovery load and load recovery commencing point.

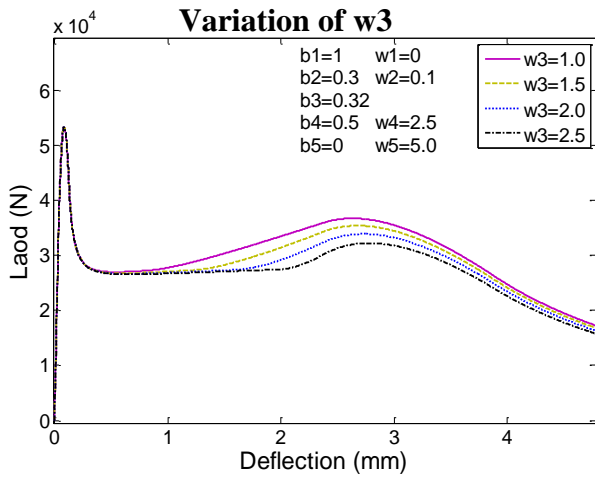
From Fig 6.10 (e) that w_3 is offsetting subsequent peak load deflection and has little contribution towards recovered load peak and from Fig 6.10 (f) we can infer that b_4 influences the subsequent peak load and from Fig 6.10 (g) it can be concluded that w_5 has its major influence on the tail part of load deflection after subsequent peak load.



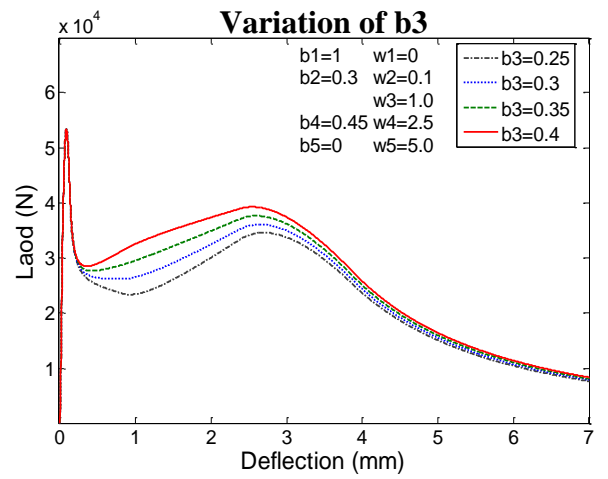
a)



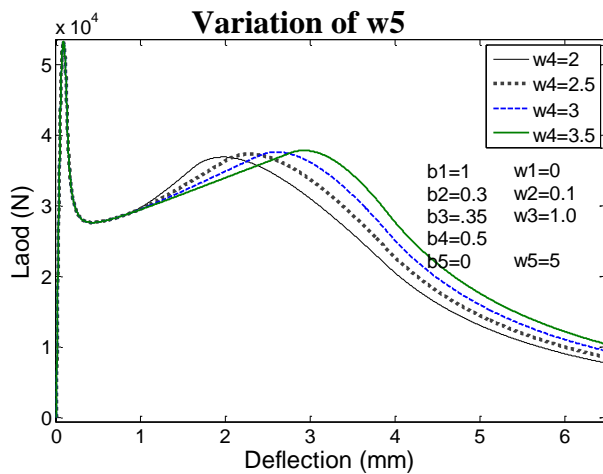
(b)



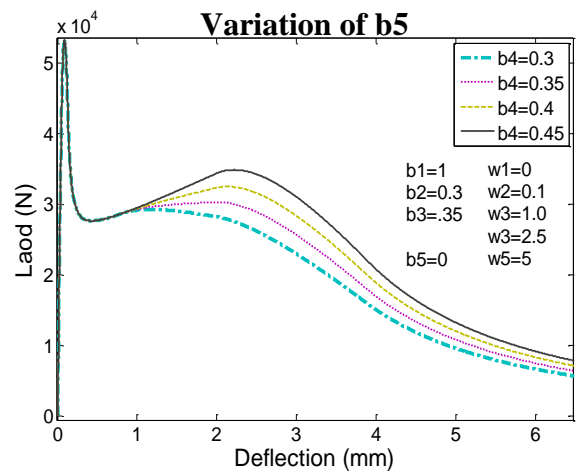
(c)



(d)



(e)



(f)

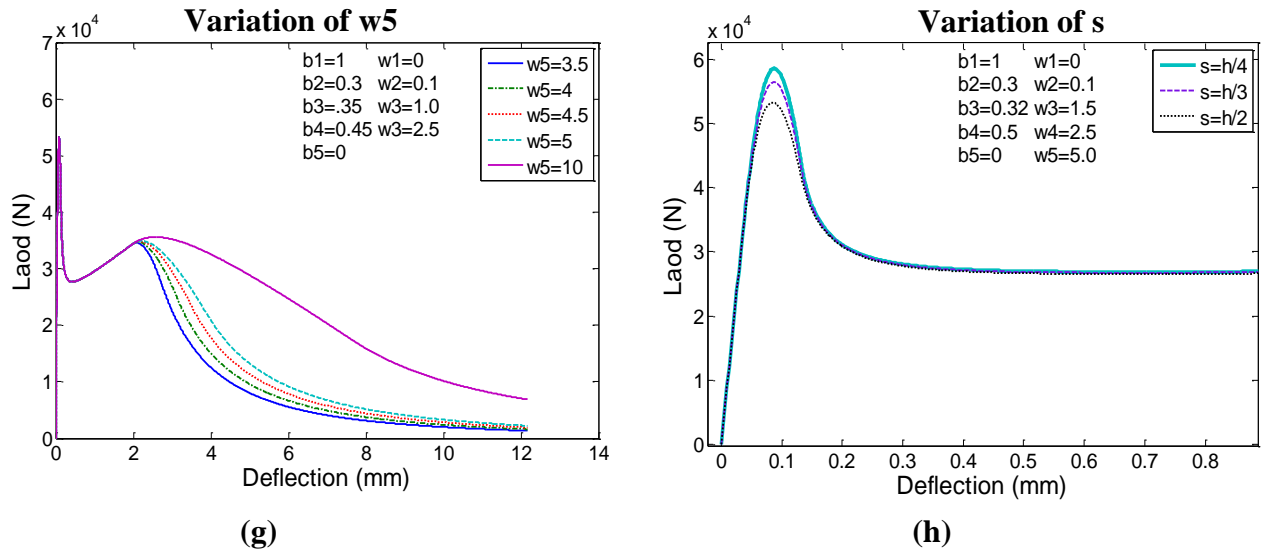


Fig 6.10 Load deflection curves by using tetra linear stress crack opening relationship

6.4 Inverse analysis

The crack hinge model provides a conceptual framework to interpret the flexural response of a beam in terms of a propagating crack with the crack closing stresses provided by fibers bridging the crack. In the previous sections the forward analysis for predicting the flexural load response using the crack hinge model with known cohesive stress-crack opening relationship has been performed. The cohesive crack closing stresses on the load response has been shown to have a significant influence on flexural the load response, from the peak load to the shape of the post-peak load response. It is established that the tensile strength and the initial slope of the cohesive stress-crack opening relationship influence the peak strength in flexure. Further, the load recovery portion of the post-peak load response has been shown to be totally the contribution of fibers bridging the crack. The measured response in flexure therefore provides a means for determining the cohesive stress-crack opening relationship.

To determine the cohesive stress-crack opening relationship from the measured flexural response an inverse analysis algorithm has been developed in which the experimentally obtained load deflection response was given as input and the difference with the predicted load response using the hinged crack is minimized. The difference between the two responses was minimized in the least squares sense. An objective function of the normalized squares of residuals for the peak load and the load response was developed.

$$\text{Norm} = |((P_u^{\text{exp}} - P_u^{\text{theoretical}}) / P_u^{\text{exp}})^2 + \sum_i ((P_i^{\text{exp}} - P_i^{\text{theoretical}}) / (P_i^{\text{exp}}))^2|$$

where P_u^{exp} and $P_u^{\text{theoretical}}$ and the peak loads obtained from the experiment and from the numerical model, respectively and P_i^{exp} and $P_i^{\text{theoretical}}$ are the i^{th} loads in the experimental and numerically predicted load responses at corresponding values of deflection, respectively.

A multilinear cohesive stress-crack opening relation of the form shown in Fig 6.7 was assumed. The parameters of the cohesive relationship were optimized to minimize the least square residual. A two-step inversion strategy was developed to separately optimize the tensile strength and the initial softening part of the cohesive behaviour. As the initial part of load deflection response is highly dependent on matrix properties, it was found to be highly sensitive to f_t and initial slope of stress crack relation and hence this part of load response was optimized separately by considering load deflection relationship up to a deflection of 0.3 mm. In first step the tensile strength (f_t) and slope of initial line of stress crack opening relationship by changing b_2 using the load response including the initial softening up to a displacement of $_$ mm. In the next step, the value of f_t obtained in the previous step was kept fixed while the other cohesive values at predefined crack openings were optimized.

The inversion procedure was implemented numerically in Matlab®. In Matlab®, constrained function minimization algorithm was used in which, constraints were applied on crack opening parameters and tensile strength of concrete. In the first step of optimization, considering the load deflection response up to 0.3 mm, the value of a_2 was fixed at 0.06 mm as it is observed that the peak is attained before an opening of 0.06 mm. The tensile strength f_t was kept fixed and the value of b_2 obtained in the first step was used as an initial guess in the next step. Value of b_2 was not fixed in the second step as it was observed to have an influence on the point of load recovery in the post-peak load response. In second step the crack opening values are predefined with a regular interval considering the sensitivity of load deflection diagram and corresponding stress values were found so as to get good match and predefined opening values also makes it easy to compare the crack bridging stresses developed by different fiber volumes.

The match between experimental and analytically developed load deflection response and corresponding stress crack opening relation for control and SPFRC and SNFRC beams with 6 kg/m³ are shown in Figures $_$. The results of all the beams tested are given in Annexure III. It can be seen that a very close match between the experimental and the predicted load response is obtained. While the cohesive stress-crack opening relationships for the control specimen exhibits a monotonic decrease in stress with crack opening, the FRC exhibits a hardening type behavior with increasing crack opening after an initial decrease following the initial post-peak softening.

The cohesive stress-crack opening relationships obtained from the inversion analysis are also plotted in Fig 6.11 and 6.12. A comparison of the distinctive points of the cohesive stress response obtained from the control, SPFRC and SNFRC is shown in Table 6.1 and 6.2. It can be observed that the stress crack opening relation is not affected up to an opening of 0.1 mm and there is deviation in the stress response after a crack opening of 0.1 mm due to crack closing stresses provided by fibers. Crack closing stresses increase after a crack opening of about 0.1 mm and the increase is in proportion with fiber volume for both FRC except for SPFRC with 4 kg/m³. However, it may be noted from Table 6.1 that the average flexural strength of the same is low, which results in higher values of the stresses in the cohesive response on the normalized scale.

On comparing Fig 6.11 and 6.12, while the stresses in both FRC are increasing after a crack opening of 0.1 mm, the increase in SPFRC is higher than that in SNFRC. SNFRC however exhibits a clear trend in an increase in closing stresses with fiber volume. This deviation from the initial softening response is observed at a smaller value of crack opening in SNFRC indicating the early activation of fibers upon crack opening.

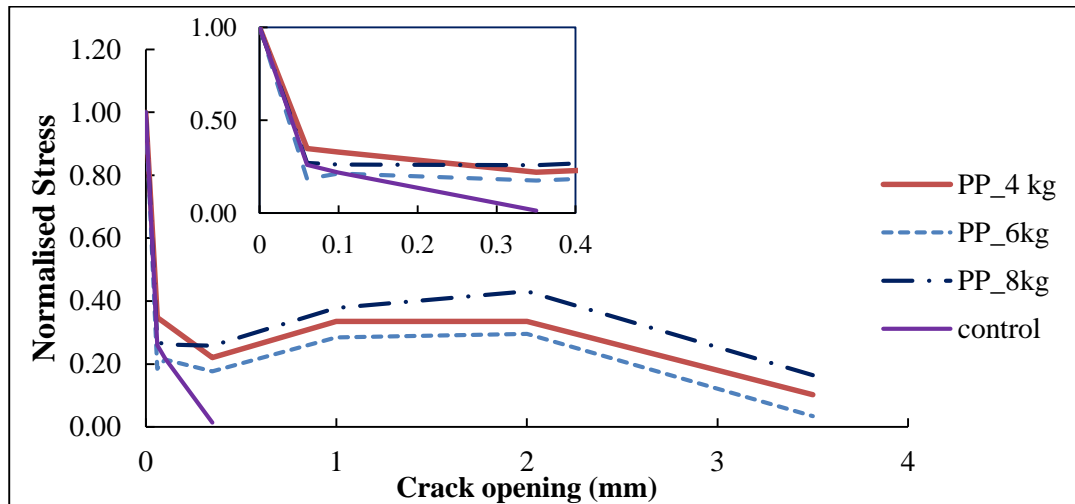


Fig 6.11. Stress Crack opening relationship of SPFRC beams

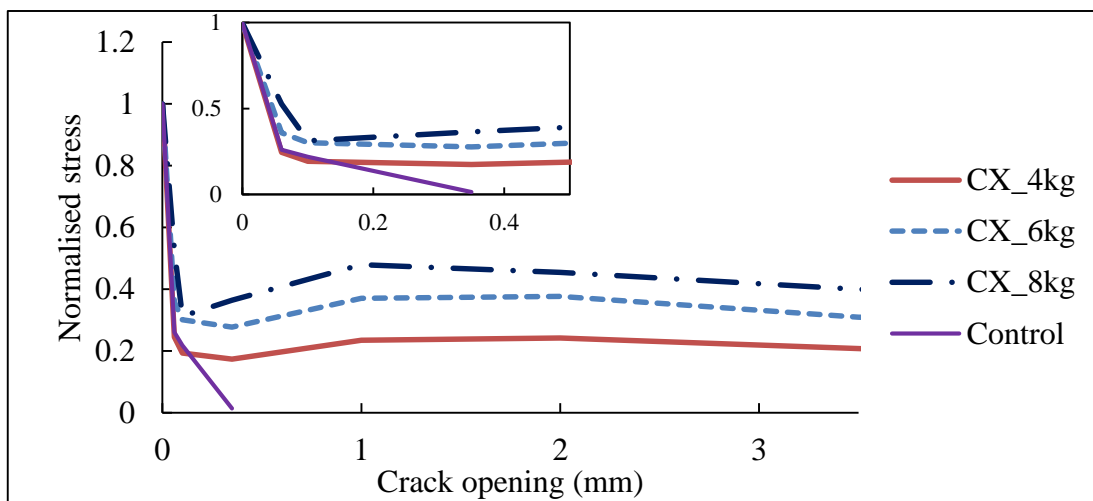


Fig 6.12 Stress Crack opening relationship of SNFRC beams

Table 6.1 Mean (Std dev) Values Of crack opening parameters of SPFRC Beam

Crack opening	Control	4 kg/m ³	6 kg/m ³	8 kg/m ³
0	1(0)	1 (0)	1(0)	1(0)
0.06	0.26(0.052)	0.35 (0.059)	0.19(0.142)	0.27(0.08)
0.1	0.22(0.024)	0.33 (0.049)	0.22(0.029)	0.26(0.042)
0.35	0.01(0.013)	0.22 (0.022)	0.18(0.049)	0.26(0.04)
1		0.34 (0.053)	0.29(0.081)	0.38(0.037)
2		0.34 (0.104)	0.3(0.074)	0.43(0.055)
3.5		0.1 (0.022)	0.04(0.059)	0.16(0.022)
f _t	1.97(0.22)	1.69(0.14)	2.24(0.044)	2.15(0.21)

Table 6.2 Mean (Std dev) Values Of crack opening parameters of SPFRC Beam

Crack opening	Control	4 kg/m ³	6 kg/m ³	8 kg/m ³
0	1(0)	1(0)	1(0)	1(0)
0.06	0.26(0.052)	0.24(0.152)	0.36(0.096)	0.53(0.071)
0.1	0.22(0.024)	0.19(0.021)	0.3(0.051)	0.31(0.096)
0.35	0.01(0.013)	0.17(0.053)	0.28(0.036)	0.36(0.051)
1		0.23(0.066)	0.37(0.046)	0.48(0.074)
2		0.24(0.051)	0.38(0.068)	0.45(0.089)
3.5		0.21(0.057)	0.31(0.054)	0.4(0.068)
f _t	1.97(0.22)	2.42 (0.15)	2.01(0.15)	2.24(0.1)

A comparison of the experimental and the numerically predicted load deflection responses of beams is shown in Fig 6.13. It can be seen that there is a good match between experimental and theoretical curves for all FRC beams. The difference in the area under curve between the experimental and the numerically predicted responses was mostly less than 1 percent. The model is able to capture the non-linearity prior to peak load, the load recovery point and also load recovery portion. But there is a small deviation in the immediate post peak response after peak where the model is unable to capture the steep load drop. This may be improved by changing predefined crack opening values which are used in the calculation of the norm.

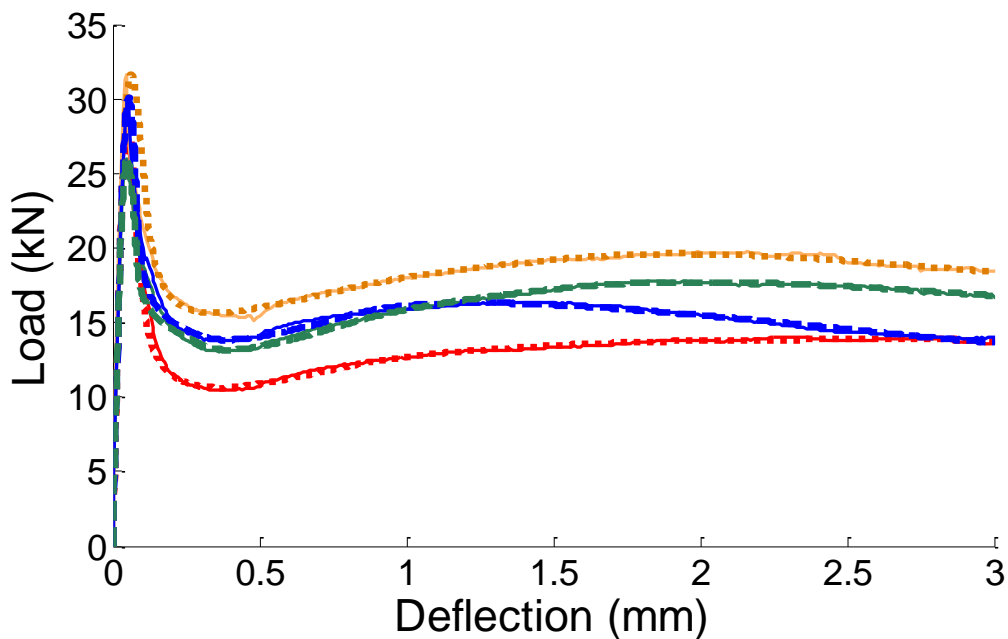


Fig 6.13 Experimental and matched theoretical curves of SNFRC 6 kg/m³ beams.

Using the results of the inversion analysis, the relationship between the crack length and the crack opening are obtained. The crack length in the hinged crack model is defined by the depth at which the stress is equal to the tensile strength, f_t . Similarly, the crack opening is the

crack opening displacement at the lowest portion of the beam. The relationship between the crack length and the crack opening displacement is plotted in Fig 6.14 and 6.15 for SPFRC and SNFRC, respectively. The relationship obtained from control beams is plotted in the figures for comparison. The results indicate that initially for a small increase in crack opening there is a large increase in the crack length. However, later there is a smaller increase in the crack length and the response is dominated by the opening of the crack. The results also indicate that crack propagation along the depth of section is significantly affected by tensile strength. For a given crack opening, the crack length in specimens with a higher f_t are smaller. The crack opening is observed to depend on crack closing stresses as it can be observed in Fig 6.15 that in 4 kg/m³ SNFRC which have higher strength, the crack propagation is less but after some crack opening SNFRC with 8 kg/m³ which has higher crack bridging stresses has smaller opening.

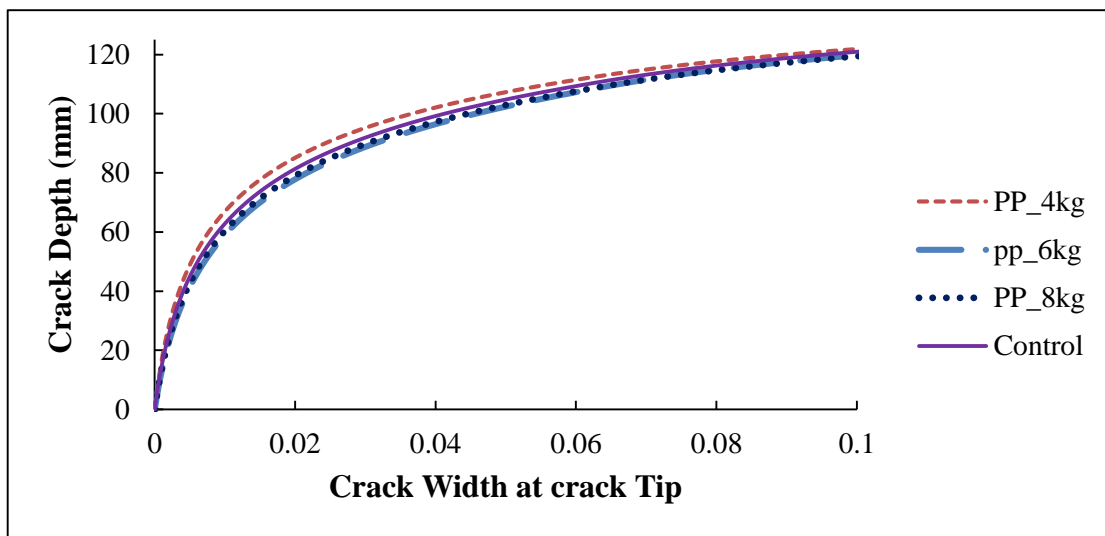


Fig 6.14 Crack depth vs Crack width for mean Crack opening parameters of SPFRC

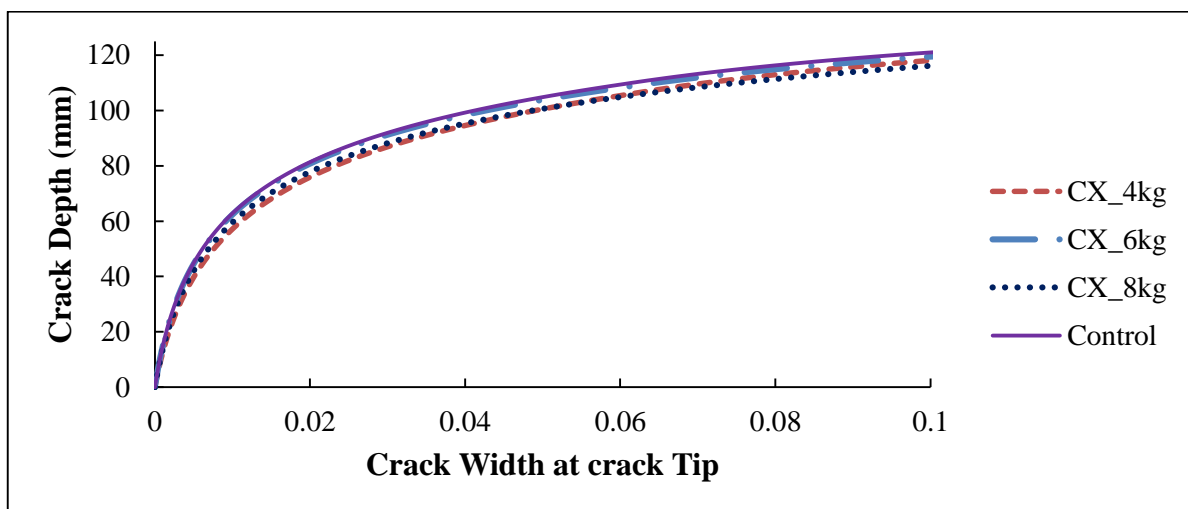


Fig 6.15 Crack depth vs Crack width for mean Crack opening parameters of SNFRC

Chapter 7

Summary of findings and Future Works

The results of the experimental investigation reveals that at low volume fractions, up to 8 kg/m^3 , once the matrix has cracked, initial part of the load response is controlled by crack propagation. In the initial softening part of the load response, there is very rapid increase in crack length for a small change in the crack opening. This part of the load response is identical for control and the fiber reinforced concrete specimens and there is little or no influence of fibers. On increasing the deflection, the load response in fiber reinforced beams exhibits a load recovery. The deviation from the softening response of control beams and the load recovery response is influenced by the fiber volume fraction. In the load recovery part of the load response, the crack growth is arrested by the fibers. There is a small increase in crack length as the crack opening continues to increase. The crack closing stresses provided by the fibers also increase with increasing crack opening allowing the composite beam to carry increasing load. The post-cracking resistance is primarily attributed to fiber pull-out. While no significant increase in composite strength is observed, considerable enhancement of the composite fracture energy and toughness is obtained.

The implications of the observed post-peak load carrying ability with fibers are discussed below

The increase in toughness obtained from the use of fibers allows cracks in indeterminate structures to work as hinges and to redistribute loads. In this way, the failure load of the structure may be substantially higher than for the unreinforced structure although the flexural strength of the plain concrete, tested on beams, is not increased.

Polypropylene fibers are not expected to bond chemically in a concrete matrix, but bonding has been shown to occur by mechanical interaction. The elastic modulus of the fiber is 10 GPa while the elastic modulus of mature concrete is expected to be higher than 20 GPa. The effective of the synthetic fibers is expected to be higher at early ages where the improvement in the fracture behaviour would be significant relative to cracking load. Synthetic fibers have been shown to be effective in the early lifetime of the composite when the matrix is itself weak, brittle, and of low modulus. Considering this, macro synthetic fibers have great potential for replacement for shrinkage steel in concrete.

Directions for future research that emerge from the findings of this study are:

1. Investigate larger length of fiber.
2. Investigate the improvements in fracture behaviour at early ages.

References

- [1] R. F. Zollo, "Fiber-reinforced concrete: an overview after 30 years of development," *Cement and Concrete Composites*, vol. 19, no. 2, pp. 107-122, 1997.
- [2] B. Belletti, R. Cerioni, A. Medo and G. Plizzari, "Design Aspects on Steel Fiber-Reinforced Concrete Pavements," *Journal of Materials in Civil Engineering*, vol. 20, no. 9, pp. 599-607, 2008.
- [3] G. L. Sorelli, A. Meda and A. G. Plizzari, "Steel Fiber Concrete Slabs on Ground: A Structural Matter," *ACI Structural Journal*, vol. 103, no. 4, pp. 551-558, 2006.
- [4] L. Ferrara and A. Meda, "Relationships between fibre distribution, workability and the mechanical properties of SFRC applied to precast roof elements.," *Materials and Structures*, vol. 39, no. 4, pp. 411-420, 2006.
- [5] G. Ravindra, B. Bryan, G. Tomas, O. Jorge and J. Rolando, "Fiber Concrete Tunnel Lining: Construction of a Subway Line in Barcelona," *Concrete International*, vol. 28, no. 8, pp. 63-69, August 2006.
- [6] L. Taerwe and A. Van Gysel, "Influence of Steel Fibers on Design Stress-Strain Curve for High-Strength Concrete," *Journal of Engineering Mechanics*, vol. 122, no. 8, pp. 695-704, 1996.
- [7] A. C. 544, "State-of-the-Art Report on Fiber Reinforced Concrete," American Concrete Institute, 1996.
- [8] A. 544.3R-93, "Guide for Specifying, Proportioning, Mixing, Placing, and Finishing Steel Fiber Reinforced Concrete," American Concrete Institute, 1993.
- [9] Z. Bayasi and M. McIntyre, "Application of Fibrillated Polypropylene Fibers for Restraint of Plastic Shrinkage Cracking in Silica Fume Concrete," *Materials Journal*, vol. 99, no. 4, pp. 337-344, 7 1 2002.
- [10] V. S. Gopalaratnam and G. Ravindra , "On the characterization of flexural toughness in fiber reinforced concretes," *Cement and Concrete Composites*, vol. 17, no. 3, pp. 239-254, 1995.
- [11] S. P. Shah and C. Ouyang, "Mechanical Behavior of Fiber-Reinforced Cement-Based Composites," *Journal of the American Ceramic Society*, vol. 74, no. 11, pp. 2727-38,2947-53, November 2005.
- [12] C. D. Johnston, "Steel Fiber Reinforced Mortar and Concrete: A Review of Mechanical Properties," *Fiber Reinforced Concrete SP-44*, vol. 44, pp. 127-142, 1974.

- [13] G. R. Williamson, "The Effect of Steel Fibers on the Compressive Strength of Concrete," *Fiber Reinforced Concrete, SP-44*, vol. 44, pp. 195-208, 1974.
- [14] C. D. Johnston and R. J. Gray, "Uniaxial Tension Testing of Steel Fibre Reinforced Cementitious Composites," in *Proceedings, International Symposium on Testing and Test Methods of Fibre-Cement Composites.*, 1978.
- [15] J. N. Kar and A. K. Pal, "Strength of Fiber-Reinforced Concrete," *Journal of the Structural Division, ASCE*, vol. 98, no. 5, pp. 1053-1068, 1972.
- [16] J. P. Romualdi and J. A. Mandel, "Tensile Strength of Concrete Affected by Uniformly Distributed and Closely Spaced Short Lengths of Wire Reinforcement," *ACI Journal Proceedings*, vol. 61, no. 6, pp. 657-672, 1964.
- [17] C. D. Johnston and R. A. Coleman, "Strength and Deformation of Steel Fiber Reinforced Mortar in Uniaxial Tension," *Fiber Reinforced Concrete, SP-44 American Concrete Institute*, vol. 44, pp. 177-194, 1974.
- [18] C. D. Johnston, "Definition and Measurement of Flexural Toughness Parameters for Fiber Reinforced Concrete," *ASTM- Cement, Concrete and Aggregates*, vol. 4, no. 2, pp. 53-60, 1982.
- [19] V. Ramakrishnan, T. Brandshaug, W. V. Coyle and E. K. Schrader, "Comparative Evaluation of Concrete Reinforced with Straight Steel Fibers and Fibers with Deformed Ends Glued Together into Bundles," *American Concrete Institute*, vol. 77, no. 3, pp. 135-143, 1980.
- [20] C. D. Johnston and R. J. Gray, "Flexural Toughness First-Crack Strength of Fibre-Reinforced-Concrete Using ASTM Standard C 1018," in *Proceedings, Third International Symposium on Developments in Fibre Reinforced Cement Concrete, RILEM*, , Sheffield, 1986.
- [21] P. J. Hannant, "FIBRE CEMENTS AND FIBRE CONCRETES," Wiley(John) & Sons, Limited, Chichester, United Kingdom, 1978.
- [22] H. Cifuentes, F. Garcia, O. Maeso and F. Medina, "Influence of the properties of polypropylene fibres on the fracture behaviour of low-, normal- and high-strength FRC," *Construction and Building Materials*, vol. 45, pp. 130-137, August 2013.
- [23] B. H. Oh, J. C. Kim and C. Y. Choi, "Fracture behavior of concrete members reinforced with structural synthetic fibers," *Engineering Fracture Mechanics*, vol. 74, no. 1-2, pp. 243-257, january 2007.

- [24] S. Singh, A. Shukla and R. Brown, "Pullout behavior of polypropylene fibers from cementitious matrix," *Cement and Concrete Research*, vol. 34, no. 10, pp. 1919-1925, October 2004.
- [25] M. N. Soutsos, T. T. Le and A. P. Lampropoulos, "Flexural performance of fibre reinforced concrete made with steel and synthetic fibres," *Construction and Building Materials*, vol. 36, pp. 704-710, November 2012.
- [26] F. Benacardino, L. Rizzuti, G. Spadea and R. N. Swamy, "Experimental evaluation of fiber reinforced concrete fracture properties," *Composites Part B: Engineering*, vol. 41, no. 1, pp. 17-24, January 2010.
- [27] N. Buratti, C. Mazzotti and M. Savoia, "Post-cracking behaviour of steel and macro-synthetic fibre-reinforced concretes," *Construction and Building Materials*, vol. 25, no. 5, pp. 2713-2722, May 2011.
- [28] A. Hillerborg, M. Modeer and P. E. Petersson, "Analysis of crack formation and crack growth in concrete by means of fracture mechanics and finite elements," *Cement and Concrete Research*, vol. 6, no. 6, pp. 773-781, November 1976.
- [29] R. T. 162_TDF, "Test and design methods for steel fibre reinforced concrete, "Design of steel fibre reinforced concrete using the (σ -w method: principles and applications)," *Materials and Structures*, vol. 35, pp. 262-278, 2002.
- [30] R. Evans and M. Marathe, "Microcracking and stress-strain curves for concrete in tension," *Materials and Structures, Matériaux et Construction*, vol. 1, no. 1, pp. 61-64, 1968.
- [31] V. S. Gopalaratnam and S. P. Shah, "Post-Cracking Characteristics of Concrete in Uniaxial Tension," in *Engineering Mechanics in Civil Engineering*, New York, 1984.
- [32] P. Petersson, "Fracture energy of concrete: Practical performance and experimental results," *Cement and Concrete Research*, vol. 10, no. 1, pp. 91-101, 1980.
- [33] H. Reinhardt, "Fracture Mechanics of an Elastic Softening Material like Concrete," pp. 5-41, 01 01 1984.
- [34] K. Visalvanich and A. E. Naaman, "Fracture Model for Fiber Reinforced Concrete," *ACI Journal*, vol. 80, no. 2, pp. 128-138, 1983.
- [35] A. Hillerborg, "Analysis of fracture by means of the fictitious crack model, particularly for fibre reinforced concrete," *International Journal of Cement Composites*, vol. 2, no. 4, pp. 177-184, 1980.

- [36] A. R. Ingraffea and W. H. Gerstle, "Non-Linear Fracture Models for Discrete Crack Propagation," in *Application of Fracture Mechanics to Cementitious Composites*, NATO ASI series, 1985.
- [37] L. Oostergaard, D. Lange and H. Stang, "Early-age stress-crack opening relationship for high performance concrete," *Cement and Concrete Composites*, vol. 26, no. 5, pp. 563-572, 2004.
- [38] H. K. Seung , Z. Zhifang and S. P. Shah, "Effect of specimen size on fracture energy and softening curve of concrete: Part II. Inverse analysis and softening curve," *Cement and Concrete research*, vol. 38, no. 8-9, pp. 1061-1069, 2008.
- [39] M. Wecharatana and S. P. Shah, "A Model for Predicting Fracture Resistance of Fiber Reinforced Concrete," *Cement and Concrete Research*, vol. 13, no. 6, pp. 819-829, November 1983.
- [40] J. F. Olesen, "Fictitious Crack Propagation in Fiber-Reinforced Concrete Beams," *Journal of Engineering Mechanics*, vol. 127, no. 3, pp. 272-280, 01 March 2001.
- [41] I. Lofgren, H. Stang and J. F. Olesen, "Fracture Properties of FRC Determined through Inverse Analysis of wedge Splitting and Three-Point Bending Tests," *Journal of Advanced Concrete Technology*, vol. 3, no. 3, pp. 423-434, October 2005.
- [42] S. Matthys and T. Soetens, "Different methods to model the post-cracking behaviour of hooked-end steel fibre reinforced concrete," *Construction and Building Materials*, vol. 73, pp. 458-471, 2014.
- [43] J. Barros, V. Cunha, A. F. Ribeiro and J. A. B. Antunes, "Post-cracking behaviour of steel fibre reinforced concrete," *Materials and Structures*, vol. 38, no. 1, pp. 47-56, January-February 2005.
- [44] U. 11039-2, "Steel Fibre Reinforced Concrete - Test Method For Determination Of First Crack Strength And Ductility Indexes," 2003.
- [45] T. C. Chu, W. F. Ranson, M. A. Sutton and W. H. Peters, "Applications of Digital Image correlation technique to Experimental Mechanics," *Exp. Mech*, vol. 25, pp. 232-244, 1985.
- [46] A. Kobayashi, *Handbook on Experimental Mechanics*, Indiana: Prentice Hall / Society for Experimental Mechanics, Inc., Lebanon, 1993.
- [47] f. Pierron , B. Green, Wisnom MR and S. R. Hallet, "Full-field assessment of the damage process of laminated composite open-hole tensile specimens. Part I: methodology," *Composites*, vol. 38, pp. 2307-2320, 2007.

- [48] K. V. Subramaniam, C. Carloni and L. Nobile, “Interface Fracture and Debonding in the FRP-Concrete Interface: Influence of the FRP Laminate width on Load Capacity,” *Engineering Fracture Mechanics*, vol. 74, no. 4, pp. 578-594, 2007.

Annexure I

For a Given bilinear stress crack opening relationship,

There are four stages as shown below. Stage 0 corresponds to precrack and remaining three stages correspond to post crack.so now here we have three transitions

Stage 0 → Stage I → Stage II → Stage III

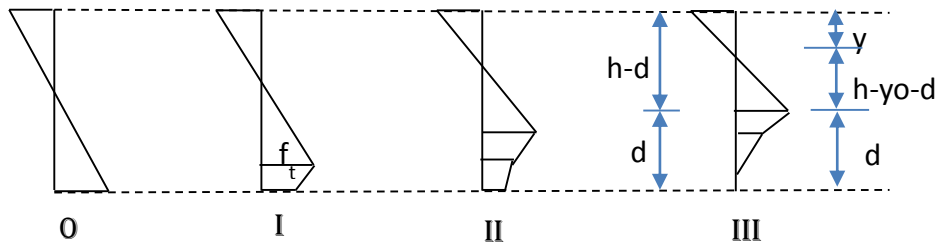


Fig 1. Stages of stress diagrams with bilinear stress crack opening relationship

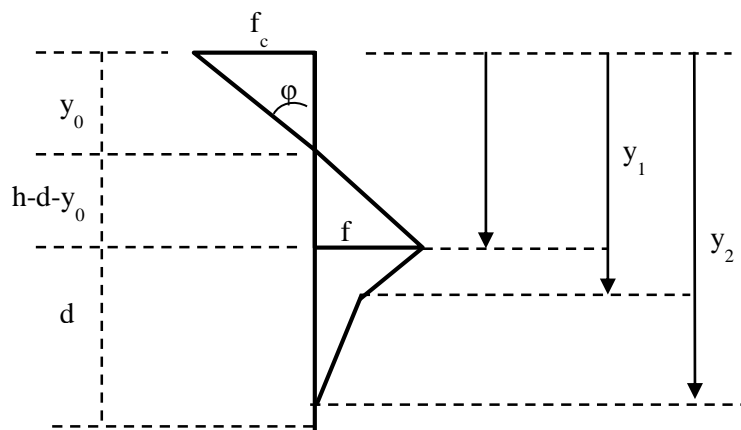


Fig 2. Stress distribution with bilinear stress crack opening relationship

To make the derivation simple, following normalization were introduced.

$$\mu = \frac{6M}{f_t h^2 t} \quad \rho = \frac{N}{f_t h t} \quad \theta = \frac{hE}{s f_t} \phi \quad \alpha = \frac{d}{h}$$

Stage 0

$$\mu(\theta) = \theta \tag{1}$$

Stage I

This case will happen when width of crack at bottom is less than w_1 or $y_1 < h$

At the crack tip, stress will be equal to tensile strength (i.e. $\sigma_w = f_t$). Therefore, keeping y as $h - d$ and $\sigma_w = f_t$ in equation 5.3 gives

$$d + y_0 = h - \frac{s \cdot f_t}{2\varphi \cdot E} = h - \frac{h}{2\theta}$$

$$d + \frac{h}{2\theta} = h - y_0 \quad (1a)$$

Now by applying force equilibrium

$$\frac{1}{2} \cdot f_c \cdot y_0 - \frac{1}{2} \cdot f_t \cdot (h - d - y_0) - T_2 + N = 0$$

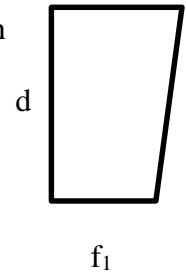
$$f_t \cdot y_0 \cdot \frac{y_0}{(h - d - y_0)} - f_t \cdot (h - d - y_0) - T_2 + N = 0$$

Using (1a) and normalization

$$\theta \left[1 - \alpha - \frac{1}{2\theta} \right]^2 - \frac{1}{4\theta} - \frac{T_2}{f_t h t} + \rho = 0 \quad (2)$$

Calculation of T_2 stress at bottom can be given by using equation (5.5b) for $y=h$

$$f_1 \cdot f_t = \sigma_w[w(h)] = \frac{\zeta_1 - 2(h - y_0)\varphi\beta_1 E}{1 - \beta_1} \frac{E}{s}$$



By Trapezoidal integration

$$\frac{T_2}{f_t h t} = \frac{1}{2} \frac{d}{f_t h} \left[f_t + \frac{E}{s(1 - \beta_1)} \left(\frac{f_t s}{E} - 2h \left[\frac{1}{2\theta} + \alpha \right] \varphi \beta_1 \right) \right]$$

$$\frac{T_2}{f_t h t} = \frac{\alpha}{1 - \beta_1} [1 - \beta_1 - \alpha \theta \beta_1] \quad (3)$$

Substituting (3) in (2)

$$\theta \left[1 - \alpha - \frac{1}{2\theta} \right]^2 - \frac{1}{4\theta} - \frac{\alpha}{1 - \beta_1} [1 - \beta_1 - \alpha \theta \beta_1] + \rho = 0$$

Upon simplification we will get an equation in terms of

$$\alpha^2 - 2\alpha[1 - \beta_1] + \left(\frac{\rho - 1}{\theta} + 1 \right) (1 - \beta_1) = 0$$

On solving the quadratic Equation we will get

$$\alpha = 1 - \beta_1 + \sqrt{(1 - \beta_1) \left[\frac{1 - \rho}{\theta} - \beta_1 \right]} \quad (4)$$

By taking moments about tip of crack

$$\frac{1}{2} \cdot f_c \cdot y_0 \cdot \left(h + d + \frac{y_0}{3} \right) - \frac{1}{2} \cdot f_t \cdot \frac{(h - d - y_0)^2}{3} + \frac{6 \cdot T_2}{f_t \cdot h^2 \cdot t} \frac{d}{3} \left(\frac{f_t + 2f_1}{f_t + f_1} \right) + \frac{6\rho}{h} \left(\frac{h}{2} - d \right)$$

Substituting for T_2 and f_1

$$\theta \left[1 + \alpha^2 + \frac{1}{4\theta^2} - 2\alpha - \frac{1}{\theta} + \frac{\alpha}{\theta} \right] \times 6 \left[\frac{1}{2\theta} + \frac{2}{3} - \frac{2\alpha}{3} - \frac{1}{3\theta} \right] - \frac{1}{4\theta^2} + \alpha^2 \left[3 - \frac{4\alpha\theta}{1 - \beta_1} \right] + 3\rho(1 - 2\alpha) = \mu$$

On simplification

$$\mu(\theta) = 4\theta \left[1 - 3\alpha + 3\alpha^2 - \frac{\alpha^3}{1 - \beta_1} \right] + (6\alpha - 3)(1 - \rho) \quad (5)$$

Stage II

Now by applying force equilibrium

$$\frac{1}{2} \cdot f_c \cdot y_0 - \frac{1}{2} \cdot f_t \cdot (h - d - y_0) - T_2 - T_3 + N = 0$$

$$f_t \cdot y_0 \cdot \frac{y_0}{(h - d - y_0)} - f_t \cdot (h - d - y_0) - T_2 - T_3 + N = 0$$

Using (1a) and normalization

$$\theta \left[1 - \alpha - \frac{1}{2\theta} \right]^2 - \frac{1}{4\theta} - \frac{T_2}{f_t h t} - \frac{T_3}{f_t h t} + \rho = 0 \quad (6)$$

From equation 5.5 (a)

$$w_1 = \frac{2(y_1 - y_0)\varphi - \zeta_1}{1 - \beta_1}$$

But from equation (5.4b)

$$w_1 = \frac{1 - b_2}{a_1 - a_2}$$

Therefore

$$\frac{2(y_1 - y_0)\varphi - \zeta_1}{1 - \beta_1} = \frac{1 - b_2}{a_1 - a_2}$$

That gives

$$\frac{y_1}{h} = \frac{(1 - \beta_1)(1 - b_2)}{2\theta(\beta_1 - \beta_2)} \quad (7)$$

Calculation of T_2 stress at bottom can be given by using equation (5.5b) for $y=y_1$

$$f_1 \cdot f_t = \frac{\zeta_1 - 2(y_1 - y_0)\varphi\beta_1 E}{1 - \beta_1} \frac{1}{s}$$

$$f_1 = \frac{f_t[\beta_1 b_2 - \beta_2]}{(\beta_1 - \beta_2)} \quad (8)$$

Calculation of T_3 stress at bottom can be given by using equation (5.5b) for $y=h$

$$f_2 \cdot f_t = \frac{\zeta_2 - 2(h - y_0)\varphi\beta_2 E}{1 - \beta_2} \frac{1}{s}$$

$$f_2 = \frac{f_t}{(1 - \beta_2)} [b_2 - \beta_2(1 + 2\alpha\theta)] \quad (9)$$

Now $\frac{T_3+T_2}{f_t h t}$

$$\frac{1}{f_t h t} \left[[f_t + f_1] \times \frac{(y_1 - (h - d))}{2} \times t + [f_1 + f_2] \times \frac{(d - y_1)}{2} \times t \right]$$

Upon substituting f_1 & f_2 gives

$$\frac{1}{2} \left[\frac{y_1}{h} \left[1 - \frac{b_2 - \beta_2(1 + 2\alpha\theta)}{1 - \beta_2} \right] + \left[\frac{[\beta_1 b_2 - \beta_2]}{(\beta_1 - \beta_2)} + \frac{[b_2 - \beta_2]}{(1 - \beta_2)} \right] \alpha - \frac{2\alpha^2\theta\beta_2}{1 - \beta_2} \right]$$

On substituting y_1 gives

$$\frac{1}{4\theta} \frac{(1 - \beta_1)(1 - b_2)^2}{(\beta_1 - \beta_2)(1 - \beta_2)} + \frac{(b_2 - \beta_2)}{(1 - \beta_2)} \alpha - \frac{\alpha^2\theta\beta_2}{(1 - \beta_2)} \quad (10)$$

Equation (10) in (6)

$$\theta \left[1 - \alpha - \frac{1}{2\theta} \right]^2 - \frac{1}{4\theta} - \frac{1}{4\theta} \left[\frac{(1 - \beta_1)(1 - b_2)^2}{(\beta_1 - \beta_2)(1 - \beta_2)} \right] - \frac{\alpha(b_2 - \beta_2)}{(1 - \beta_2)} + \frac{\alpha^2 \theta \beta_2}{(1 - \beta_2)} + \rho = 0$$

On rearranging and expressing in terms of α

$$\alpha^2 - 2\alpha \left[(1 - \beta_2) + \frac{1}{2\theta} (b_2 - 1) \right] - \frac{1}{4\theta^2} \frac{(1 - \beta_1)(1 - b_2)^2}{(\beta_1 - \beta_2)} + \frac{\rho - 1 + \theta}{\theta} (1 - \beta_2) = 0 \quad (11)$$

Solving for α gives

$$\alpha = 1 - \beta_2 - \frac{1 - b_2}{2\theta} - \sqrt{(1 - \beta_1) \left(\frac{(1 - b_2)^2}{4\theta^2(\beta_1 - \beta_2)} - \beta_2 + \frac{b_2 - \rho}{\theta} \right)} \quad (12)$$

By taking moments about tip of crack

$$\begin{aligned} \frac{1}{2} \cdot f_c \cdot y_0 \cdot \left(h + d + \frac{y_0}{3} \right) - \frac{1}{2} \cdot f_t \cdot \frac{(h - d - y_0)^2}{3} + \frac{6 \cdot T_2}{f_t \cdot h^2 \cdot t} \left(\frac{f_t + 2f_1}{f_t + f_1} \right) \frac{(y_1 - (h - d))}{3} \\ + \frac{6 \cdot T_3}{f_t \cdot h^2 \cdot t} \left((y_1 - (h - d)) + \left(\frac{f_1 + 2f_2}{f_1 + f_2} \right) \frac{(h - y_1)}{3} \right) + \frac{6\rho}{h} \left(\frac{h}{2} - d \right) \end{aligned} \quad (13)$$

Substituting for T_2 , T_3 , f_1 , f_2 and y_1

$$\begin{aligned} \theta \left[1 + \alpha^2 + \frac{1}{4\theta^2} - 2\alpha - \frac{1}{\theta} + \frac{\alpha}{\theta} \right] \times 6 \left[\frac{1}{2\theta} + \frac{2}{3} - \frac{2\alpha}{3} - \frac{1}{3\theta} \right] - \frac{1}{4\theta^2} + \frac{3\alpha^2(b_2 - \beta_2)}{(1 - \beta_2)} \\ - \frac{4\alpha^3\beta_2}{(1 - \beta_2)} + \left(\frac{c}{2\theta} \right)^2 \frac{(1 - b_2)}{(1 - \beta_2)} + 3\rho(1 - 2\alpha) = \mu \end{aligned} \quad (14)$$

Where $c = (1 - b_2)(1 - \beta_1)/(\beta_1 - \beta_2)$

On simplification

$$\mu(\theta) = 4 \left(1 - 3\alpha + 3\alpha^2 - \frac{\alpha^3}{1 - \beta_1} \right) \theta + (6\alpha - 3)(1 - \rho) - \frac{(1 - b_2) \left(3\alpha^2 - \left(\frac{c}{2\theta} \right)^2 \right)}{1 - \beta_2} \quad (15)$$

Stage III

Now by applying force equilibrium

$$\frac{1}{2} \cdot f_c \cdot y_0 - \frac{1}{2} \cdot f_t \cdot (h - d - y_0) - T_2 - T_3 + N = 0$$

$$f_t \cdot y_0 \cdot \frac{y_0}{(h - d - y_0)} - f_t \cdot (h - d - y_0) - T_2 - T_3 + N = 0$$

Using (1) and normalization

$$\theta \left[1 - \alpha - \frac{1}{2\theta} \right]^2 - \frac{1}{4\theta} - \frac{T_2}{f_t h t} - \frac{T_3}{f_t h t} + \rho = 0 \quad (16)$$

From equation 5.5 (a)

$$w_2 = \frac{2(y_2 - y_0)\varphi - \zeta_2}{1 - \beta_2}$$

But from equation (5.4b)

$$w_2 = \frac{b_2}{a_2}$$

Therefore

$$\frac{2(y_2 - y_0)\varphi - \zeta_2}{1 - \beta_2} = \frac{b_2}{a_2}$$

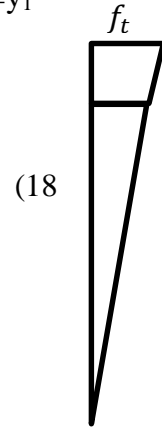
$$\frac{y_2}{h} = \frac{(b_2 - \beta_2)}{2\theta\beta_2} \quad (17)$$

Calculation of T_2 stress at bottom can be given by using equation (5.5b) for $y=y_1$

$$f_1 \cdot f_t = \frac{\zeta_1 - 2(y_1 - y_0)\varphi\beta_1 E}{1 - \beta_1} \frac{1}{s}$$

$$f_1 = \frac{f_t[\beta_1 b_2 - \beta_2]}{(\beta_1 - \beta_2)}$$

$$f_2 = 0$$



Now $\frac{T_3 + T_2}{f_t h t}$

$$\frac{1}{f_t h t} \left[[f_t + f_1] \times \frac{(y_1 - (h - d))}{2} t + f_1 \frac{(y_2 - y_1)}{2} \times t \right]$$

Upon substituting f_1, y_1 & y_2 gives

$$\frac{[\beta_2 - \beta_1\beta_2 - 2b_2\beta_2 + \beta_2^2 + \beta_1b_2^2]}{4\theta(\beta_1 - \beta_2)\beta_2}$$

Equation (19) in (16) gives

$$\theta \left[1 - \alpha - \frac{1}{2\theta} \right]^2 - \frac{1}{4\theta} - \frac{1}{4\theta} \left[\frac{[\beta_2 - \beta_1\beta_2 - 2b_2\beta_2 + \beta_2^2 + \beta_1b_2^2]}{(\beta_1 - \beta_2)\beta_2} \right] + \rho = 0 \quad (20)$$

On solving for α we get

$$\alpha = 1 - \frac{1}{2\theta} \left[1 + \sqrt{\frac{(1 - b_2)^2}{(\beta_1 - \beta_2)} + \frac{b_2^2}{\beta_2} - 4\rho\theta} \right] \quad (21)$$

By taking moments about tip of crack

$$\begin{aligned} \frac{1}{2} \cdot f_c \cdot y_0 \cdot \left(h + d + \frac{y_0}{3} \right) - \frac{1}{2} \cdot f_t \cdot \frac{(h - d - y_0)^2}{3} + \frac{6 \cdot T_2}{f_t \cdot h^2 \cdot t} \left(\frac{f_t + 2f_1}{f_t + f_1} \right) \frac{(y_1 - (h - d))}{3} \\ + \frac{6 \cdot T_3}{f_t \cdot h^2 \cdot t} \left((y_1 - (h - d)) + \frac{(y_2 - y_1)}{3} \right) + \frac{6\rho}{h} \left(\frac{h}{2} - d \right) \end{aligned} \quad (22)$$

Substituting for T_2 , T_3 , f_1 , y_1 and y_2

$$\begin{aligned} \theta \left[1 + \alpha^2 + \frac{1}{4\theta^2} - 2\alpha - \frac{1}{\theta} + \frac{\alpha}{\theta} \right] \times 6 \left[\frac{1}{2\theta} + \frac{2}{3} - \frac{2\alpha}{3} - \frac{1}{3\theta} \right] \\ - \frac{1}{4\theta^2} \left(1 - \frac{b_2}{\beta_2} \right) \left(1 - \frac{b_2}{\beta_2} + c \right) \left(1 + \frac{\beta_1 c}{1 - \beta_1} \right) + \left(\frac{c}{2\theta} \right)^2 + 3\rho(1 - 2\alpha) = \mu \end{aligned} \quad (23)$$

Where $c = (1 - b_2)(1 - \beta_1)/(\beta_1 - \beta_2)$

On simplification

$$\begin{aligned} \mu(\theta) = 4(1 - 3\alpha + 3\alpha^2 - \alpha^3)\theta + (6\alpha - 3)(1 - \rho) - 3\alpha^2 \\ + \frac{1}{4\theta^2} \left(1 - \frac{b_2}{\beta_2} \right) \left(1 - \frac{b_2}{\beta_2} + c \right) \left(1 + \frac{\beta_1 c}{1 - \beta_1} \right) + \left(\frac{c}{2\theta} \right)^2 \end{aligned} \quad (24)$$

Thus equations 1, 15, 24 represents moment rotation relationship

Calculation for transitions

Stage 0 → Stage I

(25)

$$\theta_{0-I} = 1 - \rho$$

Stage I → Stage II

From equation 5.5 (a)

$$w_1 = \frac{2(h - y_0)\varphi - \zeta_1}{1 - \beta_1}$$

But from equation (5.4b)

$$w_1 = \frac{1 - b_2}{a_1 - a_2}$$

Therefore

$$\frac{2(h - y_0)\varphi - \zeta_1}{1 - \beta_1} = \frac{1 - b_2}{a_1 - a_2} \quad (26)$$

(1.1a) in (26) after rearranging for d

$$\frac{d}{h} = \frac{(1 - \beta_1)(1 - b_2)}{2\theta(\beta_1 - \beta_2)} = \alpha \quad (27)$$

Now substituting (27) in (4)

$$\theta_{I-II} = \frac{1}{2} \left(1 - \rho - c + \sqrt{(1 - \rho - c)^2 + \frac{c^2}{\beta_1 - 1}} \right) \quad (28)$$

Stage II → Stage III

From equation 5.5 (a)

$$w_2 = \frac{2(h - y_0)\varphi - \zeta_2}{1 - \beta_2}$$

But from equation (5.4b)

$$w_2 = \frac{b_2}{a_2}$$

Therefore

$$\frac{2(h - y_0)\varphi - \zeta_2}{1 - \beta_2} = \frac{b_2}{a_2} \quad (29)$$

Substituting from (1.1a) gives

$$\frac{d}{h} = \frac{(b_2 - \beta_2)}{2\theta\beta_2} = \alpha$$

Now substituting (30) in (12) gives

$$\theta_{II-III} = \frac{1}{2} \left(\frac{b_2}{\beta_2} - \rho + \sqrt{\rho^2 + 2\rho \frac{b_2}{\beta_2} + \frac{(1 - b_2)^2}{(\beta_1 - \beta_2)} + \frac{b_2^2}{\beta_2}} \right) \quad (31)$$

Thus equations 25, 28, 31 gives transition rotations

Annexure II

Derivation of relation of k_i in terms of coordinates.

Equation 5.3 is given by $\sigma_w(w(y)) = (2(y - y_0)\varphi - w(y)) \frac{E}{s}$

Now at i_{th} coordinate $f_t \cdot b_i = (2(y'_i - y_0)\varphi - w_i) \frac{E}{s}$ (1)

$i+1_{th}$ coordinate $f_t \cdot b_{i+1} = (2(y'_{i+1} - y_0)\varphi - w_{i+1}) \frac{E}{s}$ (2)

(2) - (1) gives

$$b_{i+1} - b_i = (y'_{i+1} - y'_i)\varphi \frac{E}{sf_t} - (w_{i+1} - w_i) \frac{E}{sf_t}$$

$$b_{i+1} - b_i = (y_1)\varphi \frac{E}{sf_t} - (w_{i+1} - w_i) \frac{E}{sf_t}$$

By taking $\frac{\theta}{h} = \frac{E}{sf_t} \varphi$ and rearranging gives

$$k_i = (b_{i+1} - b_i) + (w_{i+1} - w_i) \frac{E}{sf_t}, \quad \text{Where } k_i = \frac{2\theta y_i}{h} \quad (3)$$

Derivation of relation of θ_i in terms of k_i and coordinates

From Equation 5.10,

$$\frac{y_0}{h} = 1 - \alpha - \frac{1}{2\theta} \quad \text{and} \quad \frac{h - d - y_0}{h} = \frac{1}{2\theta} \quad (4)$$

Force equilibrium for any θ_i

$$\frac{1}{2} \cdot f_c \cdot y_0 - \frac{1}{2} \cdot f_t \cdot (h - d - y_0) - \frac{1}{2} \cdot f_t \cdot (b_1 + b_2) y_1 - \frac{1}{2} \cdot f_t \cdot (b_2 + b_3) y_2 - \dots$$

$$- \frac{1}{2} \cdot f_t \cdot (b_i + b_{i+1}) y_i$$

$$f_t \cdot y_0 \cdot \frac{y_0}{(h - d - y_0)} - f_t \cdot (h - d - y_0) - \frac{h f_t}{2\theta} \sum k_i (b_{i+1} - b_i)$$

Dividing with f_t and replacing with (4) gives

$$2\theta \left(1 - \alpha - \frac{1}{2\theta}\right)^2 - \frac{1}{2\theta} - \frac{h}{2\theta} \sum k_i (b_{i+1} - b_i)$$

We know $d = \sum y_i$ and hence $\alpha = k_i / (2\theta)$ Substituting and rearranging

$$\theta^2 - \theta \cdot (1 + \sum k_i) + \frac{1}{4} [(\sum k_i)^2 + 2 \cdot \sum k_i - \sum k_i \cdot (b_{i+1} - b_i)]$$

Solving for θ gives

$$\theta_i = \frac{1}{2} \left[(1 + \sum k_i) + (1 + \sum k_i \cdot (b_{i+1} - b_i))^{1/2} \right] \quad (5)$$

To get Moment Curvature relationship

Start with $\theta=0$ and increase it gradually

Case I $\theta \leq 1$

$$\mu(\theta) = \theta \quad (6)$$

Case II $\theta > 1$ and $\theta \leq \theta_{n-1}$

n represents no of coordinates of stress crack relationship.

Force equilibrium gives when $\theta_{i-1} \leq \theta \leq \theta_i$

$$\frac{1}{2} \cdot f_c \cdot y_0 - \frac{1}{2} \cdot f_t \cdot (h - d - y_0) - \frac{1}{2} \cdot f_t \cdot (b_1 + b_2) y_1 - \frac{1}{2} \cdot f_t \cdot (b_2 + b_3) y_2 - \dots$$

$$- \frac{1}{2} \cdot f_t (b_i + b_b) \cdot d \cdot \sum y_{i-1} = 0 \quad (7)$$

To calculate b_b

Slope of any line can be given as

$$m_i = \frac{b_{i+1} - b_i}{w_{i+1} - w_i}$$

Using equation 5.3 by placing $y=h$

$$f_t \cdot b_b = (2(h - y_0)\varphi - w) \frac{E}{S} \quad (8)$$

Where w is crack width at bottom can be calculated using slope of line

$$w = \frac{b_b - b_i}{m_i} + w_i$$

Substituting in equation (8) gives

$$b_b = \left(2(h - y_0)\varphi \frac{E}{sf_t} - \left[\frac{b_b - b_i}{m_i} + w_i \right] \frac{E}{sf_t} \right)$$

On simplification by using $\frac{\theta}{h} = \frac{E}{sf_t} \varphi$

$$b_b = \frac{(1 + 2\alpha\theta) + j_i(b_i - m_i w_i)}{1 + j_i} \quad (9)$$

$$\text{where } j_i = \frac{E}{m_i s j_i}$$

Then $b_i + b_b$ in equation (7) becomes

$$b_b + b_i = \frac{(b_i + 1 + 2\alpha\theta) + j_i(2b_i - m_i w_i)}{1 + j_i}$$

Upon substitution in equation (7)

$$\begin{aligned} & \frac{1}{2} \cdot f_c \cdot y_0 - \frac{1}{2} \cdot f_t \cdot (h - d - y_0) - \frac{1}{2} \cdot f_t \cdot (b_1 + b_2) y_1 - \frac{1}{2} \cdot f_t \cdot (b_2 + b_3) y_2 - \dots \\ & - \frac{1}{2} \cdot f_t (b_i + b_b) \cdot d \cdot \Sigma y_{i-1} \end{aligned}$$

$$2\theta \left(1 - \alpha - \frac{1}{2\theta} \right)^2 - \frac{1}{2\theta} - \left(\frac{hf_t}{2\theta} \sum k_{i-1} (b_i - b_{i-1}) \right)$$

$$- \frac{(b_i + 1 + 2\alpha\theta) + j_i(2b_i - m_i w_i)}{1 + j_i} \cdot (2\alpha\theta - \Sigma k_{i-1}) = 0$$

$$2\theta \left(1 - \alpha - \frac{1}{2\theta} \right)^2 - \frac{1}{2\theta} - \left(\frac{hf_t}{2\theta} \sum k_{i-1} (b_i - b_{i-1}) \right)$$

$$- \frac{(b_i + 1 + 2\alpha\theta) + j_i(2b_i - m_i w_i)}{1 + j_i} \cdot (2\alpha\theta - \Sigma k_{i-1}) = 0$$

On simplification we will get

$$a\alpha^2 + b\alpha + c = 0$$

Where

$$a = \theta j_i$$

$$b = - \left(2\theta + \frac{(b_i - \Sigma k_{i-1} - 1)}{2} + j_i(2\theta - 1 + b_i - m_i w_i/2) \right) \quad (10)$$

$$c = (\theta - 1)(1 + j_i) - \left[\sum_{g=1}^{i-1} (b_g + b_{g+1}) \cdot k_g + \frac{(b_i + 1) + j_i(2b_i - m_i w_i)}{1 + j_i} \sum_{g=1}^{i-1} k_g \right] \cdot \frac{1 + j_i}{4\theta}$$

Upon solving quadratic equation we will get α in terms of theta

$$\alpha = \min \left(\frac{-b + \sqrt{b^2 - 4ac}}{2a}, \frac{-b - \sqrt{b^2 - 4ac}}{2a} \right) \quad (11)$$

Then by substituting for α in equation (9) we will get stress at bottom.

By considering moments about tip of crack

$$\begin{aligned} \frac{1}{2} \cdot f_c \cdot y_0 \cdot \left(h + d + \frac{y_0}{3} \right) - \frac{1}{2} \cdot f_t \cdot \frac{(h - d - y_0)^2}{3} - \frac{1}{2} \cdot f_t \cdot (b_1 + b_2) y_1 \cdot \frac{(b_1 + 2b_2) \cdot y_1}{3(b_1 + b_2)} \\ - \frac{1}{2} \cdot f_t \cdot (b_2 + b_3) y_2 \cdot \frac{(b_2 + 2b_3) \cdot y_2}{3(b_2 + b_3)} - \dots \\ - \frac{1}{2} \cdot f_t (b_i + b_b) \cdot (d - \Sigma y_{i-1}) \cdot \left(\Sigma y_{i-1} + \frac{(b_i + 2b_b) \cdot (d - \Sigma y_{i-1})}{3(b_i + b_b)} \right) = M \end{aligned}$$

By substitutions with normalizations we will get

$$\begin{aligned} \mu(\theta) = \left(1 - \alpha - \frac{1}{2\theta} \right)^2 \cdot (1 + (2 - 2\alpha)2\theta) - \frac{1}{4\theta^2} + \frac{1}{4\theta^2} \{ [\sum_{z=1}^{i-1} 3k_z \cdot (\sum_{v=1}^{z-1} k_z) \cdot (b_z + b_{z+1})] + [\sum_{z=1}^{i-1} (k_z^2 \cdot (b_z + 2b_{z+1}))] + (2\alpha\theta - (\sum_{z=1}^{i-1} (k_z)) [3 \cdot (b_i + 2b_b) \cdot (\sum_{z=1}^{i-1} (k_z) + (2\alpha\theta - \sum_{z=1}^{i-1} (k_z)) \cdot (b_i + 2b_b)]) \} \end{aligned} \quad (12)$$

Case III $\theta > \theta_{n-1}$

In this case stress at bottom will become zero as the crack width has crossed critical width.

By proceeding in similar manner we will get

$$a\alpha^2 + b\alpha + c = 0$$

Where

$$a = \theta$$

$$b = -(2\theta - 1) \quad (13)$$

$$c = (\theta - 1) - \left(\sum_{g=1}^{i-1} (b_g + b_{g+1}) \cdot k_g \right) \cdot \frac{1}{4\theta}$$

Upon solving quadratic equation we will get α in terms of theta

$$\alpha = \min\left(\frac{-b + \sqrt{b^2 - 4ac}}{2a}, \frac{-b - \sqrt{b^2 - 4ac}}{2a}\right) \quad (14)$$

Moment equilibrium will give

$$\mu(\theta) = \left(1 - \alpha - \frac{1}{2\theta}\right)^2 \cdot (1 + (2 - 2\alpha)2\theta) - \frac{1}{4\theta^2} + \frac{1}{4\theta^2} \left\{ \left[\sum_{z=1}^{i-1} 3k_z \cdot \left(\sum_{v=1}^{z-1} k_v \right) \cdot (b_z + b_{z+1}) \right] + \sum_{z=1}^{i-1} (k_z^2 \cdot (b_z + 2b_{z+1})) \right\} \quad (15)$$

Thus equations 6, 12 and 15 establishes the moment rotation relationship for multi linear stress-crack opening relationship

Annexure III

28- Day Compression Results

Specimen	Weight (kg)	Load (kN)	Compressive Strength(MPa)	Mean (MPa)	Standard Deviation (MPa)
Control-1	7.895	813.8	36.1	34.6	1.05
Control-2	7.875	760.0	33.7		
Control-3	7.832	768.4	34.1		
PP_4kg/m ³ -1	7.986	765.1	34.0	34.4	0.82
PP_4kg/m ³ -2	7.966	800.2	35.5		
PP_4kg/m ³ -3	8.011	757.9	33.6		
CX_4kg/m ³ -1	7.886	909.4	40.4	40.0	1.88
CX_4kg/m ³ -2	7.910	953.5	42.3		
CX_4kg/m ³ -3	7.970	850.3	37.7		
PP_6kg/m ³ -1	7.900	923.0	41.0	38.0	2.27
PP_6kg/m ³ -2	7.978	843.9	37.5		
PP_6kg/m ³ -3	7.920	804.0	35.5		
CX_6kg/m ³ -1	7.993	847.9	37.6	39.4	1.28
CX_6kg/m ³ -2	7.920	909.1	40.4		
CX_6kg/m ³ -3	7.849	904.9	40.2		
PP_8kg/m ³ -1	7.864	788.5	35.0	35.6	0.54
PP_8kg/m ³ -2	7.931	799.7	35.5		
PP_8kg/m ³ -3	7.958	817.9	36.3		
CX_8kg/m ³ -1	7.930	913.7	40.6	40.5	0.12
CX_8kg/m ³ -2	7.950	912.9	40.5		
CX_8kg/m ³ -3	7.920	907.3	40.3		

90 Day Compression Results

Specimen	Weight (kg)	Load(kN)	Compressive Strength(MPa)	Mean (MPa)	Standard Deviation (MPa)
Control-1	7.928	921.9	40.9	43.6	2.72
Control-2	7.932	1066.3	47.3		
Control-3	7.949	957.0	42.5		
PP_4kg/m ³ -1	7.876	1143.1	50.8	48.5	1.92
PP_4kg/m ³ -2	7.921	1038.8	46.1		
PP_4kg/m ³ -3	7.942	1095.00	48.6		
CX_4kg/m ³ -1	8.057	1237.3	54.99	53.7	2.04
CX_4kg/m ³ -2	8.026	1142.7	50.79		
CX_4kg/m ³ -3	8.053	1242.6	55.23		
PP_6kg/m ³ -1	8.082	1155.9	51.3	50.4	1.32
PP_6kg/m ³ -2	8.049	1156.4	51.3		
PP_6kg/m ³ -3	7.911	1091.8	48.5		
CX_6kg/m ³ -1	8.042	1103.3	49.0	49.4	0.43
CX_6kg/m ³ -2	8.09	1106.5	49.2		
CX_6kg/m ³ -3	7.962	1125.2	50.0		
PP_8kg/m ³ -1	7.958	1014.3	45	43.6	1.07
PP_8kg/m ³ -2	7.832	977.7	43.4		
PP_8kg/m ³ -3	7.849	954.4	42.4		
CX_8kg/m ³ -1	7.916	1092.8	48.6	48.2	0.90
CX_8kg/m ³ -2	7.94	1056.8	47.0		
CX_8kg/m ³ -3	8.057	1104.6	49.1		

Table 3 Key Parameters of Polypropylene Fibers at 28 day

Specimen	Fiber Volume (kg/m ³)	P _u (kN)	Mean P _u (kN) (stdev)	δ _u (μm)	Mean δ _u (kN) (stdev)	P _{crit} (kN)	Mean P _{crit} (kN) (stdev)	δ _{crit} (μm)	Mean δ _{crit} (μm) (stdev)
1	4	25.6	23.1 (2.40)	53.2	42.1 (7.15)	10.4	9.5 (0.74)	461.4	468.3 (24.21)
2	4	25.6		37.6		8.3		446.6	
3	4	23.3		34.5		9.4		511.8	
4	4	19.2		47.7		10.1		475	
5	4	21.8		37.3		9.2		446.5	
1	6	34.4	30.8 (2.29)	47.2	44.2 (3.39)	11.0	9.4 (2.09)	294.2	386.9 (80.38)
2	6	31.1		43.6		11.7		326.5	
3	6	29.0		47.1		8.1		494.3	
4	6	28.6		38.9		6.6		432.4	
1	8	25.5	27.9 (2.34)	41.3	44.2 (9.57)	8.1	10.7 (1.89)	747.1	441.7 (216.21)
2	8	27.2		34.2		12.6		276.7	
3	8	31.1		57.1		11.4		301.2	
1	Control	25.5	27.0 (2.51)	47.6	44.7 (5.73)				
2	Control	24.6		35.2					
3	Control	26.8		50.3					
4	Control	31.1		45.8					

Table 4 Key Parameters of Nylon fibers at 28 day loading

Specimen	Fiber Volume (kg/m ³)	P _u (kN)	Mean P _u (kN) (stdev)	δ _u (μm)	Mean δ _u (kN) (stdev)	P _{crit} (kN)	Mean P _{crit} (kN) (stdev)	δ _{crit} (μm)	Mean δ _{crit} (μm) (stdev)
1	4	31.2	32.3 (1.63)	43.1	44.4 (6.502)	5.9	9.7 (2.11)	500.2	417.0 (74.20)
2	4	33.2		38.0		12.0		330.3	
3	4	34.2		37.8		10.8		461.6	
4	4	29.7		55.1		10.6		324.8	
5	4	33.2		47.8		8.9		468.0	
1	6	28.6	29.2 (2.11)	49.8	47.9 (3.36)	10.4	12.8 (1.45)	355.5	393.5 (47.63)
2	6	26.1		45.6		13.0		367.4	
3	6	31.8		43.9		14.2		475.0	
4	6	30.4		52.4		13.7		376.0	
1	8	31.1	32.2 (1.72)	53.2	51.2 (8.05)	17.8	16.8 (1.87)	504.2	328.8 (102.48)
2	8	33.7		42.1		15.5		248.4	
3	8	29.9		46.1		19.3		269.9	
4	8	34.0		63.3		14.5		292.6	
1	control	25.5	27.0 (2.51)	47.6	44.7 (5.73)				
2	control	24.6		35.2					
3	control	26.8		50.3					
4	control	31.1		45.8					

28 day SPFRC Notched Beam Parameters

Specimen	Vol. Fibers (kg/m ³)	Peak load (kN)	Mean (kN) (stdev)	CMOD (μm)	Mean (μm) (stdev)	CTOD (μm)	Mean (μm) (stdev)	Load critical (kN)	Mean (kN) (stdev)	CMOD critical (μm)	Mean (μm) (stdev)	CTOD critical(μm)	Mean (μm) (stdev)
1	4	12.8	11.8 (0.60)	34.8	35.9 (2.52)	23.1	24.0 (3.93)	4.6	4.1 (0.35)	684.3	731.1 (154.62)	552.2	537.2 (23.98)
2	4	11.6		38.8		29.2		3.9		658.7		556.1	
3	4	11.2		32.3		25.2		4.2		589.4		503.4	
4	4	11.6		37.6		18.3		3.7		992.1		#N/A	
1	6	13.4	13.2 (0.71)	22.1	32.9 (9.54)	31.3	27.2 (8.55)	4.1	4.5 (0.49)	577.9	606.2 (21.54)	488.4	531.5 (32.88)
2	6	12.3		31.3		45.3		4.2		610.7		568.2	
3	6	14.0		45.3		0.0		5.2		630.1		537.8	
2	8	14.3	13.5 (0.56)	29.5	32.2 (2.43)	22.3	23.8 (1.31)	5.3	5.8 (0.40)	538.6	526.9 (12.56)	428.1	429.5 (7.09)
3	8	13.0		35.4		25.5		5.8		532.7		438.8	
4	8	13.1		31.8		23.6		6.3		509.5		421.6	
1	control	13.9	13.8 (1.44)	26.7	31.9 (6.37)	17.4	21.5 (6.54)						
2	control	11.6		25.7		18.4							
3	control	13.8		33.6		17.4							
4	control	15.7		41.6		32.8							

28 day SNFRC Notched Beam Parameters

Specimen	Vol. Fibers (kg/m ³)	Peak load (kN)	Mean (kN) (stdev)	CMOD (μm)	Mean (μm) (stdev)	CTOD (μm)	Mean (μm) (stdev)	Load critical (kN)	Mean (kN) (stdev)	CMOD critical (μm)	Mean (μm) (stdev)	CTOD critical(μm)	Mean (μm) (stdev)
1	4	15.5	14.6 (0.56)	29.5	31.2 (7.17)	20.1	18.1 (10.18)	4.3	4.1 (0.19)	934.5	929.0 (86.55)	798.9	616.8 (263.10)
2	4	14.3		22.6		12.5		4.2		785.9		662.9	
3	4	14.7		30.1		6.3		3.8		998.5		174.4	
4	4	14.0		42.5		33.6		4.1		997.0		831.0	
1	6	14.0	13.1 (0.61)	36.1	32.9 (4.36)	34.4	25.2 (4.4)	5.4	4.8 (0.43)	565.4	529.5 (112.75)	466.2	439.2 (87.61)
2	6	13.5		34.4		25.4		4.2		628.8		523.5	
3	6	12.7		25.4		35.6		4.8		338.3		292.2	
4	6	12.4		35.6		0.0		4.7		585.6		474.7	
1	8	15.2	15.2 (0.29)	30.1	31.4 (1.12)	22.1	17.7 (4.30)	5.8	6.3 (0.36)	611.2	616.2 (139.48)	515.2	495.8 (95.36)
2	8	15.0		33.0		13.1		6.4		556.2		444	
3	8	15.7		30.7		21.9		6.5		838.5		640	
4	8	14.9		31.9		13.7		6.7		458.8		383.9	

